2006

Thermal and Mechanical effects of a Shallow Asthenosphere in the Acadian Orogen: An Investigation through Numerical Modeling

Lucy E. Brown

Recommended Citation

Brown, Lucy E., "Thermal and Mechanical effects of a Shallow Asthenosphere in the Acadian Orogen: An Investigation through Numerical Modeling" (2006). *Electronic Theses and Dissertations*. 110.
http://digitalcommons.library.umaine.edu/etd/110

THERMAL AND MECHANICAL EFFECTS OF A SHALLOW ASTHENOSPHERE IN THE ACADIAN OROGEN: AN INVESTIGATION THROUGH NUMERICAL MODELING

By

Lucy E. Brown

B.A. Wellesley College, 2003

A THESIS

Submitted in Partial Fulfillment of the
Requirements for the Degree of
Master of Science
(in Earth Sciences)

The Graduate School
The University of Maine
December, 2006

Advisory Committee:

Peter O. Koons, Professor of Earth Sciences, Advisor
Scott E. Johnson, Professor of Earth Sciences
Martin G. Yates, Associate Scientist

THERMAL AND MECHANICAL EFFECTS OF A SHALLOW ASTHENOSPHERE IN THE ACADIAN OROGEN: AN INVESTIGATION THROUGH NUMERICAL MODELING

By Lucy E. Brown

Thesis Advisor: Dr. Peter O. Koons

An Abstract of the Thesis Presented
in Partial Fulfillment of the Requirements for the
Degree of Master of Science
(in Earth Sciences)
December, 2006

A high-temperature region associated with Acadian deformation extends 200 km through north-central New England. The scale of this heat source is investigated in order to better understand the rheology and mechanics of deforming orogens. In central Maine, on the boundary of the high-temperature region, isograds in pelitic rocks are normal to the accretionary structures and record a steep northeast-southwest thermal gradient. The isogradic sequence, geobarometry, and the mineral assemblages indicate low-pressure, high-temperature metamorphism, moderately low pressures of 3 kbar, and temperatures ranging from 600° to 450° C over a 10 km region. The spacing between these isograds and the temperature at each isograd are used in combination with thermal modeling to extract information about the scale and nature of the heat source. Three-dimensional conductive thermal models fall into two broad categories based on scale and type of heat source: models with a local plutonic heat source and models with a regional asthenospheric heat source. The results show that the likely source of the isograds in central Maine is local granitic plutons that dip shallowly to the northeast, but the regional thermal structure is best described by models with an asthenospheric heat source at crustal depths.

Integrating existing Bouguer gravity data with the thermal models, I found that, on the local scale, the quality of gravity data is such that it cannot confirm or refute the presence of a shallowly dipping pluton. On a regional scale, there is a large mass deficiency over southern Maine that cannot be explained entirely by low-density plutons and implies an overthickened crust. The presence of a thick crust contradicts the high-density signature expected from a region of shallow, cooled asthenosphere. These opposing pieces of evidence may be a sign of flat subduction in which the asthenospheric heat source was replaced by crustal material.

Using information from the thermal and gravity modeling, I constructed three-dimensional mechanical models that deform the orogen obliquely with west-dipping subduction. The patterns of strain that emerge show curvature at the transition between the strong and the weak rheological zones, and high uplift in the weakened zone relative to the strong region. This curvature in the orogen is not observed in Maine. Further numerical modeling could explore possible ways of accommodating both a shallow asthenosphere and a lack of curvature, but this discrepancy suggests that there may not be an abrupt change in rheology in central Maine. In turn, the possibility of along-strike rheological uniformity supports the idea that central Maine represents a change in the erosional level associated with underplating.

ACKNOWLEDGEMENTS

I thank Phaedra Upton for creating the basic mechanical model that I used in this project. She enabled me to begin my project with a working model, and she kindly allowed me to tinker with and modify this model for my own purposes. I owe Phaedra further thanks for patiently explaining many aspects of her model to me and for teaching me much about modeling in general.

When I first came to the University of Maine, I was quite ignorant about the mechanics of the earth, and since then my understanding has improved. I largely have Peter Koons to thank for this progress. I thank Peter for maintaining infinite patience while teaching me about the behavior of the earth, and I thank Peter for allowing me the space and time to make the numerous mistakes that were necessary in order for me to learn.

I thank Scott Johnson and Marty Yates for serving on my thesis committee, and for, several times, pointing me in new but relevant directions.

I thank my parents for the inspiration that their unabashed eccentricity and inquisitiveness has provided me, and I thank David for the unrelenting honesty that can be expected only from a sibling.

I thank the University of Maine and the National Science Foundation (Grants EAR-0207717 and EAR-0236756) for financial support.

TABLE OF CONTENTS

Chapter

LIST OF TABLES

LIST OF FIGURES

Chapter 1

INTRODUCTION

Eastern North America has experienced multiple episodes of deformation and metamorphism associated with a long history of subduction. In Maine this history has been preserved in multiply strained rocks, major structural faults, polymetamorphosed rocks, and a large number of plutonic bodies. Of particular interest in this study are the intrusive bodies and the metamorphism associated with the Acadian orogeny (Figure 1.1).

Southern Maine was the site of a large thermal anomaly recorded by the high-grade metamorphic rocks. This high-temperature region extends into New Hampshire and central Massachusetts where migmatites and gneiss domes are preserved. Intriguingly, this thermal anomaly is normal to the general grain of the Appalachians (Figure 1.2).

The anomalously high temperatures recorded in southern Maine potentially could have caused a change in the rheology of the crust. Large-scale along-strike weakening in an active orogen could have a significant effect on the distribution of strain within the orogen. The goal of this study is to understand the potential effects of a high-temperature anomaly on the mechanics of a deforming orogen. To accomplish this goal, I numerically explore the scale and source of the heat that produced the thermal anomaly in Maine; I construct a possible thermal and rheological structure produced by the heat source; and I incorporate this rheological structure into a mechanical model of an obliquely deforming orogen.

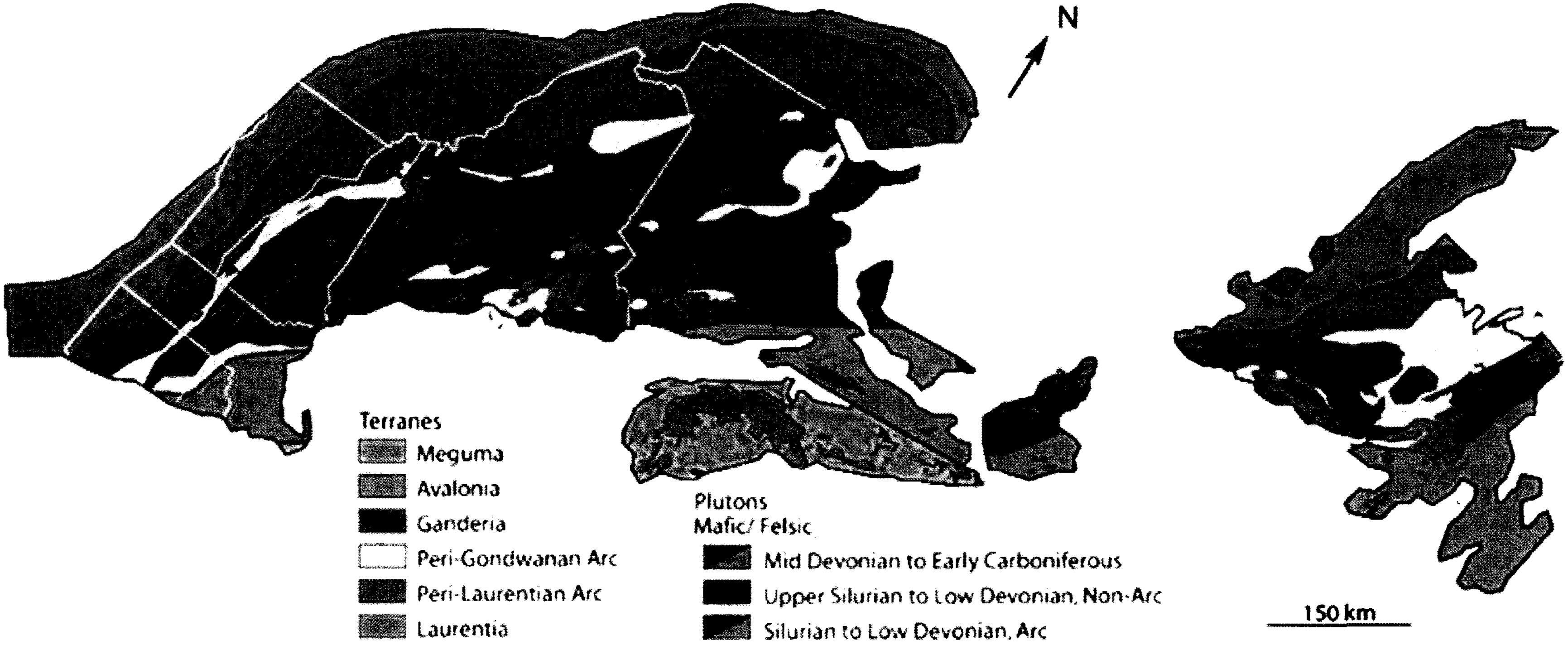

Figure 1.1. Simplified tectonic map of the northern Appalachians. Shown are the relations between Avalon, Laurentia, and Acadian and neo-Acadian plutons (modified from Hibbard et al., 2006).

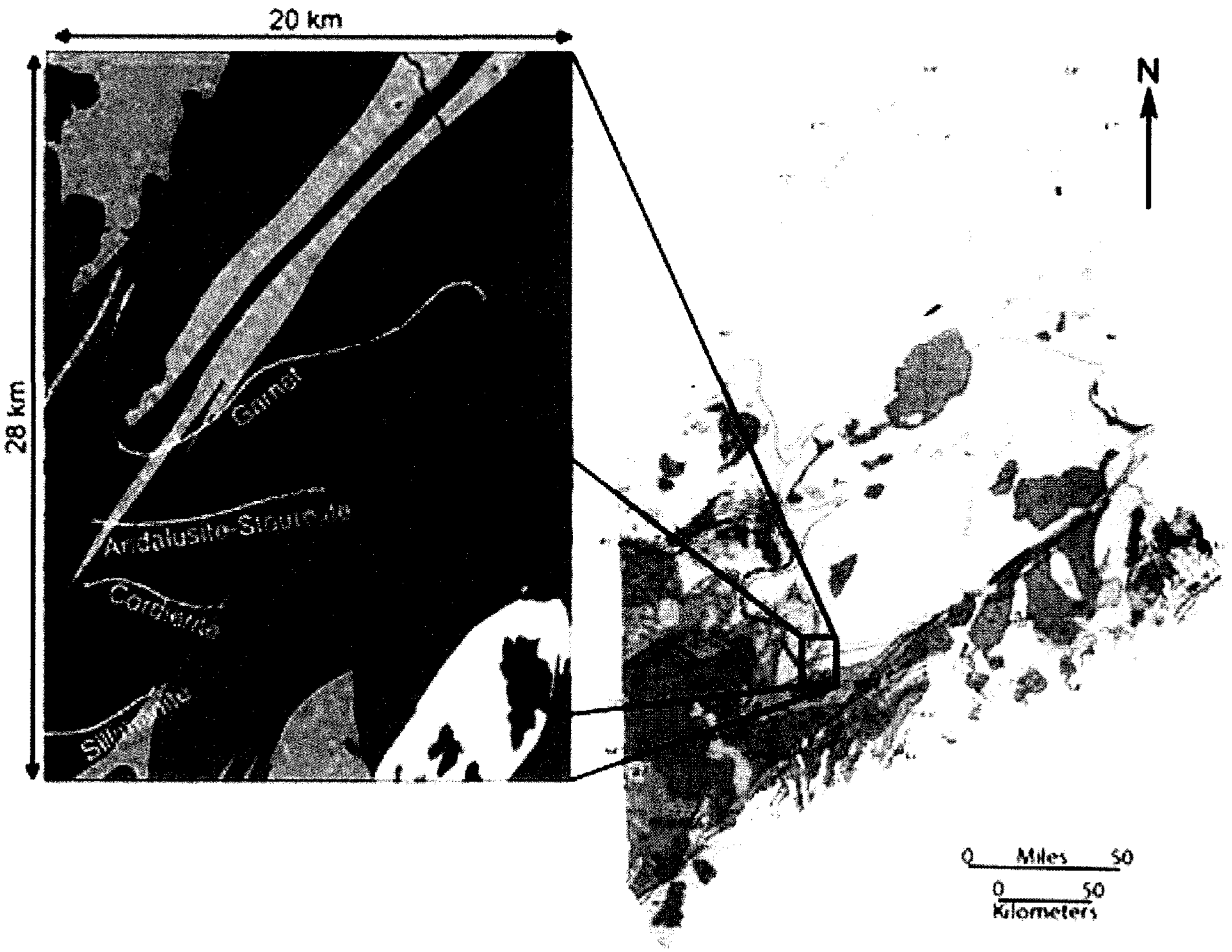

Figure 1.2. A geologic map of the study area and a metamorphic map of Maine. Shown are the relationship between the plutons, isograds, and the major lithologies in the study area (modified from Osberg, 1968). Plutons are shown in orange, brown, and yellow. The various units of the Sangerville Formation are shown in shades of green, the Waterville Formation in blue, and the Mayflower Hill Formation in pink. Isograds formed in the pelitic units of the Waterville formation are shown as yellow lines. Bodies of water are shown, for reference, in light blue.

The map is placed in the larger context of metamorphism in Maine (from Guidotti, 1985). The study area falls in a transition between high grade metamorphism (red) in southern Maine and low grade metamorphism (yellow) in northern Maine. Plutons are shown in grey.

1.1. Tectonic Setting

1.1.1. Geometric Considerations

Devonian-aged deformation in eastern Canada and eastern Massachusetts is referred to as the Acadian orogeny, which was the site of a subduction related collision between the composite microcontinent of Avalon and the continent of Laurentia (Barr et al., 2002a). For simplicity, references to Devonian-aged deformation in Maine will also be referred to as Acadian deformation. The period of active deformation is thought to have lasted from 423-385 Ma (Robinson et al., 1998). Various tectonic models have been proposed for the Acadian deformation. These models are based on the location, type, and timing of plutonism, metamorphism, deformation, and structures in the Appalachians.

By tracking the deformation front through time, the convergence rate has been conservatively estimated as 10 to 12mm a^{-1} (Robinson et al., 1998, Bradley et al., 1998). Regions of high-strain contain sense of shear indicators, which record significant evidence for right lateral movement (Swanson 1992, 1999, Solar and Brown, 2001, Short and Johnson, in press).

The Coastal Volcanic Zone in eastern Maine is usually considered to be part of the Acadian terrane (Robinson et al., 1998, Bradley and Tucker, 2002). The volcanic units in this region are syndeformational. However, there are also syndeformational plutons that have intruded into western Maine, New Hampshire, New Brunswick, and Quebec, which were part of the Laurentian continent (Robinson et al., 1998). The presence of magmatism on both sides of the orogen led to confusion about the geometry of the subduction zone; in a simple subduction zone, magmatism would be expected only in the lithosphere above the subducting slab. The plutons of western Maine and the Coastal Volcanic Zone include both gabbroic and granitic plutons (Tucker et al., 2001, Aleinikoff and Moench 1987). Some of the granitic plutons are interpreted to have formed entirely from a crustal source, but the gabbroic plutons require a mantle contribution (Murphy et al., 1999, Bradley and Tucker, 2002). An additional piece of information is that, at the same time that the magmatism was taking place in Maine, the deformation front of the Acadian orogen was moving northwest across Maine (Bradley et al., 1998).

Some researchers suggested that the volcanic rocks in the Coastal Volcanic Zone imply that the slab dipped east beneath Avalon (Keppie and Dostal, 1994, Tucker et al., 2001). With this model, the presence of volcanism in Laurentia, the overlying slab, was explained through lithospheric flexure (Bradley and Kidd, 1991) or through a onetime event such as slab break-off or mantle delamination (Tucker et al., 2001). Such a onetime event could expose the asthenosphere to the base of the crust beneath Laurentia and cause melting. The weaknesses of this model are that it does not explain the spatial gap in magmatism in central Maine or the northwest movement of the deformation front across Maine.

Other researchers suggested that the record of Acadian related volcanism is evidence for two-sided subduction (McKerrow and Zeigler 1971, Bradley, 1983, Ludman et al., 1993). In this model the oceanic slab separating Avalon from Laurentia was subducting in two locations with one zone dipping east beneath Avalon and the other dipping west beneath Laurentia. The advantage of this model is that as Laurentia and Avalon approached one another, the oceanic slab separating them could delaminate and sink into the mantle. This would expose the asthenosphere to the base of the crust, and it would explain the high-temperature regions that were recorded in the Appalachians. However, there are few modern examples of this type of mechanical situation. This has led to skepticism about the realism of this type of model (Robinson et al., 1998). Additionally, because high-temperature regions and complex patterns of volcanism have been produced in modern orogenic settings without two-sided subduction (Bibby et al., 1995, McMahon, 2000), this raises the possibility that two-sided subduction is an unnecessarily complicated and unlikely model.

Still others have suggested a west-dipping subduction zone. In this scenario, the igneous rocks of the Coastal Volcanic Zone formed in a backarc setting. Supporting this idea is the presence of subduction-like melange in New Hampshire (Eusden et al., 1996). One proposal places a mantle plume beneath the subduction zone, and as the subduction zone overrode the plume, the plutons of western Maine were formed in a continental arc setting, and this model can explain the westward movement of the deformation front by means of flat subduction. This region of underplating could have pushed the location of subduction and deformation farther into the interior of Laurentia. This event would have produced a gap in magmatism beneath the underplated region and pushed the zone of deformation towards the interior of the continent (Murphy et al., 1999). However, other causes for flat subduction are possible (Cloos, 1993), and mechanisms other than flat subduction could explain the magmatic gap (Nelson, 1992, McMahon, 2000). Additionally, there is now evidence that the Coastal Volcanic Zone does not represent a part of Avalon (van Staal et al., 2002, Barr et al., 2002b). This eliminates the confusion over the relationship between subduction geometry and volcanism in this part of the orogen, and in parts of the orogen where Avalon is visible, there are no igneous rocks with syndeformational ages (Hibbard et al., 2006).

It is possible that during Maine's long history of subduction, the dynamics of the region changed significantly, and there have been several kinematic models proposed for subduction during the Acadian orogeny. Despite this uncertainty, I will assume subduction was oblique, right lateral, and that the subduction zone dipped to the west, under North America.

1.1.2. Thermal and Metamorphic Age Considerations

The metamorphic history of Maine has been shown to be complex. A high-temperature region extended through southern Maine, New Hampshire, and central Massachusetts. Temperatures throughout this region were likely greater than 500° C (West et al., 1988). However, age dating and petrographic analyses show that the high-temperature region was not produced by a single event (Eusden and Barreiro, 1988, West et al., 1988, Lux and Guidotti, 1985). Rather, the high-grade metamorphism is the result of polymetamorphism from spatially overlapping but temporally disparate heating events. Most significantly, much of the highest temperature metamorphism in southern Maine was likely a late event, possibly associated with the emplacement of the Sebago Pluton (Lux and Guidotti, 1985). However, a petrographic analysis suggests that this high-temperature event overprinted the more widespread metamorphism associated with the Acadian orogeny (Holdaway et al., 1982, Guidotti, 1970). Thus the Acadian event likely overprinted existing metamorphism, and subsequently was overprinted by later events. This integration of metamorphic events with time makes it difficult to determine the spatial extent of Acadian metamorphism, but it does not decrease the likelihood that there was a widespread heating event associated with the Acadian deformation. Even within the Acadian orogeny, two possible episodes of metamorphism have been identified. They have typically been distinguished from one another by the presence or absence of andalusite. This petrographic change has been attributed to a slight increase in pressure between the two events (Holdaway, et al., 1982).

The cause of this metamorphism has been modeled as deep-level contact metamorphism (Guidotti, 1989, DeYoreo et al., 1989). This model suggests that the normal geothermal temperatures at a depth of 12-15 km along with the additional heat of plutons emplaced at and above this level combine to significantly increase the geothermal gradient and produce unusually high-grade metamorphism at low to moderate pressures (DeYoreo et al., 1991). In this model, the cause of the petrologically inferred increase in pressure during the Acadian orogeny, referred to above, is attributed to an increase in the volume of plutonic and volcanic material overlying the currently exposed section of the mid-crust (Guidotti, 1989).

The high-temperature region coincides with a region of deeper crustal exposure levels. Although temperature is expected to increase with depth, the high temperatures that are reached could not be attained with a normal geotherm (DeYoreo et al., 1989). However, this deepening of the exposure surface does raise the possibility that the high temperature region may have extended farther to the north at depth, and the high temperature record may not be visible in the north because the exposure level is too shallow for the anomaly to be visible.

1.2. Modern Analogues

There are numerous areas of the world in which active subduction is currently taking place. Some of these regions may be similar enough in their geometry or kinematics that a comparison between these modern orogens and the Acadian orogen may be helpful in improving our understanding of certain aspects of the dynamics of the Acadian orogen. In particular, the volcanism of New Guinea and the high temperatures associated with the Taupo Volcanic Zone of the North Island, New Zealand may be instructive modern analogues. Knowledge of the tectonics of these locations can serve as a guide when thinking about the possible processes that were at work during the Acadian orogeny.

1.2.1. Taupo Volcanic Zone

In the North Island of New Zealand, convergence of 50 mm a^{-1} causes the Pacific Plate to subduct obliquely beneath the Australian Plate at the Hikurangi Trough. The coupling between these two plates at the subduction zone becomes stronger to the south along the length of the South Island. The subduction of sediments in the north has led to an area of flat subduction, and the presence of these sediments is thought to be responsible for the weak interface between the two plates in this part of the subduction zone (Eberhart-Phillips and Reyner, 1999, Bourne and Stewart, 2000). The flat subduction has essentially thickened the crust in the northern part of the North Island, and crustal thickening has led to high uplift rates (Reyner et al., 1999, Bourne and Stewart, 2000). Numerical modeling has shown that a weakly coupled subduction zone can lead to extension in the overlying slab when the overlying slab is much stronger than the interface (Upton et al., 2003). Additionally, slab rollback likely accounts for some of the extension (Upton et al., 2003, Hochstein, 1995). Another proposed explanation for the extension is the presence of a mantle plume initiated by subduction-induced flow in the backarc (Hochstein, 1995). These various mechanisms of producing extension within a convergent setting are probably not incompatible with one another.

Associated with the extension in the North Island are a number or geophysical anomalies observed in the Central Volcanic Region (CVR). A smaller region within the CVR, the Taupo Volcanic Zone (TVZ), produces active rhyolitic and andesitic volcanism. Seismic surveys have indicated that the Moho in the CVR is at a shallow depth of 15 km, and the lithosphere may be thinned to as little as 30 km (Stern and Davey 1987, Bibby et al., 1995). Bibby et al. (1995) studied many other geophysical anomalies associated with the TVZ. Strong seismic reflections in the lower crust and near the Moho suggest that there may be partial melting in the lower crust. Seismicity indicates that most faulting is normal and that earthquakes rarely extend to depths greater than 10 km. Heat flow is high in the TVZ, and is convectively concentrated into volcanic and geothermal fields. The average heat flow across the central TVZ, where most of the geothermal activity takes place, is 700 mW/m^2 (Bibby et al., 1995). Some studies have suggested that these high values of heat flow require a combination of lithospheric thinning and a mantle plume (Hochstein, 1995).

Taupo demonstrates the possibility of extension within a convergent setting. It demonstrates the effect of lithospheric thinning on heat flow, and gives several possible mechanisms for generating extremely high heat flow.

1.2.2. New Guinea

New Guinea is the site of a recent arc-continent collision at the boundaries between the Australian and Pacific plates which produced a complex pattern of volcanism. A belt of Miocene plutons extends along the eastern side of the island. To the south, farther from the subduction zone, there is a belt of younger igneous rocks that are less than 7 Ma. In the central portion of the island, there is a gap in the magmatism, and on the western side of the island, there is a second group of Miocene plutons as well as plutons less than 5 Ma (McMahon, 2000a). Additionally, there are volcanic rocks that form the collided arcs.

The only area of current volcanism is offshore of New Guinea above a north-facing subduction zone. In fact, this volcanism is part of one of the only modern examples of a double-sided subduction zone. Convergence on the south facing subduction zone in this system is very slow, and currently no volcanism is taking place in this region. The geometry of the double-sided subduction zone suggests that it may have extended farther to the west previously, and some of the complexity in the volcanism on the eastern side of New Guinea is attributed to the closing of this subduction zone (McMahon, 2000b).

On the western side of the island, the tectonic response to collision was different from the east. Some models involve south-dipping subduction on the western side of New Guinea that later changes polarity to north-dipping (McMahon, 2000b, Cloos et al., 1998). However, the evidence for this switch is ambiguous. There is a temporal gap in magmatism at this point. A common explanation for the younger igneous rocks on this side of the island is lithospheric delamination of the subducting slab. The delamination exposed the asthenosphere to the base of the crust causing the volcanism (McMahon, 2000b).

The tectonics of New Guinea are complex, and despite the relative youth of this orogen, there have been various tectonic models and geologic processes proposed to explain the features observed on New Guinea. The processes that have been postulated for New Guinea are not necessarily the same ones that took place in the development of the Acadian orogen. The relevance of New Guinea to the Acadian orogen is that New Guinea demonstrates that there are significant temporal and along-strike variations in subduction geometry, volcanism, and heat flow.

Chapter 2

STUDY AREA AND PETROLOGY

The rock types that occur in the Waterville region are of interest for two reasons. First of all, the rock type provides information about the thermal and mechanical properties of the region. This geological information can be used to constrain numerical models. Secondly, the initial rock type and composition determine the type of metamorphic rock that will be produced under given P-T conditions.

There are three small plutons in the southern portion of the study area and one larger pluton in the northwest. Because the southern plutons appear to have a spatial relationship to the local metamorphic isograds, these plutons are of most interest for this study. Two of these plutons, the Hallowell and Togus plutons, have a binary quartz monzonitic composition, and the third, the Threemile Pond pluton, has a biotite granodioritic composition (Osberg, 1968). There are also very small amounts of diorite found in the same location as the larger plutons. Radiometric dating has shown the Hallowell pluton to be 387±11 Ma, the Togus pluton to be 378±1 Ma, and the Threemile Pond pluton to 381±1 Ma (Zartman et al., 1970, Dallmeyer and van Breeman 1981, Tucker et al., 2001).

Osberg (1968) has described the stratigraphy of the three relevant formations, Sangerville (Vassalboro), Mayflower Hill, and Waterville. The Sangerville Formation is primarily a calcareous wacke. In addition to the wacke, there are smaller amounts of two phyllites, one dominated by biotite and the other by muscovite.

The Mayflower Hill Formation is primarily a wacke with minor phyllites.

The Waterville Formation contains four members: a pelite, a wacke, a limestone, and a phyllite. The pelite contains biotite, chlorite, garnet, variable amounts of quartz, and muscovite at low grades of metamorphism. At high grades it contains quartz, biotite, muscovite, garnet, andalusite, staurolite, and cordierite. The wacke contains clasts of quartz, feldspar, slate, and volcanic fragments in a matrix of quartz, biotite, muscovite, chlorite, and calcite. In the chlorite and garnet zones of metamorphism, the limestone contains biotite, actinolite, garnet, calcite, and variable amounts of quartz. At the higher grades of metamorphism, the limestone has been metamorphosed to a marble containing quartz, biotite, actinolite, diopside, garnet, and calcite. The limestone alternates with the phyllite, which contains muscovite, quartz, graphite, and pyrrotite (Osberg, 1968).

The rock in the study area has undergone low-pressure, high-temperature metamorphism. Garnet, andalusite-staurolite, cordierite, and sillimanite isograds record an increase in temperature with increasing proximity to the plutons (Figure 1.2). The distance of each isograd from the pluton is variable, but roughly sillimanite is 1 km, cordierite is 3 km, andalusite-staurolite is 6 km, and garnet is 10 km from the edge of the pluton.

The mineral assemblages in each metamorphic zone were determined by Osberg (1968), and the geochemistry of the pelitic and calcareous units of the Waterville and Sangerville formations was determined by Ferry (1976a, 1976b, 1982). The assemblages and geochemistry suggest that K_2O, FeO, MgO, Al_2O_3, SiO_2, H_2O, and MnO are the dominant components in the pelitic rocks. The presence of magnetite in some of the lower-grade rocks suggests that Fe_2O_3 may also be an important component.

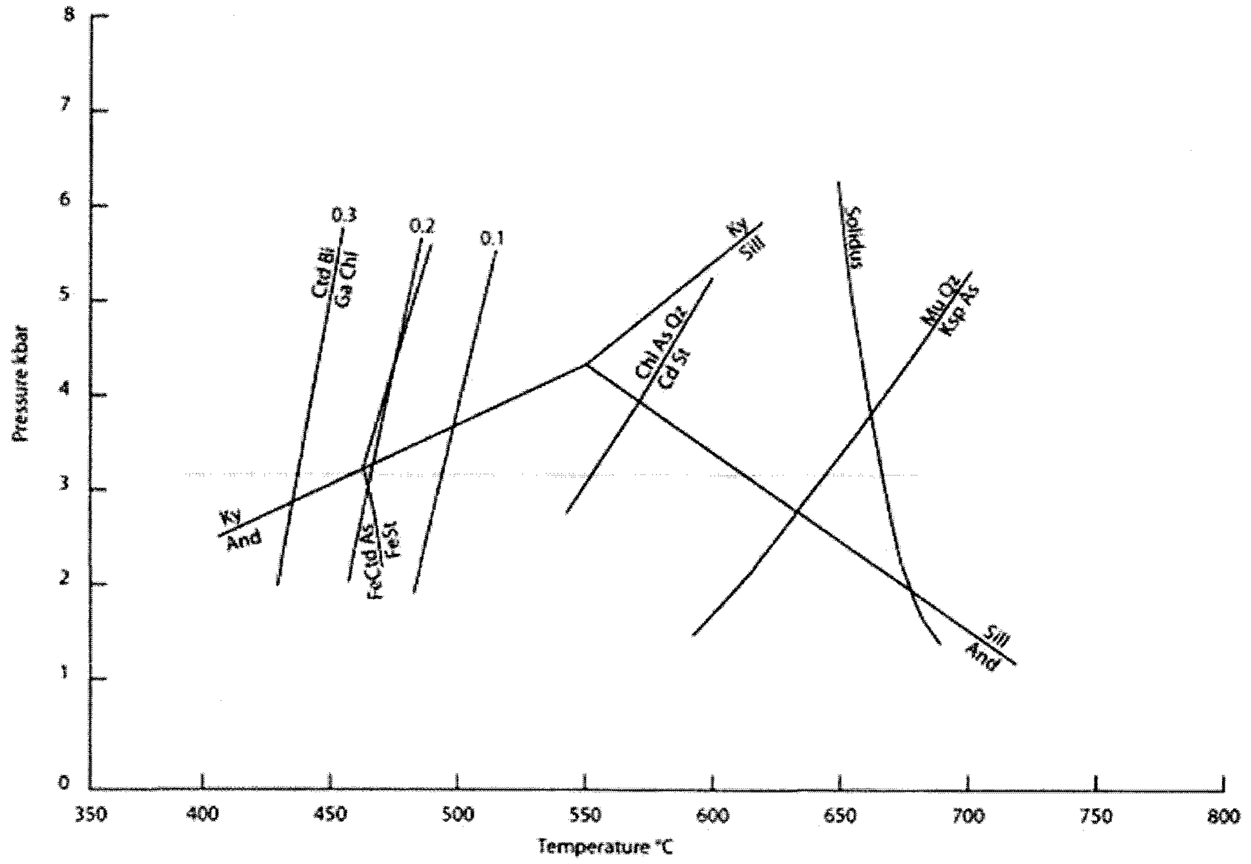

Figure 2.1. Simplified petrogenetic grid for pelites. Shown are univarient curves in the KFMASH system that are used to estimate the temperature at each isograd. The abbreviations used are And=andalusite, As=aluminum silicate, Bi=biotite, Cd=cordierite, Chl=chlorite, Ctd=chloritoid, Ga=garnet, Ksp=potassium feldspar, Ky=kyanite, Mu=muscovite, Qz=quartz, Sill=sillimanite, and St=staurolite. Three different curves are shown for garnet stability depending on whether the Mn/(Mn+Fe+Mg) ratio is 0.1, 0.2, or 0.3. In the study area, this ratio was found to be approximately 0.2. Also shown is a light grey line at the 12 km depth that is estimated as the current erosional surface (after Spear and Cheney, 1989 and Xu et al., 1994).

Ferry (1980) used biotite-garnet-andalusite-sillimanite, garnet-plagioclase-quartz-andalusite-sillimanite, biotite-garnet-plagioclase-quartz-aluminum silicate, and garnet-cordierite-sillimanite-quartz geobarometry to determine that the pressure was between 3.0 and 4.0 kbar. Based on this analysis, I used a depth of 12 km as the present day erosional surface.

If the temperatures of each of the isograds can be determined, thermal modeling of heat flow around the pluton can put some constraints on what conditions could have created the present day distribution of metamorphism. Ideally, the temperature of each isograd would be determined petrologically from the reactions implied by the assemblages on either side of each isograd. A petrogenetic grid could then be used to determine the temperature of each reaction at 3.5 kbar. However, in this region, there are complications that make this approach difficult. There is a disequilibrium assemblage, cordierite, staurolite, biotite, and muscovite, found in some areas surrounding the pluton (Pattison et al., 1999). Polymetamorphism is a likely cause of this disequilibrium assemblage but does not necessarily mean that the isograds are also in disequilibrium. However, the possibility of polymetamorphism does raise the question: which metamorphic event caused the isograd to form? Because the purpose of the modeling is to evaluate different sources of heat as causes of metamorphism, the modeling itself may be able to address the issue of polymetamorphism. For the purposes of modeling, it is enough to know that the temperature at each isograd is approximately constant. However, the requirement of constant temperature may not apply to at least one isograd. The andalusite and staurolite isograds are lumped together as one because the order in which these two minerals first appear is not consistent (Osberg, 1968). This may be an indication that these two reactions are sensitive to bulk composition and that variations in bulk composition caused significant variations in the temperature at which these reactions took place.

The minerals are in the KFMASH system for which numerous petrogenetic grids have been determined (Hess, 1969, Spear and Cheney, 1989, Xu et al., 1994). However, garnet has a significant amount of Mn^{2+}, which changes the stability of garnet in P-T space. The effects of bulk composition and disequilibrium make it difficult to determine the reactions that took place here, and the effect of the extra components outside of the KFMASH system make it uncertain whether a reaction temperature determined from the KFMASH system has validity. Instead, the minimum temperature at which each isogradic mineral is stable is used as an estimate of temperature at each isograd (Figure 2.1).

Because quartz behaves ductilly, the background temperature is assumed to have been at least 350° C (Brace and Kohlstedt, 1980). This temperature is also supported by thermal closure data from muscovite and biotite (Dallmeyer and van Breeman, 1981). Ferry (1980) measured the composition of numerous garnet samples from this area. His measurements showed a significant spessartine content, leading to a ratio of Mn/(Mn+Fe+Ca) of approximately 0.2 (Ferry, 1980). This ratio places the lower limit on the garnet stability at 460° C (Spear, 1993). At 12 km depth, the lower range of staurolite is slightly below the value for garnet, and the lower range for andalusite is significantly below the value for garnet (Spear and Cheney, 1989). Given that staurolite and andalusite first appear at a higher grade than garnet, the staurolite value seems to be more realistic than the andalusite value. The ordering of garnet before staurolite can easily be explained by variations in bulk composition, geobarometrical error, or petrological error. For this reason, a value of 470° C was used for the andalusite-staurolite isograd. Of the four isograds considered, this is the most questionable, and may not be a good indicator of temperature. The lower limit of cordierite stability is placed at 550° C (Xu et al., 1994). The sillimanite isogradic temperature is based on the andalusite-sillimanite transition, and is placed at 600° C (Xu et al., 1994). However, the sillimanite formed on biotite rather than on andalusite. This may be an indication that the metastability of andalusite was significant, and the estimated temperature at this isograd may be an underestimate. Closer to the pluton, sillimanite and K-feldspar coexist, suggesting a temperature of 660° C was reached.

Based on the petrological uncertainty presented above, as well as the uncertainty in thermodynamic data, I estimate that there is an error of ± 50° C in the temperature at each isograd. Because of the close spacing between some of the isograds, there is significant overlap in the temperature range that is possible at these isograds (Figure 2.2). The degree of overstepping that is required at each isograd to cause each reaction to proceed from a metastable state is unknown. Overstepping is likely at the sillimanite isograd and could cause the actual temperature at other isograds to be higher than estimated as well. Additionally, it is unclear whether the temperature recorded by the isograds is the peak temperature or whether retrograde metamorphism may cause a lower temperature to be recorded. Both of these unknowns would cause the peak temperature at each isograd to be higher than my estimate.

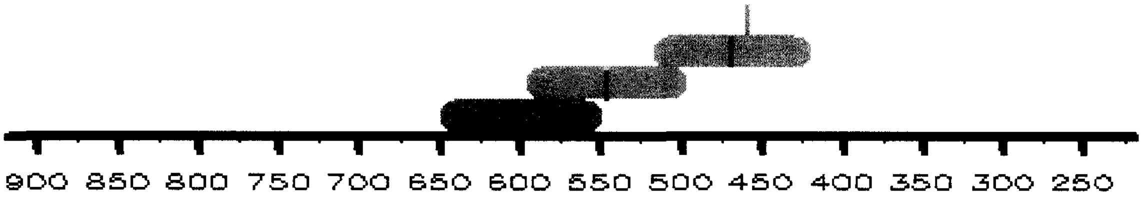

Figure 2.2. Temperatures of relevant metamorphic reactions. Each color represents the preferred petrogenetically determined temperature of each isograd and the error associated with the petrological data. Sillimanite is shown in blue, cordierite in red, staurolite in black and garnet in orange. There is overlap in the temperature range of garnet, staurolite, and cordierite and in the range of cordierite and sillimanite.

Chapter 3

LOCAL-SCALE THERMAL MODELS

3.1. Model Setup

3.1.1. Horizontal Pluton Geometry

This group of models was designed to determine whether the steep thermal gradient recorded on the edge of the regional thermal anomaly in southern Maine could have been produced locally by plutons.

Local heat flow is modeled with a rectangular volume of dimensions x=50 km, y=50 km, z=30 km (Figure 3.1). The grid spacing is 2 km in the x-direction, 0.5 km in the y-direction, and 1 km in the z-direction. The box has a geothermal gradient for which the temperature varies with depth and is constant in the horizontal directions. An area of anomalously high temperature is placed into this steady-state geotherm, which represents an instantaneously emplaced pluton. In this model, the pluton is placed in the center of one edge of the model. The pluton extends 20 km along the edge in the x-direction, 10 km towards the center of the model in the y-direction, and is 2 km thick.

This geometry is a simplification of the actual geometry. In Augusta there are three small plutons. Radiometric dating has shown that, within error, these plutons could be the same age, but, within error, they could be separated in age by over one hundred thousand years (Dallmeyer and van Breeman 1981, Tucker et al., 2001). I have chosen to assume that the plutons were emplaced simultaneously and to simplify the geometry by combining the three plutons into a single larger pluton with approximately the same area

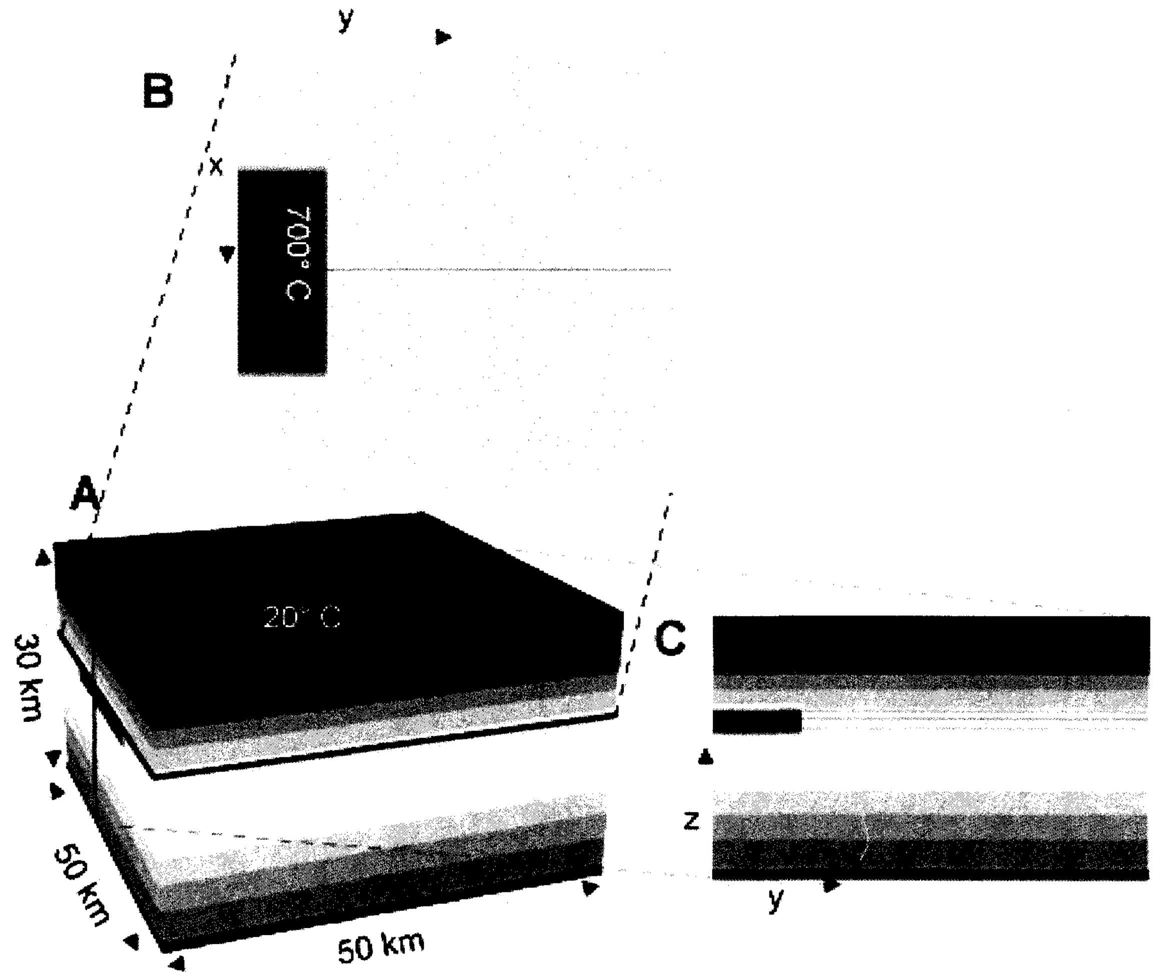

Figure 3.1. Small-scale thermal model setup for horizontal plutons. Image A shows the model dimensions and the steady-state geothermal gradient in the z-direction. Image B shows the location of the pluton in a map view at a depth of z=12 km. Image C shows a cross-section through the pluton. The black lines going across images B and C show the lines along which the temperature-time data were recorded, and likewise, the lines going across image C show the variation in depth of the erosional surfaces that was explored.

of surface exposure. The importance of the timing and lifespan of the plutons is discussed below in Sections 3.1.2 and 3.2.2.2.

The background steady-state geothermal gradient used in this model was reached by applying a constant heat flux to the base of the model, a constant temperature of 20° C to the top of the model, and a constant radioactive heat source throughout the volume of the model (Table 3.1). The edges of the models have adiabatic boundaries. Under these conditions, the model was allowed to run until it reached a steady state.

The model assumes that heat flow is primarily conductive, based on the equation $\frac{\partial T}{\partial t} = \kappa\left(\frac{\partial^2 T}{\partial x^2} + \frac{\partial^2 T}{\partial y^2} + \frac{\partial^2 T}{\partial z^2}\right) + A$, where T is temperature, t is time, A is a source term and κ is the thermal diffusivity, which is equal to $\frac{k}{\rho c}$ where k is the thermal conductivity, ρ is the density, and c is the specific heat. This assumption is valid because the low permeability at 12 km depth impedes convection. Additionally, although in all cases the release of metamorphic fluids would accelerate cooling, Dutrow (2002) has shown that the amount of fluid produced by the pluton is unlikely to transport significant amounts of heat. The conductive heat flow equation was solved in three-dimensions with a finite difference code, FLAC^{3D} (Itasca, 2005).

Many of the thermal parameters that went into this model can vary significantly within the earth, and some factors constrained by petrology are not well known. An understanding of the role these factors play, why certain values were chosen, and the effect that a variation in these properties has on the result is important. In order to determine the range of outcomes that might reasonably be expected, I varied the values of several thermal properties as well as some variables related to the pluton geometry. Table 3.1 shows the values for the thermal properties used in each model.

The standard basal flux used in this model was 0.04 Wm^{-2}. This is a realistic value for the mantle contribution to the geotherm in a normal geothermal environment (Turcotte and Schubert, 2002). This condition resulted in a steady-state geotherm with a basal temperature of 670° C. In some areas of a subduction zone, the geothermal gradient is elevated because of backarc extension, slab break-off, or slab induced upward mantle flow. To account for the possibility of a high mantle contribution to the thermal gradient, some models use a fixed basal temperature of 900° C. (Chapter 4 addresses the possibility of high regional heat flow). Near the basal boundary, the use of a fixed temperature base will affect the downward flow of heat away from the pluton. However, the base of the models was sufficiently far from the plutons that this effect is unlikely to be significant.

The standard conductivity in the model was 2.9 $Jm^{-1}{}^{\circ}C^{-1}s^{-1}$. This is a value appropriate for typical crustal material. The conductivity was varied to 1.9 $Jm^{-1}{}^{\circ}C^{-1}s^{-1}$, a value appropriate for a rock which is coarse grained, has a low percentage of quartz, or has a high porosity, and 3.9 $Jm^{-1}{}^{\circ}C^{-1}s^{-1}$, a value for a rock with high quartz or calcite. A value of 2.9 $Jm^{-1}{}^{\circ}C^{-1}s^{-1}$ is sensible in this area because the rock in the study is sedimentary and has a significant amount of quartz. At the time of metamorphism, the rock was at 12 km depth, thus it probably had a low permeability. Because the conductivity of the rocks could have changed with grain size during metamorphism, testing the variation in conductivity is important, but 2.9 $Jm^{-1}{}^{\circ}C^{-1}s^{-1}$ is probably a reasonable value to use as a starting point.

Model Name	Conductivity	Specific Heat	Density	Thermal Diffusivity	Basal Heat Flux	Fixed Basal Temperature	Radioactive Heat Production	Surface Temperature	Pluton Temperature	Time Span of Pluton Activity	Pluton Depth	Erosional Surface Depth	Dip Angle (Pluton)	Dip Angle (Erosional Surface)	Pluton Thickness	Steps				
					Basal Boundary Condition												Step Size		Total Run Time	
	W/m/°C	J/kg/°C	kg/m^3	m^2/s	W/m^2	°C	W/m^3	°C	°C	kyr	km	km	°	°	km		s	years	s	kyr
3.3A	2.9	1000	2700	1.1E-06	0.04		1.5E-06	20	700	0	11	12	0	0	2	500	8.51E+10	2699	4.E+13	1350
3.3B	3.9	1000	2700	1.4E-06	0.04		1.5E-06	20	700	0	11	12	0	0	2	672	6.33E+10	2007	4.E+13	1350
3.3C	1.9	1000	2700	7.0E-07	0.04		1.5E-06	20	700	0	11	12	0	0	2	328	1.30E+11	4119	4.E+13	1350
3.3D	2.9	1000	2700	1.1E-06		900	1.5E-06	20	700	0	11	12	0	0	2	500	8.51E+10	2699	4.E+13	1350
3.3E	2.9	1000	2700	1.1E-06	0.04		1.5E-06	20	900	0	11	12	0	0	2	500	8.51E+10	2699	4.E+13	1350
3.3F	2.9	1000	2700	1.1E-06	0.04		1.5E-06	20	700	infinite	11	12	0	0	2	500	8.51E+10	2699	4.E+13	1350
3.3G	3.9	1000	2700	1.4E-06	0.04		1.5E-06	20	700	infinite	11	12	0	0	2	672	6.33E+10	2007	4.E+13	1350
3.3H	1.9	1000	2700	7.0E-07	0.04		1.5E-06	20	700	infinite	11	12	0	0	2	328	1.30E+11	4119	4.E+13	1350
3.3I	2.9	1000	2700	1.1E-06		900	1.5E-06	20	700	infinite	11	12	0	0	2	500	8.51E+10	2699	4.E+13	1350
3.3J	2.9	1000	2700	1.1E-06	0.04		1.5E-06	20	900	infinite	11	12	0	0	2	500	8.51E+10	2699	4.E+13	1350
3.3K	2.9	1000	2700	1.1E-06	0.04		1.5E-06	20	700	0	11	11	0	0	2	500	8.51E+10	2699	4.E+13	1350
3.3L	2.9	1000	2700	1.1E-06	0.04		1.5E-06	20	700	0	11	12	0	0	2	500	8.51E+10	2699	4.E+13	1350
3.3M	2.9	1000	2700	1.1E-06	0.04		1.5E-06	20	700	0	11	13	0	0	2	500	8.51E+10	2699	4.E+13	1350
3.3N	2.9	1000	2700	1.1E-06	0.04		1.5E-06	20	700	0	12	12	0	0	2	500	8.51E+10	2699	4.E+13	1350
3.3O	2.9	1000	2700	1.1E-06	0.04		1.5E-06	20	700	0	12	13	0	0	2	500	8.51E+10	2699	4.E+13	1350
3.3P	2.9	1000	2700	1.1E-06	0.04		1.5E-06	20	700	0	13	13	0	0	2	500	8.51E+10	2699	4.E+13	1350

Table 3.1. Local Scale Thermal Modeling Parameters. The model names correspond to the labeling of the figures in Section 3.2.

Model Name	Conductivity	Specific Heat	Density	Thermal Diffusivity	Basal Heat Flux	Fixed Basal Temperature	Radioactive Heat Production	Surface Temperature	Pluton Temperature	Time Span of Pluton Activity	Pluton Depth	Erosional Surface Depth	Dip Angle (Pluton)	Dip Angle (Erosional Surface)	Pluton Thickness	Steps				
					Basal Boundary												Step Size		Total Run	
	W/m/°C	J/kg/°C	kg/m^3	m^2/s	W/m^2	°C	W/m^3	°C	°C	kyr	km	km	°	°	km		s	years	s	kyr
3.4A	2.9	1000	2700	1.1E-06	0.04		1.5E-06	20	700	0	dipping	12	12	0	2	1000	4.29E+09	136	4.E+12	136
3.4B	2.9	1000	2700	1.1E-06	0.04		1.5E-06	20	700	0	11	dipping	0	12	2	1000	4.29E+09	136	4.E+12	136
3.4C	2.9	1000	2700	1.1E-06	0.04		1.5E-06	20	700	0	dipping	12	5	0	2	1000	4.29E+09	136	4.E+12	136
3.4D	2.9	1000	2700	1.1E-06	0.04		1.5E-06	20	900	0	dipping	12	12	0	2	1000	4.29E+09	136	4.E+12	136
3.4E	2.9	1000	2700	1.1E-06	0.04		1.5E-06	20	900	0	11	dipping	0	12	2	1000	4.29E+09	136	4.E+12	136
3.4F	2.9	1000	2700	1.1E-06	0.04		1.5E-06	20	900	0	dipping	12	5	0	2	1000	4.29E+09	136	4.E+12	136
3.4G	2.9	1000	2700	1.1E-06	0.04		1.5E-06	20	700	infinite	dipping	12	12	0	2	1000	4.29E+09	136	4.E+12	136
3.4H	2.9	1000	2700	1.1E-06	0.04		1.5E-06	20	700	infinite	11	dipping	0	12	2	1000	4.29E+09	136	4.E+12	136
3.4I	2.9	1000	2700	1.1E-06	0.04		1.5E-06	20	700	infinite	dipping	12	5	0	2	1000	4.29E+09	136	4.E+12	136
3.4J	2.9	1000	2700	1.1E-06		900	1.5E-06	20	700	0	dipping	12	12	0	2	1000	4.29E+09	136	4.E+12	136
3.4K	2.9	1000	2700	1.1E-06		900	1.5E-06	20	700	0	11	dipping	0	12	2	1000	4.29E+09	136	4.E+12	136
3.4L	2.9	1000	2700	1.1E-06		900	1.5E-06	20	700	0	dipping	12	5	0	2	1000	4.29E+09	136	4.E+12	136
3.4M	2.9	1000	2700	1.1E-06		900	1.5E-06	20	700	infinite	dipping	12	12	0	2	1000	4.29E+09	136	4.E+12	136
3.4N	2.9	1000	2700	1.1E-06		900	1.5E-06	20	700	infinite	11	dipping	0	0	2	1000	4.29E+09	136	4.E+12	136
3.4O	2.9	1000	2700	1.1E-06		900	1.5E-06	20	700	infinite	dipping	12	5	0	2	1000	4.29E+09	136	4.E+12	136
3.5A	2.9	1000	2700	1.1E-06		900	1.5E-06	20	700	1	dipping	12	5	0	2	1000	4.29E+09	136	4.E+12	136
3.5B	2.9	1000	2700	1.1E-06		900	1.5E-06	20	700	3	dipping	12	5	0	2	1000	4.29E+09	136	4.E+12	136
3.5C	2.9	1000	2700	1.1E-06		900	1.5E-06	20	700	11	dipping	12	12	0	2	1000	4.29E+09	136	4.E+12	136
3.5D	2.9	1000	2700	1.1E-06		900	1.5E-06	20	700	6	dipping	12	12	0	4	1000	4.29E+09	136	4.E+12	136
3.5E	2.9	1000	2700	1.1E-06	0.04		1.5E-06	20	700	3	dipping	12	5	0	2	1000	4.29E+09	136	4.E+12	136
3.5F	2.9	1000	2700	1.1E-06	0.04		1.5E-06	20	700	4	dipping	12	5	0	2	1000	4.29E+09	136	4.E+12	136

Table 3.1 Continued.

Changing the value of any of the thermal variables in Table 3.1 will affect the geotherm. I have chosen to vary only two of these properties: the basal boundary condition and the thermal conductivity. Changing the basal boundary condition will affect the geotherm without affecting how a given amount of heat will flow through an area of the model with a specified thermal gradient. Changing the conductivity will affect both the geothermal gradient and the ease with which heat will flow through a region with a given gradient. For this reason, the effect of changing these two variables has a fundamentally different effect on the model, and it is important to see the effect of these two types of changes. If other thermal variables were varied, they too would change the geotherm and some would also affect the ease of heat flow in the model. Changes in each thermal property might result in a geotherm of a slightly different shape. However, the change in shape resulting from a variation of these parameters is not as significant as the overall increase or decrease in the geotherm, which can be observed as easily from changing the basal boundary condition and conductivity as from changing any other thermal parameter.

The standard temperature used for the pluton was 700° C. This is based on the minimum melting temperature of a granite (Tuttle and Bowen, 1958) (Figure 2.1). This temperature was varied to 900° C to consider the possibility that the melt was heated to significantly higher than the minimum temperature before it was emplaced. These two situations represent end members with the actual temperature of emplacement probably closer to the 700° C end.

In some models, the pluton temperature was allowed to decay as soon as it was emplaced. In other models, the temperature was held constant at the initial temperature for the duration of the run. The first situation represents emplacement that is rapid relative to the timescale of heat flow, while the second situation represents emplacement that is on the same timescale as heat flow. Neither of these two cases perfectly represents reality. Clearly, emplacement of a pluton will never be entirely instantaneous. Thus, the size of the pluton will increase as it is emplaced. The two cases used here, can be seen as end members between which reality is likely to lie. Given the small size of the pluton, the emplacement time is likely to be short. This means that the first case is probably the more realistic of the two. In some models, where more control over the time span of emplacement was needed, the pluton temperature was held constant for a set period of time, after which, the temperature was allowed to decay. Rates of emplacement are discussed further in Section 3.1.2.

In addition to varying the thermal properties of the model, the sensitivity of the model to changes in geometry was evaluated. Because of uncertainty in the geobarometry the depth of the current erosional surface was varied from 11 to 13 km (Figure 3.1C). This changed the location within the model at which the temperature was observed without changing anything about the setup or thermal structure of the model. Because it is certain that the pluton is exposed at the earth's surface today, the surface depth was not varied by more than 2 km, the thickness of the pluton in the model. The other way to accomplish a relative change in the position of the pluton and the erosional surface is to change the depth of emplacement of the pluton. Again, in this case, the depth of the pluton was changed only to such an extent, relative to the erosional surface, that the pluton would be exposed at the surface.

3.1.2. Dipping Pluton Geometry

Because gravity data were not able to determine whether or not the pluton dips beneath the study area (Chapter 5), models were run with a pluton dipping relative to the erosional surface (Figure 3.2). In these models a different grid was used because it was necessary to have a higher resolution in the z-direction. For most of the volume of the model, the spacing was 2 km in each direction. However, in one section, the spacing was 2 km in the x-direction, 0.5 km in the y-direction, and 0.1 km in the z-direction. This high-resolution zone encompassed the entire region where metamorphic isograds are found.

In some models, the erosional surface was assumed to be horizontal and the pluton to be dipping beneath it. In other models the pluton was assumed to be initially horizontal, and the erosional surface to have formed at an angle relative to the pluton. These two situations differ from one another because, the orientation of the pluton and the erosional surface relative to the geothermal gradient are not the same. In the latter case, the background temperature changes with location along the erosional surface while in the former case the background temperature is uniform along the erosional surface.

Many of the variations in thermal properties that were described above were also examined with a dipping pluton geometry. Models were run where the pluton temperature was allowed to decay immediately, models were run where the pluton temperature was held constant for the duration of the run, models were run where the pluton temperature was elevated to 900° C, and models were run in a setting with an elevated geotherm. In addition to these variables some models were run where the pluton

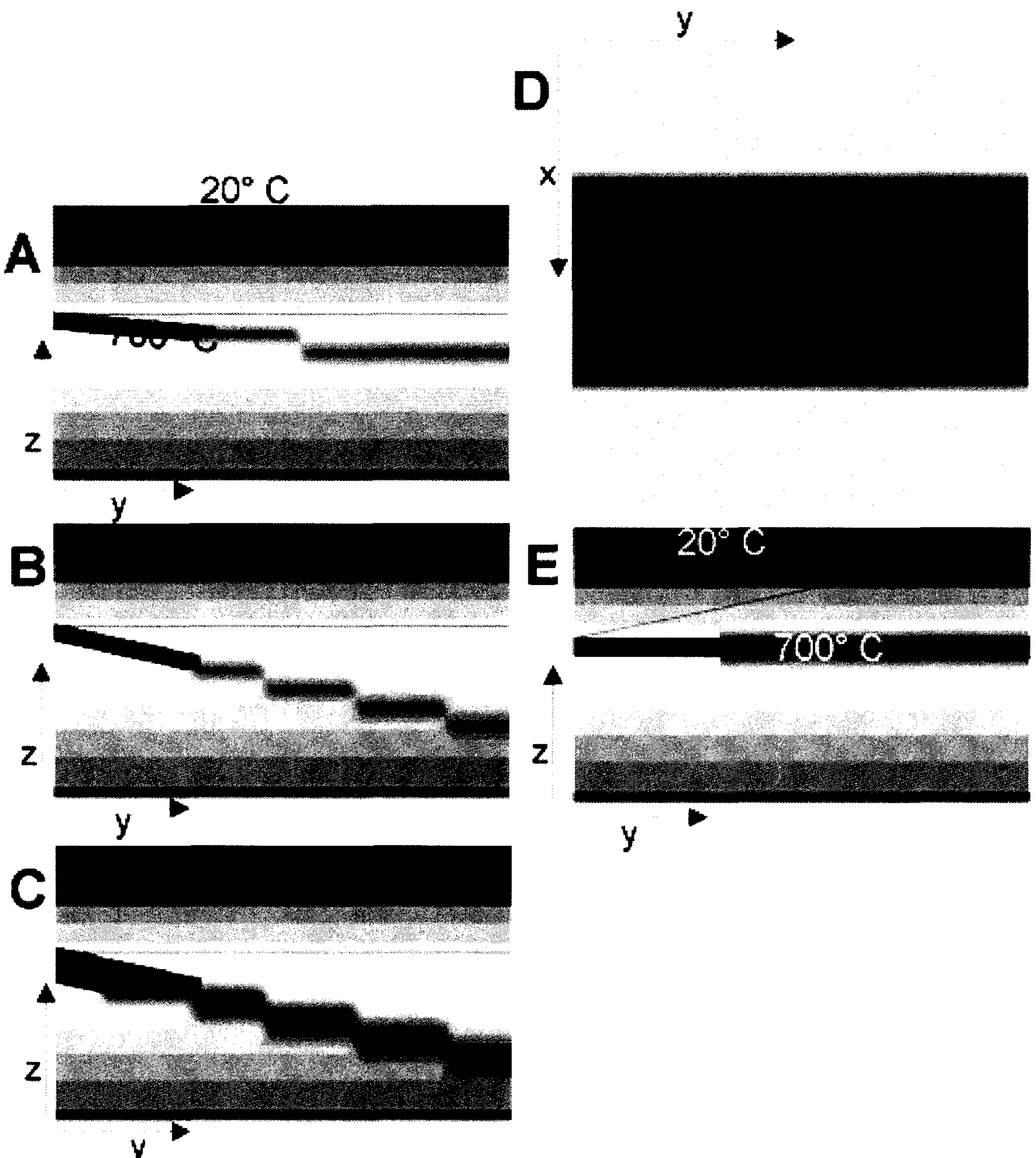

Figure 3.2. Small-scale thermal model setup for dipping plutons. The scale is the same as in Figure 3.1. Image A shows a pluton dipping at 5°. Image B shows a pluton with a dip of 12°. Image C also shows a pluton with a dip of 12°, but the pluton thickness has been increased such that the intersection of the pluton and the erosional surface is approximately equal to the intersection for the pluton in image A. Image D shows a map view of a horizontal pluton, and image E shows a cross-section of the same pluton with an erosional surface dipping at 12°. For all cross-sections, the black lines represent the erosional surface where temperature-time data was collected. Visible on most of these images is the location where the pluton crosses from the finely gridded portion of the model to the portion with a coarser grid. This transition is not very close to the locations at which temperature-time data is collected and should not have a significant effect on the results.

had a 12° dip while others were run where the pluton had a 5° dip. For some models, the results were such that it was appropriate to look more closely at the effect of the length of time over which plutonic activity lasted. For this reason, there were models in which the pluton temperature was held constant for a set period of time, and after this time, the temperature of the pluton was allowed to decay.

In the models with a dipping pluton, the effect of pluton thickness was examined. The reason for this was that, because these plutons are modeled as sheet-like bodies, the current exposure area of the pluton on the surface of the earth depends on the thickness, dip angle, and width of the pluton. The pluton dimension normal to the dip direction will be determined by the width, but the dimension of interest is the length of the pluton in the dip direction. This dimension is determined by the thickness of the pluton and the dip of the pluton relative to the erosional surface. The plutons in Augusta have a length, in the dip direction, of about 20 km. Models with a 5° dip that are 2 km thick have a dimension comparable with that observed in Augusta. Models that dip at 12° were tested with a thickness of 2 km as well as 4 km. For a 2 km thick pluton that dips at 12°, the intersection of the pluton and the erosional surface produces a surface exposure for the pluton that is less than what is observed in Augusta, but with a thickness of 4 km, the surface exposure is comparable.

Models were run for a period of time that varied from 140 kyr to 1400 kyr. Some information is known about the amount of time a pluton remains active. Assuming dike emplacement, one way of estimating the time scale for emplacement is to look at the minimum speed at which melt can move through a dike (Gerbi et al., 2004). With this constraint, it would be difficult for a small pluton, such as is found in Augusta, to remain active for much longer than 5 kyr. Other methods of estimating emplacement times result in comparable amounts of time. (Johnson et al., manuscript in preparation, White et al., 2006). Thus the timescale for which these models were run is long. However, this timescale allows for the possibility that the pluton was emplaced at the tectonic rate at which space dilatationally becomes available in the lithosphere; a life of one million years is appropriate for a small pluton emplaced at a strain rate of $10^{-14}s^{-1}$. Regardless of the length of time the pluton was active, running a model for a long period of time means that the full extent of the conductive heating is visible. The time step for each model was determined based on the thermal properties and the grid spacing. The time steps used for these models ranged from $4.287 \cdot 10^9$ to $1.299 \cdot 10^{11}$s. Based on the time step, I ran models for 328 to 1000 steps, such that the time elapsed during a run would be constant for each group of models.

3.2. Model Results

References to a model producing sillimanite metamorphism, for example, are shorthand for the model having reached the temperature of sillimanite stability. Likewise, references to the sillimanite isograd, within the context of modeling, refer to the temperature at which sillimanite becomes stable.

3.2.1. Horizontal Pluton Geometries

Figure 3.3 shows temperature-time plots at the position of each isograd for different models. These plots are compared with the petrologically calculated temperature at each isograd to see how closely each model matches the field data.

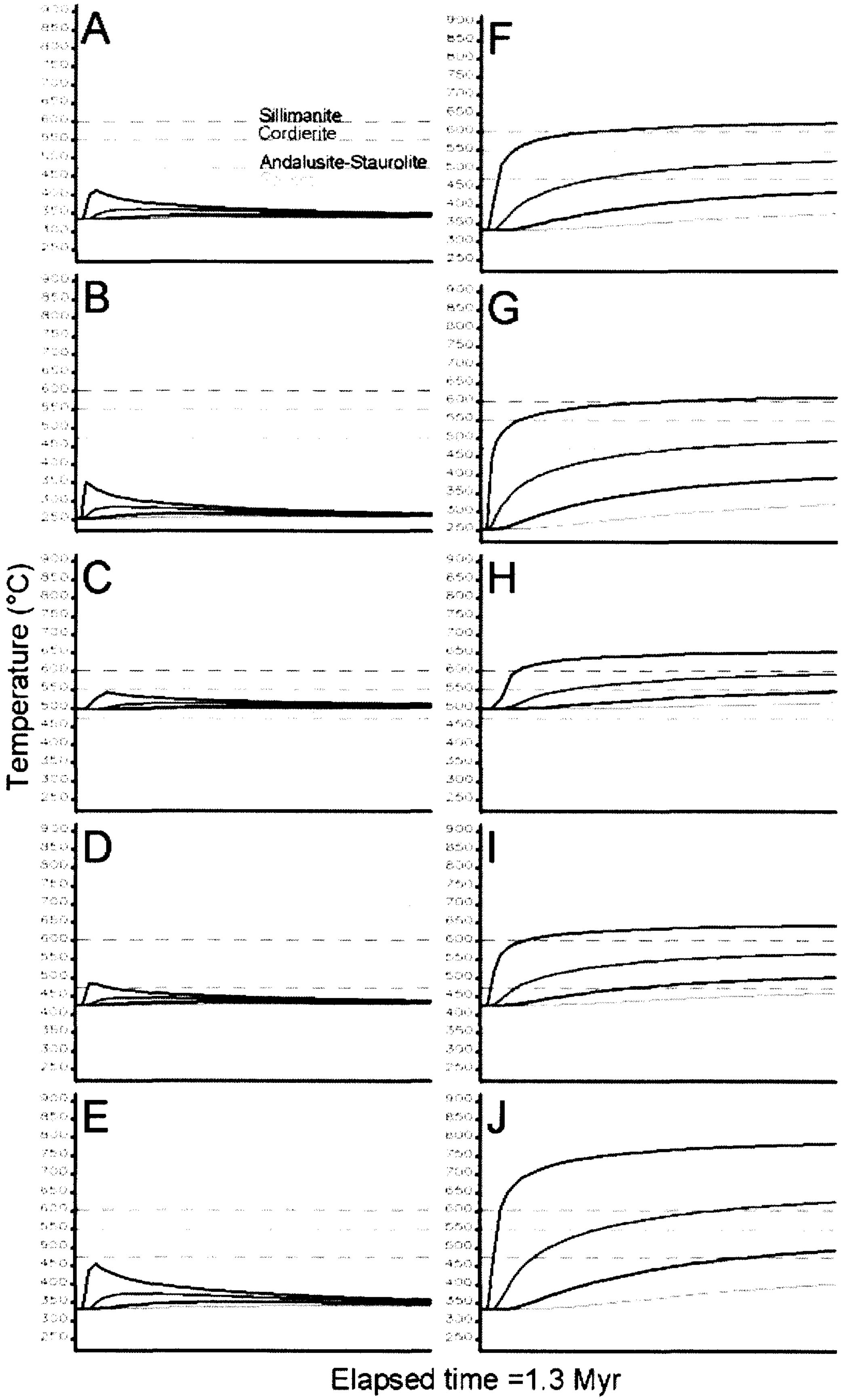
A
B
C
D
E
F
G
H
I
J
Sillimanite
Cordierite
Andalusite-Staurolite
Temperature (°C)
900
850
800
750
700
650
600
550
500
450
400
350
300
250
Elapsed time =1.3 Myr

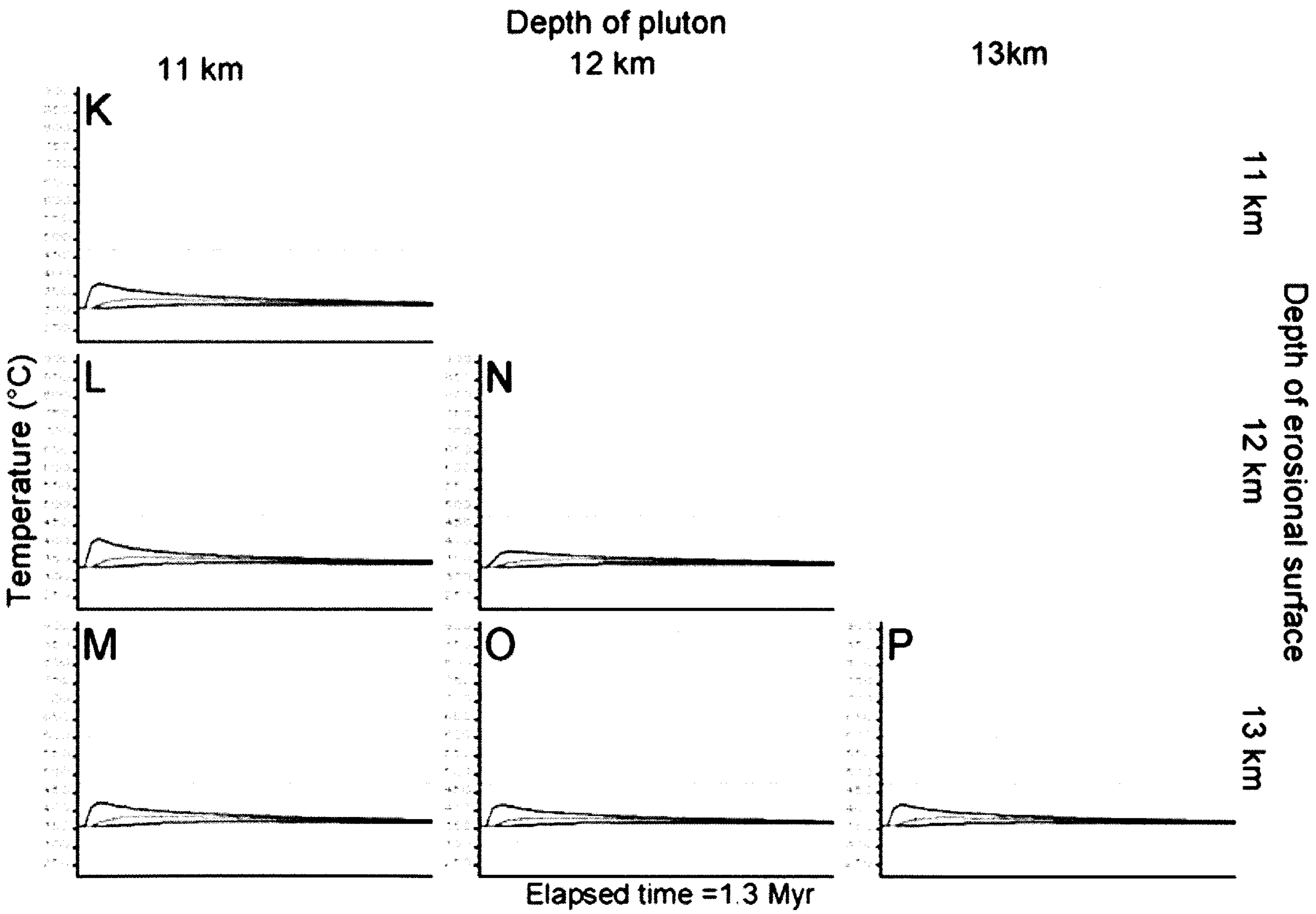

Figure 3.3 Continued.

3.2.1.1. Pluton temperature allowed to decay: models A-E and K-P. With one exception, the temperatures required for metamorphism were not reached in any model where the pluton was horizontal and had a temperature that was allowed to decay. The one exception was the model with low conductivity (C). In this model the temperatures were high enough to produce garnet and staurolite. However, the thermal perturbation caused by the pluton was similar to that of other models, and the reason metamorphism could take place was that the background temperature was elevated to an extent that garnet and staurolite were produced regionally. This means that the pluton was not the cause of these isograds, and because these minerals are not found regionally, this model is unrealistic.

Despite the lack of metamorphism, several instructive observations can be made from these models. Unsurprisingly, the largest effect caused by changing the conductivity was that the geothermal gradient changed. The change in temperature caused by the pluton was comparable in models with similar background temperatures regardless of the conductivity. Since the background geotherm is most easily controlled with the basal temperature, the conductivity is kept at 2.9 J $m^{-1}°C^{-1}s^{-1}$ for all subsequent models.

The distribution of isograds was fairly insensitive to small variations in the depth of the pluton or the present day erosional surface (models K-P). Changing the current erosional depth affects two things: the background temperature and the position of the erosional surface relative to the pluton. The latter of these two factors affects whether heating from the pluton is being caused predominantly by vertical or lateral heat flow. The results suggest that most of the change in these models came from changing the background temperature with depth rather than changing the direction of heat flow.

For these geometries, it appears that there are only small thermal perturbations caused by the pluton. For this reason a necessary factor for metamorphism is a background temperature that is close to the temperature necessary for metamorphism. Because of the wide range of metamorphic temperatures near Augusta, it is not possible to meet this condition for all of the isograds.

3.2.1.2. Pluton temperature is constant: models F-J. Several models reached the temperatures needed to produce metamorphism, but there were also reasons that these models are unlikely to be a realistic representation of the situation that produced the metamorphism in Augusta. The model that required the shortest amount of time to reach sillimanite grade metamorphism, model J, had an elevated pluton temperature of 900° C. This model required 30-60 kyr to produce sillimanite metamorphism. This is a long time for a small pluton to be active, and this model required an even longer amount of time to produce lower grades of metamorphism. (Section 3.1.2 provides constraints on the amount of time that a small pluton is likely to remain active). Many of the models required significantly more than 60 kyr to produce any metamorphism. Based on the timescale of plutonic activity required to cause metamorphism, none of the thermal models explored here could produce a temperature distribution that can match all of the isograds found in Augusta.

Additionally, for some models, in the time required to reach low-grade metamorphism 10 km from the pluton, sillimanite forms in locations where there should only be cordierite-grade metamorphism. This consideration places a time limit on some of the models; the pluton cannot be active so long that it causes overheating that results in metamorphism higher than that which is observed. Given that these models represent a wide range of realistic physical conditions, it is unlikely the thermal structure recorded by the isograds in Augusta was caused by plutons with a geometry similar to the one used in these models.

3.2.2. Dipping pluton geometries

3.2.2.1. Constant Pluton Temperatures and Decaying Pluton Temperatures.

The results for shallowly dipping plutons are shown in Figure 3.4. In model A, the pluton has a 12° dip and the temperature is allowed to decay. The peak temperature at each model isograd is not high enough to produce metamorphism. Varying the angle of the erosional surface and the dip of the pluton (models B and C) produced similar results. Subsequent models also look at variation in dip angle but under different thermal conditions.

In models D-F, the pluton temperature was increased. With the increase in temperature, two of the models were within error of the appropriate metamorphic temperature at the sillimanite, cordierite, and staurolite isograds.

When the pluton temperature was held constant (models G-I), all of the models reached the temperatures needed for sillimanite, cordierite, and staurolite metamorphism, but the amount of time required to produce this metamorphism varied considerably between models. Model I produced metamorphism in the least amount of time. In this model, it took 2-5 kyr to produce sillimanite, 5-7 kyr to produce cordierite, 6-9 kyr to produce staurolite, and 17-20 kyr to produce garnet. However, overheating in which sillimanite would be produced at the cordierite isograd begins to take place at 17-20 kyr.

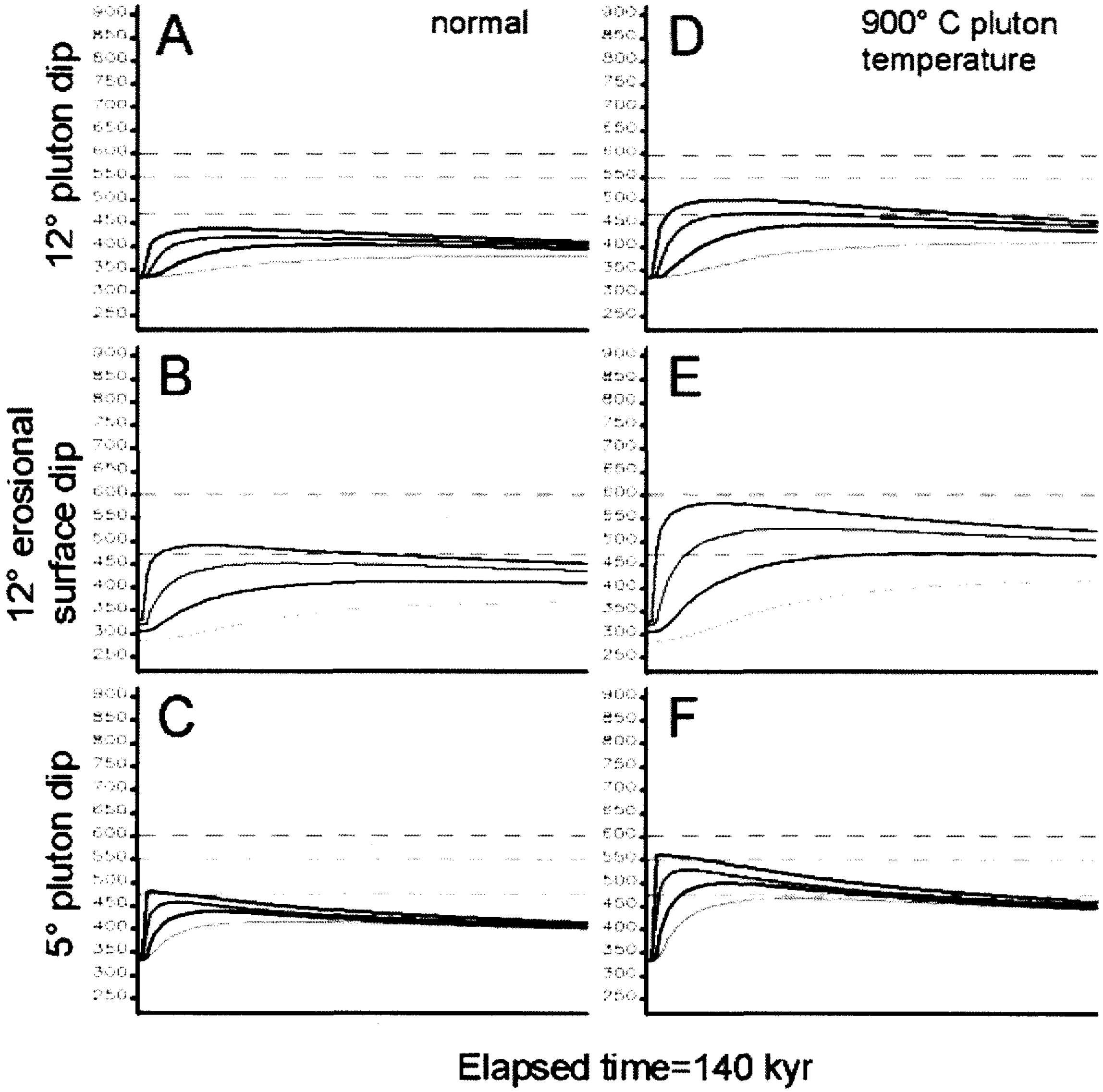
A
normal
D
900° C pluton temperature
B
E
C
F
12° pluton dip
12° erosional surface dip
5° pluton dip
900
850
800
750
700
650
600
550
500
450
400
350
300
250
Elapsed time=140 kyr

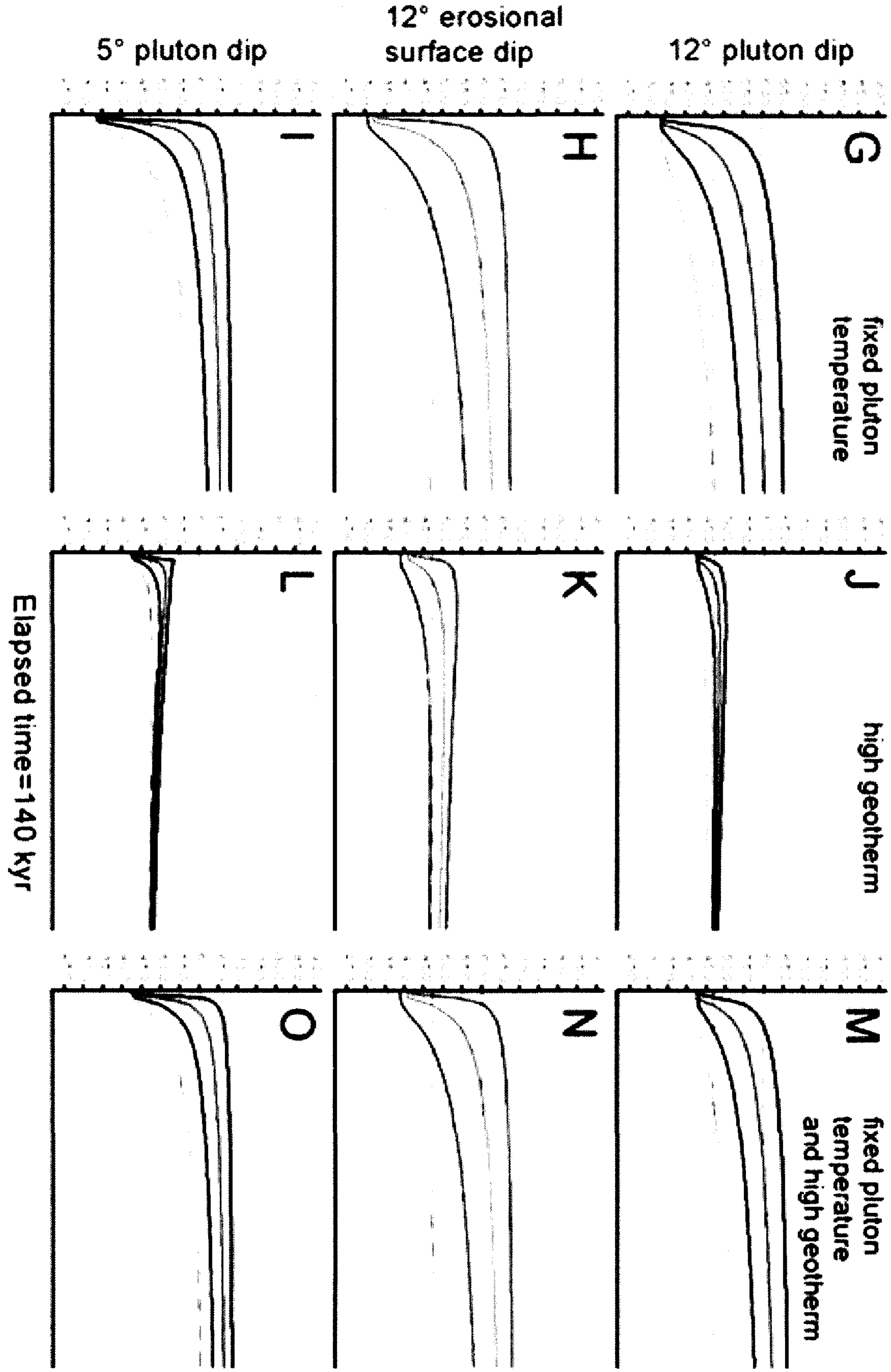

5° pluton dip
12° erosional surface dip
12° pluton dip
G
H
I
J
K
L
M
N
O
fixed pluton temperature
high geotherm
fixed pluton temperature and high geotherm
Elapsed time=140 kyr

For this reason, it is unlikely that model I could produce garnet metamorphism, even if the pluton were active for a long time. Other models produced sillimanite in a reasonable amount of time but require at least 23 kyr to produce cordierite. However, as is shown below, the length of plutonic activity that appears to be needed to reach the metamorphic temperature at each isograd may be an overestimate. The reason for this overestimate is that it takes a significant amount of time for heat to flow, for example, the 10 km from the pluton to the garnet isograd. This idea is explored further below.

All the models with a high geothermal gradient (J-L), within petrological error, produce staurolite metamorphism. Additionally, the plutons with a 12° (J) and 5° (L) dip produce garnet metamorphism. When considering these results it is significant that the plutons in these two models were free to thermally decay; if either of these models, when run with a fixed pluton temperature, could produce sillimanite and cordierite metamorphism in a reasonable amount of time, this model could account for all of the observed metamorphism. The models with a fixed pluton temperature and a high geothermal gradient (M-O) explore this possibility.

For the pluton with a 12° dip (M), sillimanite and cordierite metamorphism are produced in less than 14 kyr when the pluton temperature is fixed and the background temperature is high. Similarly, for a horizontal pluton with a dipping erosional surface (N), sillimanite and cordierite metamorphism are produced in less than 14 kyr. For a pluton with a 5° dip (O), sillimanite and cordierite are reached in less than 5 kyr. This means that a pluton dipping at 5° can account for all of the isograds observed in Augusta in a time period of less than 5 kyr. Even though staurolite and garnet do not appear to be produced quickly in this model, model L showed that these minerals will eventually form as the thermal pulse travels away from the pluton with no additional heat.

3.2.2.2. Plutons with a set period of plutonic activity. The idea that all the observed isograds could be produced from a single pluton was suggested by models L and O and is refined in the models shown in Figure 3.5. The following models allow the pluton to remain active with a constant temperature for a set period of time. At the end of this time, the temperature is allowed to decay. Model A shows results for a pluton that has a 5° dip, is active for 1 kyr, and is emplaced into an region with an elevated geotherm. Model B has the same conditions as model A, but extends the life of the pluton to 3 kyr. Both models produce results that are within error of the metamorphism observed in Augusta. However, model B is slightly more likely because it places the temperature at each isograd well into the range that produces metamorphism. This is important because there are several factors that could contribute to the peak isogradic temperatures being higher than estimated or higher than recorded. In each of these models, the temperature at the staurolite isograd is slightly over 50° C above the minimum temperature needed to produce staurolite. Despite the fact that staurolite is the most uncertain of the isograds, this result raises some doubt as to whether this isograd could be produced by this geometry. Similarly, the temperature at the garnet isograd is high enough that the petrology indicates that staurolite should be produced. However, because of the close temperature spacing estimated between the garnet and staurolite isograds, there is a necessary overlap in the temperature range of these two minerals. Although the model temperature at the garnet isograd is high in both models A and B, this result highlights

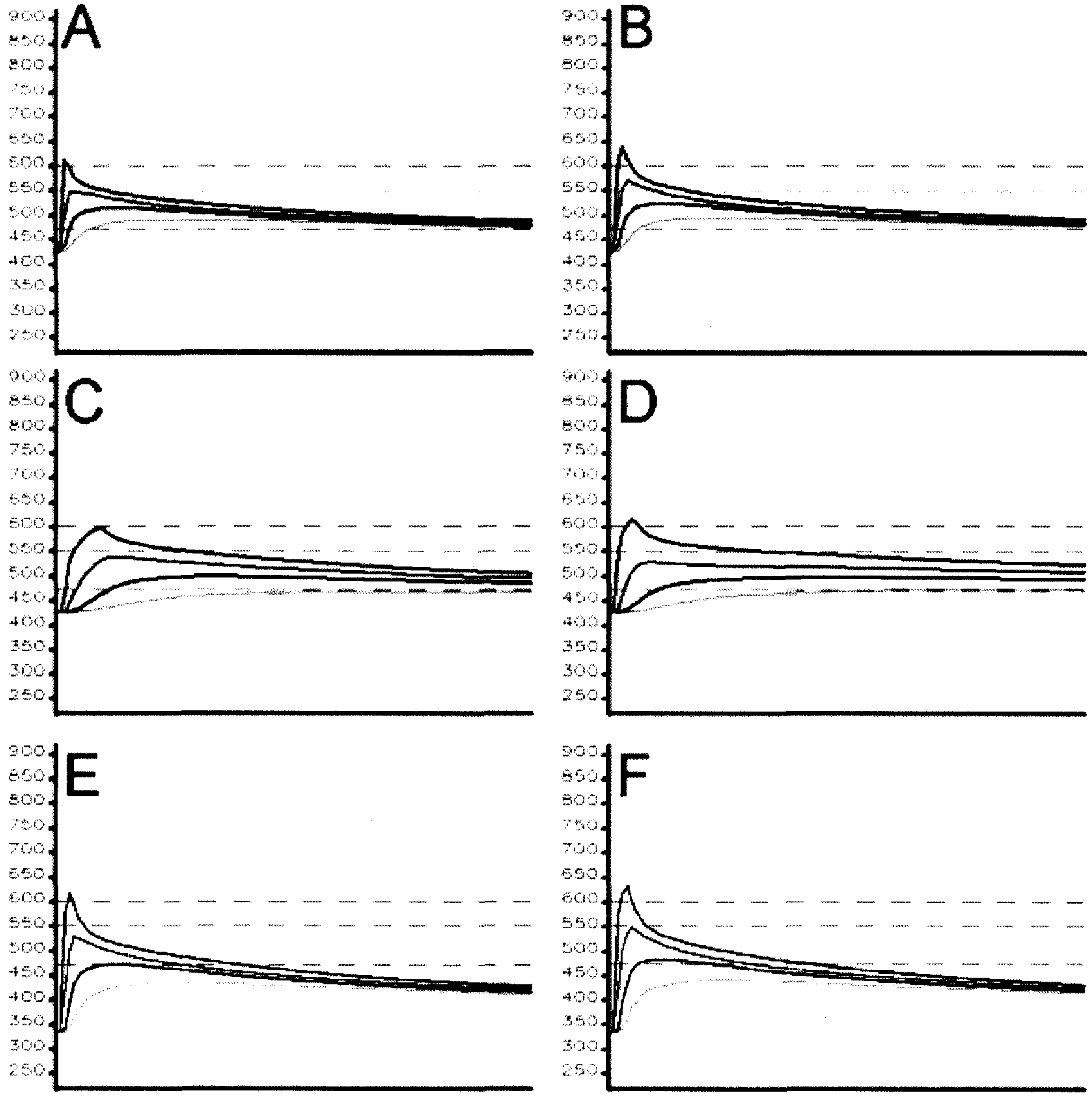

Elapsed time=140 kyr

the uncertainty in the petrological data rather than the impossibility of producing garnet from this model.

Model C has a pluton that is 2 km thick and dips at 12°. The thickness of the pluton in model C is the same as in models A and B, but because the dip is greater, the area of the pluton exposed at the earth's surface was smaller than it would be in models A and B or than what is observed in Augusta. In model D, the conditions are the same as model C, but the pluton thickness was increased to 4 km. Thus the surface area was similar to what it had been in previous models. For model C, to produce metamorphism comparable to that observed in Augusta, the pluton needed to be active for over 11 kyr, but model D it took only 6 kyr to produce comparable metamorphism. Models C and D show that when the pluton temperature is allowed to decay, the thickness of the pluton can substantially change the peak temperature at any given isograd. This is because the amount of total heat available to the system changes. The models with a 5° dip and model D shows that there is a balance between the size and angle of the pluton. The steeper the angle, the larger the pluton can be without changing the surface exposure, but as the total available heat increases with size, the distance between the pluton and the observed locations of the isograds increases.

Models E and F have plutons that dip at 5° in a normal geothermal environment. The plutons in these 2 models are active for 3 and 4 kyr, respectively. As with the previous models, the results are a reasonable fit to the metamorphism observed in Augusta. With the given level of petrological uncertainty, it is not possible to determine whether these results are more or less likely to account for the observed metamorphism than models A and B. By varying the geothermal gradient, the time scale of plutonic activity, and the angle of the pluton, it may be possible to build models that more closely match the observed metamorphism for the region. However, given the high uncertainty in the petrological data, this does not seem to be a worthwhile goal. The importance of models E and F is that they demonstrate that an elevated geotherm is not necessary to produce the observed metamorphism.

3.2.3. Summary of Results

There are a number of models with dipping plutons or dipping erosional surfaces that can account for some of the isograds observed near Augusta, and some models can produce all of the isograds. The simplest method of producing the isograds around Augusta is with a short-lived shallowly dipping pluton. Although this model does not perfectly fit the petrological data, it is likely that this geometry could account for all of the observed isograds. The angle, thickness, and geothermal gradient cannot be uniquely determined from these models. The alternative to this model is that the pluton had a geometry such that it was able to produce only some of the isograds, and the remainder of isograds were produced by another heat source. This type of solution may allow for more flexibility in the thermal distribution, and this flexibility may allow for solutions that more closely approximate the petrogenetic data. However, given the degree of uncertainty in the petrology, there is no reason to think that this trade of simplicity for accuracy is necessary.

Chapter 4

OROGEN-SCALE THERMAL MODELS

4.1. Model Setup

This group of models is designed to evaluate crustal thinning and asthenospheric upwelling as a source of heat for widespread regional metamorphism.

This model is a rectangular volume for which x=320 km, y=500 km, z=50 km (Figure 4.1). The grid spacing in this volume was 10 km in the x-direction, 12.5 km in the y-direction, and 2.5 km in the z-direction. This spacing is large relative to the isograd spacing, and if it were found that this heat source was a possible cause of those isograds, a finer grid would have been necessary to further evaluate that possibility. Like the small-scale models, the system initially has a steady-state vertical geothermal gradient. On one edge of the model, extending along the entire length in the x-direction is an area of elevated temperature, representing a mantle heat source.

The top surface of the model was fixed at 20° C. The bottom surface had a constant heat flux of 0.04 Wm^{-2}, which simulated the mantle contribution to the geotherm. Because the model was 50 km thick, giving the model crustal levels of radioactivity throughout the model yields a gradient that is inappropriately high except for areas with a long history of crustal overthickening. For this reason, models were tested with a radioactive input in only the top 30 km of the model. Other models were tested with crustal levels of radioactivity throughout the model. The value given for radioactive heat production in the upper 30 km was $1.5 \cdot 10^{-6}$ Wm^{-3}. Clearly, the amount of radioactive heat produced in the mantle lithosphere is greater than zero, but these two

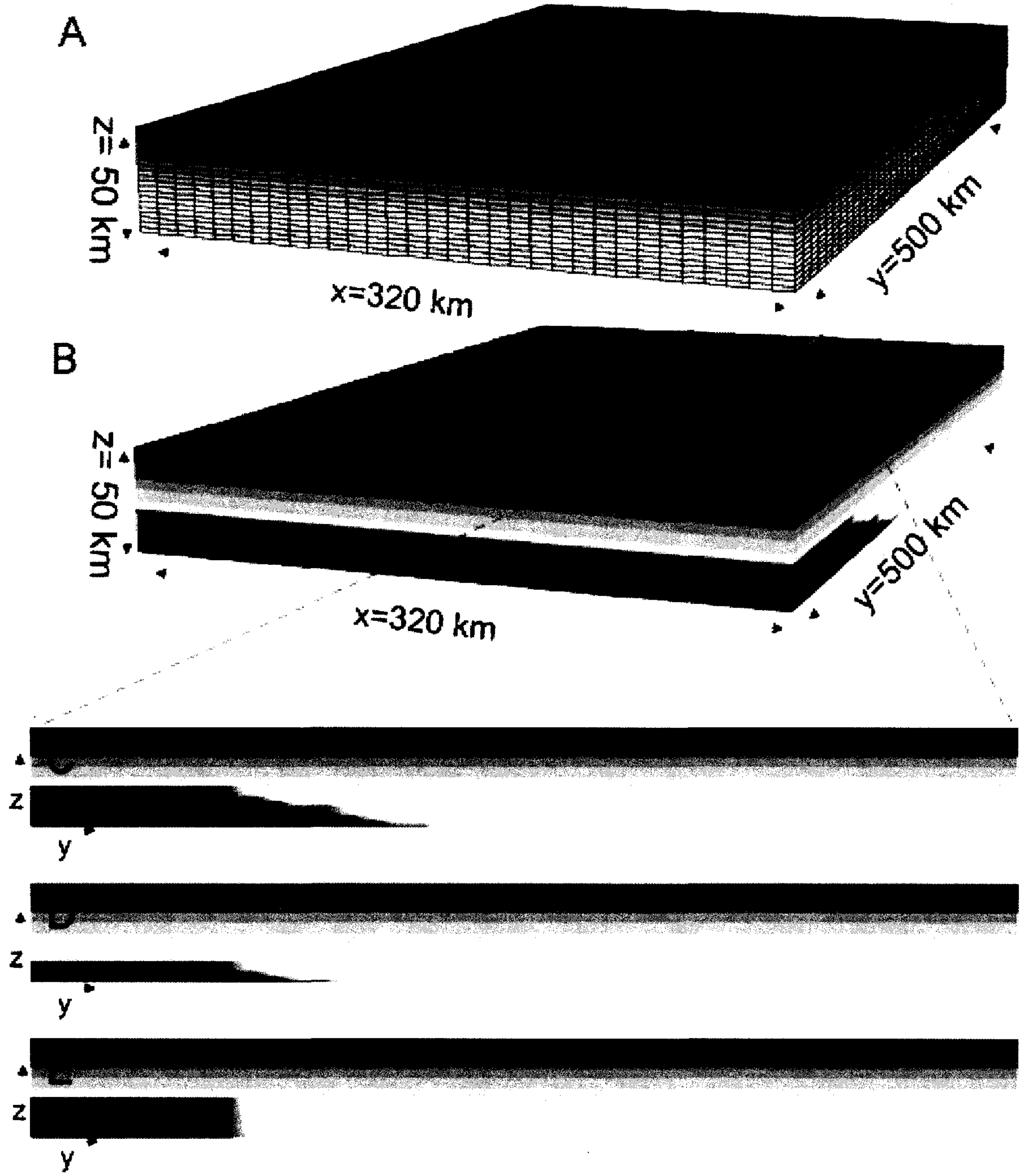

Figure 4.1. Orogen-scale thermal model setup. Image A shows the model dimensions, the background geotherm, and the grid spacing. B shows a 3-dimensional view of the location and geometry of the mantle source. C shows the same setup as B but in a cross-sectional view. Like C, image D shows a cross-sectional view of the model, but the top of the mantle source has been lowered from a depth of 30 to 40 km below the surface. Several other depths were tested as well. Image E is similar to C, but the dip angle of the source has been increased from 12° to vertical.

models of radioactive production provide end members of likely levels of heat production. With these boundary conditions, the model was run until it reached a steady state.

The standard model used a temperature of 1400° C for the mantle heat source. This was changed to 1100° C in some models. This variation allows for the possibility that the transition to the asthenosphere takes place at less than 1400° C or that a process such as adiabatic cooling is significant.

The standard model had the asthenospheric source extend horizontally in the y-direction for 100 km. At this location the source dipped at an angle of 12°. This geometry was compared to one with a dip angle of 90°. In addition, the standard model had the asthenosphere extend upward to a depth of 30 km below the surface. The depth of the source was varied to 25, 35, and 40 km below the surface.

Two models looked at the effect of radioactive heat production in the lithosphere. One of these models established a steady-state geotherm with a constant radioactive heat source throughout the entire model. This simulates a situation where the crust has long been overthickened before the emplacement of the asthenospheric heat source. The other model started with the standard steady-state geotherm with radioactive heat production in only the upper 30 km. At the time the asthenospheric heat source was added, the volume of the model that included radioactive heat production was expanded to include the entire model. This model looked at the case where crustal thickening in one part of the model occurs simultaneously with crustal thinning in another part of the model. In addition to looking at the effect of crustal thickening, these models look at the variation that might be expected in radioactive heat production in the upper mantle. It can be expected that the mantle contribution to radioactive heat will be less than the contribution in the first model. This gives some limit to the possible background temperature.

Each model was run for 500 steps with a time step of $12 \cdot 10^{11}$s. This means that each model run covers a time period of approximately 20 Myr. This is a reasonable amount of time for a mantle source to be active. This time span was varied to 10 Myr

4.2. Results

Figures 4.2 and 4.3 show the thermal profiles that result after running each regional scale model for 20 Myr. Also shown are the locations where the petrologically-determined temperature of each isograd is found and the present day erosional surface, a depth of 12 km. Future references to the sillimanite isograd, for example, refer to the petrologically determined temperature at which sillimanite becomes stable.

Geometrically, there are two distinct geothermal regions. One is the normal background geothermal gradient, and the other is an elevated geothermal region above the mantle heat source. The isograd spacing is determined by the thermal contrast between these two distinct regions as well as the steepness of the transition between these two areas.

An increase in the depth of the mantle source caused all of the isograds to translate, horizontally along the 12 km erosional surface, closer to the edge of the source. Increasing the depth of the source also caused an increase in the spacing of the isograds, but this effect was minor compared to the horizontal movement of all of the isograds. The change in spacing was most noticeable in the isograds closest to the source. For all the depths tested, the spacing between each pair of isograds was too large, except for the

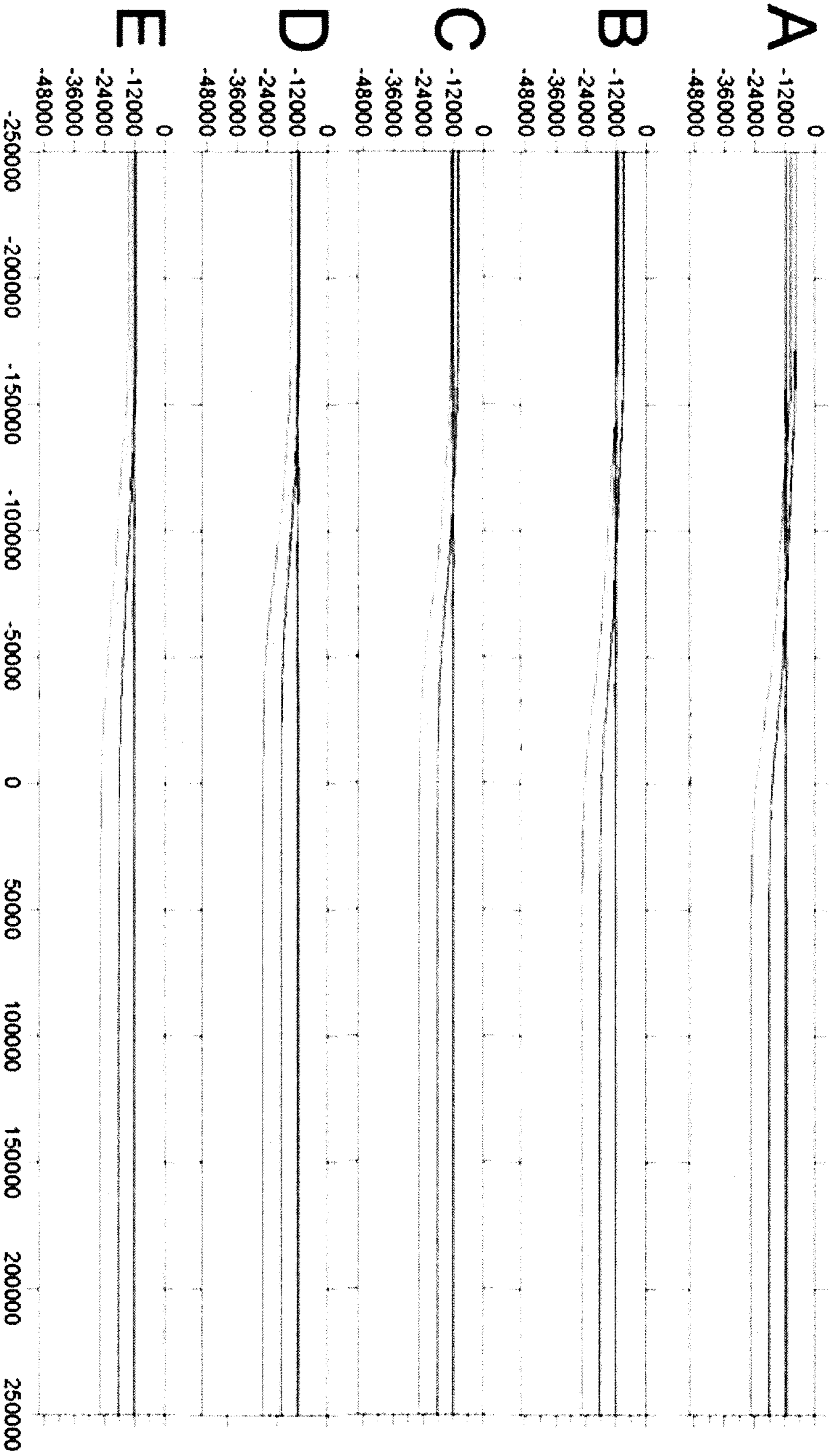
A
B
C
D
E
0
-12000
-24000
-36000
-48000
-250000
-200000
-150000
-100000
-50000
0
50000
100000
150000
200000
250000

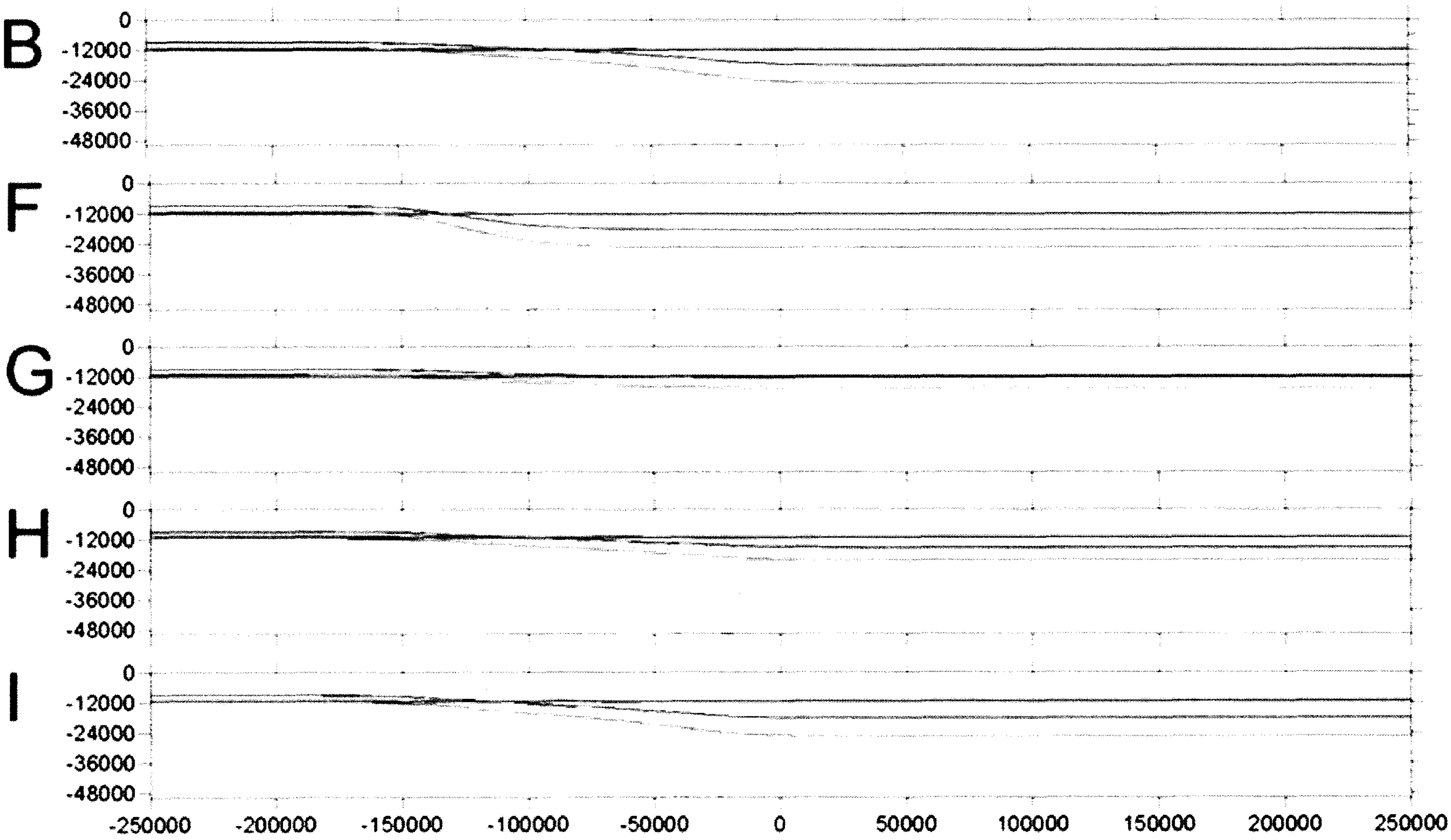

Figure 4.2 Continued. Image B is repeated for reference.

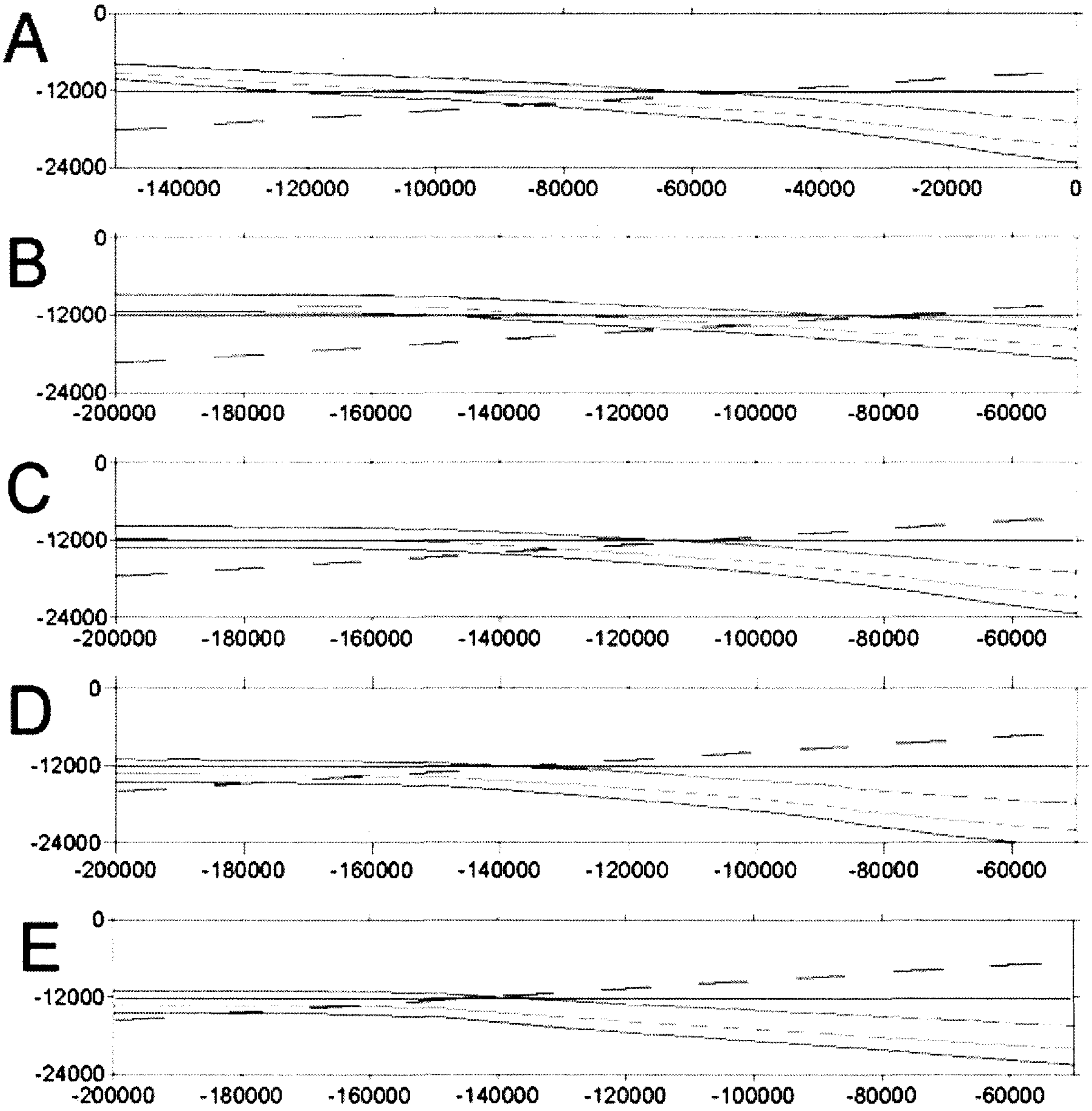

Figure 4.3. Orogen-scale thermal model results: magnified. These profiles show the same results as Figure 4.2, but these cross-sections show an enlarged view of the four isograds as they cross the 12 km erosional surface. In addition to showing the four isograds, the solid pink line marks the depth of z=12 km, and the dashed pink line shows an erosional surface that dips at 3.5°, the angle suggested by DeYoreo et al. (1989). The labeling of the images corresponds to the labeling in Figure 4.2.

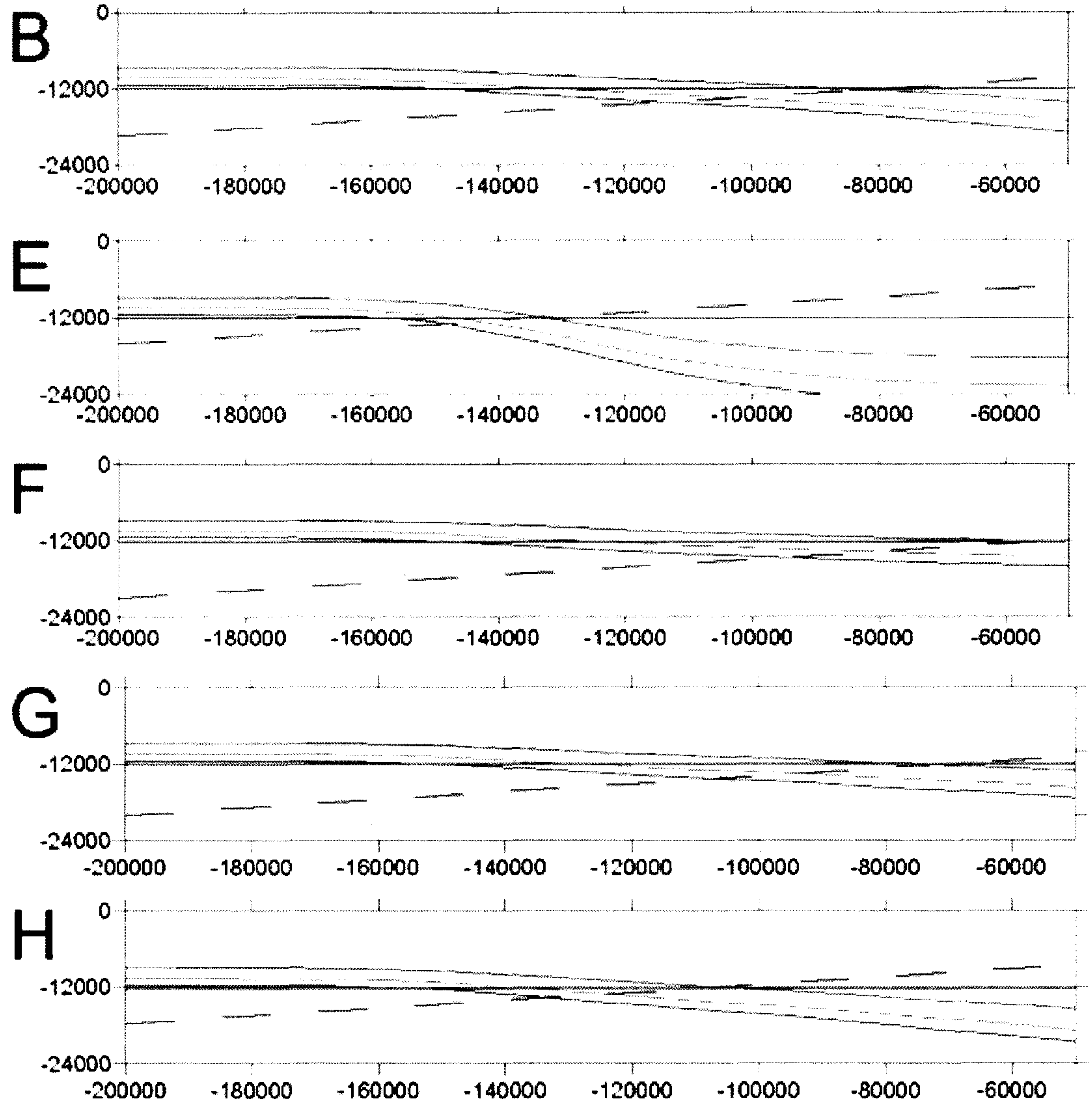

Figure 4.3 Continued.

andalusite-staurolite and garnet isograds, and the spacing between the andalusite-staurolite and garnet isograds, was quite similar for heat sources of different depths.

The effect of decreasing the source temperature was similar to the effect of increasing the depth of the source. At a depth of 12 km the isograds moved horizontally closer to the source, and the isograd spacing increased. Again, the change in the spacing between the andalusite-staurolite and garnet isograds was very small, and the isograd spacing was too large between each pair of isograds except andalusite-staurolite and garnet.

Changing the dipping contact to a vertical contact steepened the horizontal thermal gradient between the elevated and normal geothermal regions. The decrease in the spacing of the isograds was considerable, but the spacing between isograds was still too large for each isogradic pair except andalusite-staurolite and garnet.

If the background geothermal gradient is increased by thickening the crust such that the levels of radioactive heat production in the lower 20 km of the model are increased, the isograd spacing is increased. This effect is most noticeable in the isograds farthest from the source. In some cases, the background temperature was high enough that garnet, andalusite, and staurolite were produced regionally at a depth of 12 km. These results are important because they suggest that crustal thickening and the accompanying increase in radiogenic heat production are not capable of producing temperatures high enough to account for the metamorphism in Maine.

It is worth noting two potential problems with the interpretation of the large-scale modeling. The andalusite-staurolite isograd is the most difficult one to characterize petrologically. Its high dependence on bulk composition makes the assumption of constant temperature along this isograd questionable. For this reason, despite the excellent agreement between the isograd spacing of andalusite-staurolite and garnet in the model with the spacing in Augusta, the spacing should be taken as no more than a rough estimate. The second problem is that there is some waviness to lines that should be smooth. This is an artifact of the grid spacing in the model and the method of contouring. This problem seems to be most pronounced near boundaries, where the error caused by the waviness can exceed 4 km, the spacing between the andalusite-staurolite isograd and the garnet isograd. However, this problem appears to be much less significant away from boundaries. For this reason, it may not have a significant effect in the region of interest.

The large-scale profiles show isograds every 100° C. This representation of the thermal structure gives a rough idea of the uncertainty in isograd location caused by petrologic error. Clearly, even with the uncertainty in the sillimanite, cordierite, and andalusite-staurolite isograds, the spacing between each of these isograds is still much larger than the spacing between isograds in Augusta.

Modeling of a local heat source suggested that all the isograds in Augusta could have been produced from a single dipping pluton. The large-scale mantle heat source was able to produce isograds of the approximate spacing of the andalusite-staurolite and garnet isograds, but the spacing between all other isograds was too large. Unlike the local heat source, the mantle heat source could not produce the distribution of isograds by itself. Although the distribution of isograds could have resulted from an overlap of isograds produced by a local source and isograds produced by a mantle source, there is no reason to suspect that this is the case.

The regional thermal structure is well matched by the large-scale models. The large-scale heat source produces a thermal distribution in which temperatures of greater than 600° C can be maintained for hundreds of kilometers. This model can be used to explain the thermal gradient across Maine and the high-temperature rocks in central Massachusetts. However, the scale of heating that is necessary is unclear because not all metamorphism in central New England was produced at the same time (Robinson, 1998). The thermal models presented here assume an exhumation rate that was essentially constant over the small area studied in Augusta and exhumation rates that changed linearly over the regional scale. However, within these constraints, there are many models that produce a thermal distribution similar to that which is observed.

There are other possible heat sources that could produce a large high-temperature area. For example, the aureoles around many plutons could overlap to produce a large region of elevated temperature (DeYoreo et al., 1989). However, results from the pluton modeling show that a small pluton cannot produce temperatures over 600° C .3 km from the edge of the pluton after 3 ka of activity. This suggests that in order to maintain high temperatures over a large region, the plutons would need to have a very close spacing or be much larger than the plutons modeled. Additionally, there are areas of the Acadian orogeny which record high temperatures in which very few plutons are found. Another possibility is that the thermal gradient was constant over the region, and the exhumation rate was much higher in the south than in the north. This possibility is explored in Figure 4.4 where the temperature is fixed at 1100° C at 30 km depth. It is found that if, as in previous models, the gradient in exhumation is linear, then the thermal gradient is too high in northern Maine. This implies that for a constant geotherm to have caused the

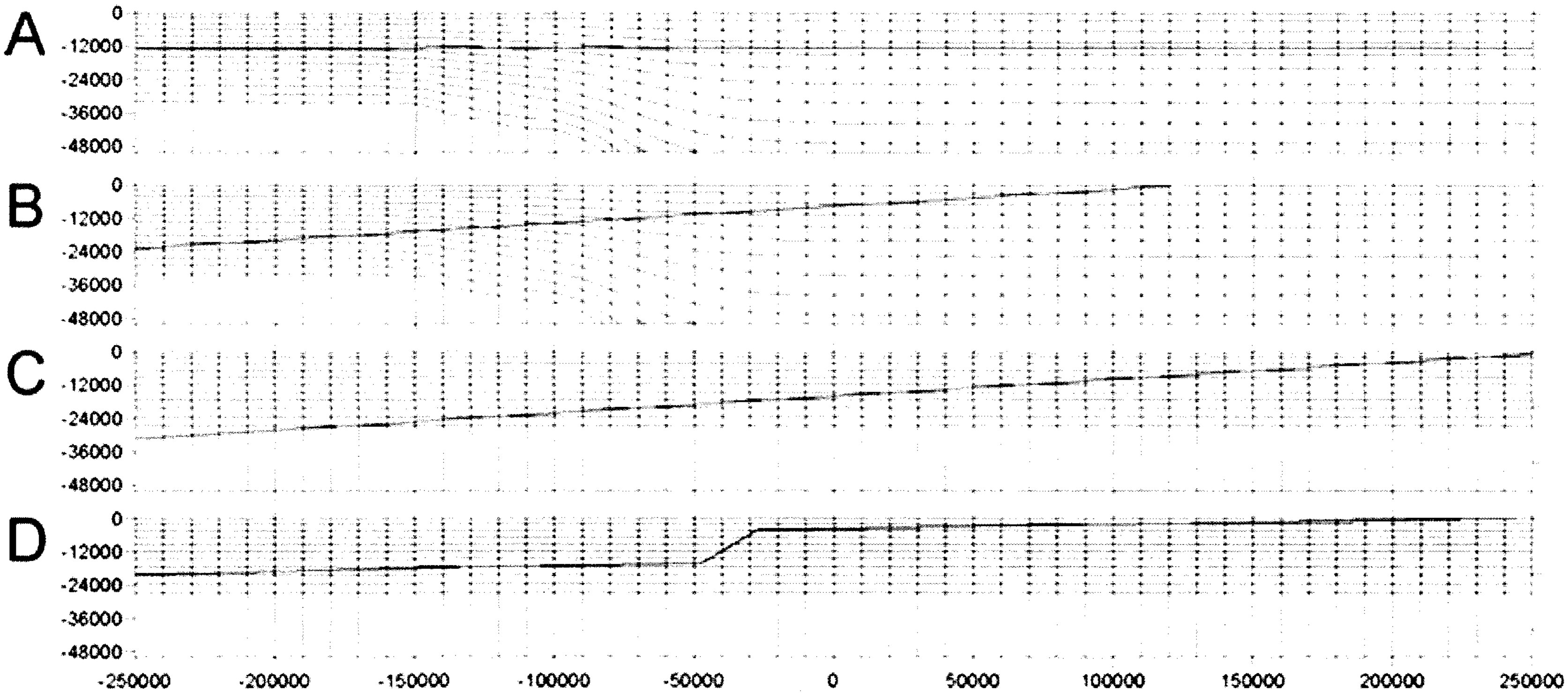

Figure 4.4. Various models of exhumation. Model A shows a situation where exhumation is constant on an orogen scale. B and C show a situation where the exhumation rate linearly increases to the south as DeYoreo et al. (1989) suggested. Figure D shows a situation where the exhumation rate increases nonlinearly in the south. Depicted on each figure is an erosional surface such that if it were the current erosional surface, the recorded thermal distribution exposed at the surface would be reasonably consistent with the regional thermal distribution. The thermal gradient could represent a transition from a high to a normal geotherm, or it could represent a uniformly high geotherm. These two possibilities imply different spatial extents for the mantle source.

high-temperature region, the exhumation rate would need to be low across northern Maine and increase rapidly in central Maine. In this scenario, the Augusta area would represent a transition between high and low exhumation rates rather than a transition between a high and a low geothermal gradient. Geobarometry has shown that the exposed crustal level increases from 2 km in northern Maine to 25 km in central Massachusetts (DeYoreo et al., 1989). It is not clear whether the crustal level increases linearly. Differential erosion remains an alternative to horizontal variation in the geotherm.

Differential erosion rates would signify a greater amount of uplift in the southern portion of Maine than in the north. If this mechanism for producing the regional thermal pattern were adopted, a mechanism to explain the high erosion rate would need to be found. Additionally, this model does not take into account the high degree of deformation that likely took place around the time of metamorphism. This deformation adds complexity to the situation, and the relationship between crustal thickening and metamorphism must be understood.

The two most likely causes for the regional thermal pattern are a high geotherm in the south and high erosion rates in the south. These two possibilities should be geologically distinguishable from one another. A shallow asthenospheric heat source in southern Maine would produce a thermally weakened rheology in an isolated portion of the orogen. Differential weakening within the orogen would localize strain, and these strain patterns would be visible in the regional geology. The alternate possibility is that the geotherm was horizontally uniform throughout the orogen but the erosion rate was high in the south. Geological support for this model would consist of using regional geobarometric data to establish the depth of the erosional surface. Additionally, with this information, it would be possible to determine the steepness of the regional geotherm, and thus determine whether the geotherm was normal or elevated at the time of metamorphism. If there were an elevated geotherm, thermal weakening could be expected to take place in this model as it did in the first model. However, despite this weakening, the rheology would be uniform throughout the model, and this would cause the strain partitioning to be minimal in comparison to the partitioning expected in the first model. Thus, this model should be distinguishable from the first model through regional strain patterns and geobarometry.

The problem of polymetamorphism and the overlap of several temporally distinct metamorphic regions is a difficult one. Even when looking at a smaller section of the high-grade rock of central New England, which is all of the same metamorphic age, it is difficult to explain such a widespread thermal anomaly without a regional source of heat. However, the presence of multiple overlapping metamorphic lobes of different ages suggests the need for this regional heat source to either shift with time or to periodically reoccur. This problem is not well addressed by this modeling.

Chapter 5

GRAVITY

Bouguer gravity data over Maine show that there is a pronounced regional low with a magnitude of -40 mgal over much of central Maine (Figure 5.1) (Stewart et al., 1991, National Image and Mapping Agency, 2001). In places this anomaly reaches values of -70 mgal. On a smaller scale, there is a steep gradient to the northwest of the study area. This gradient is an indication that the study area is on the edge of a regional low.

My gravity modeling uses the software GM-SYS (Northwest Geophysical Associates, Inc, 2004), and it looks at plutons as a possible source of the anomaly. A region of granitic material in the first 10 km of the earth's crust creates an anomaly of approximately -30 mgal (Figure 5.2). This result is the same approximate change in gravity as observed in Maine, but the modeling shows the gravitational gradient at the edge of the pluton is steep. This means that to maintain the anomaly over a large area, the granitic layer would need to be nearly continuous. Additionally, many plutons with a surface exposure are visible as small-scale gravitational anomalies within the regional low. For these reasons, it would be difficult for the regional anomaly to be caused by plutons. More likely, the anomaly is the result of thickened crust displacing mantle material. Modeling of this situation shows that a crust thickened by 2 km would cause an anomaly of -50 mgal. This anomaly is of a similar magnitude to the one observed in Maine.

Over the pluton, there appears to be a slight decrease in gravity of -2 to -6 mgal in magnitude. The small magnitude of this decrease indicates that the pluton is quite thin.

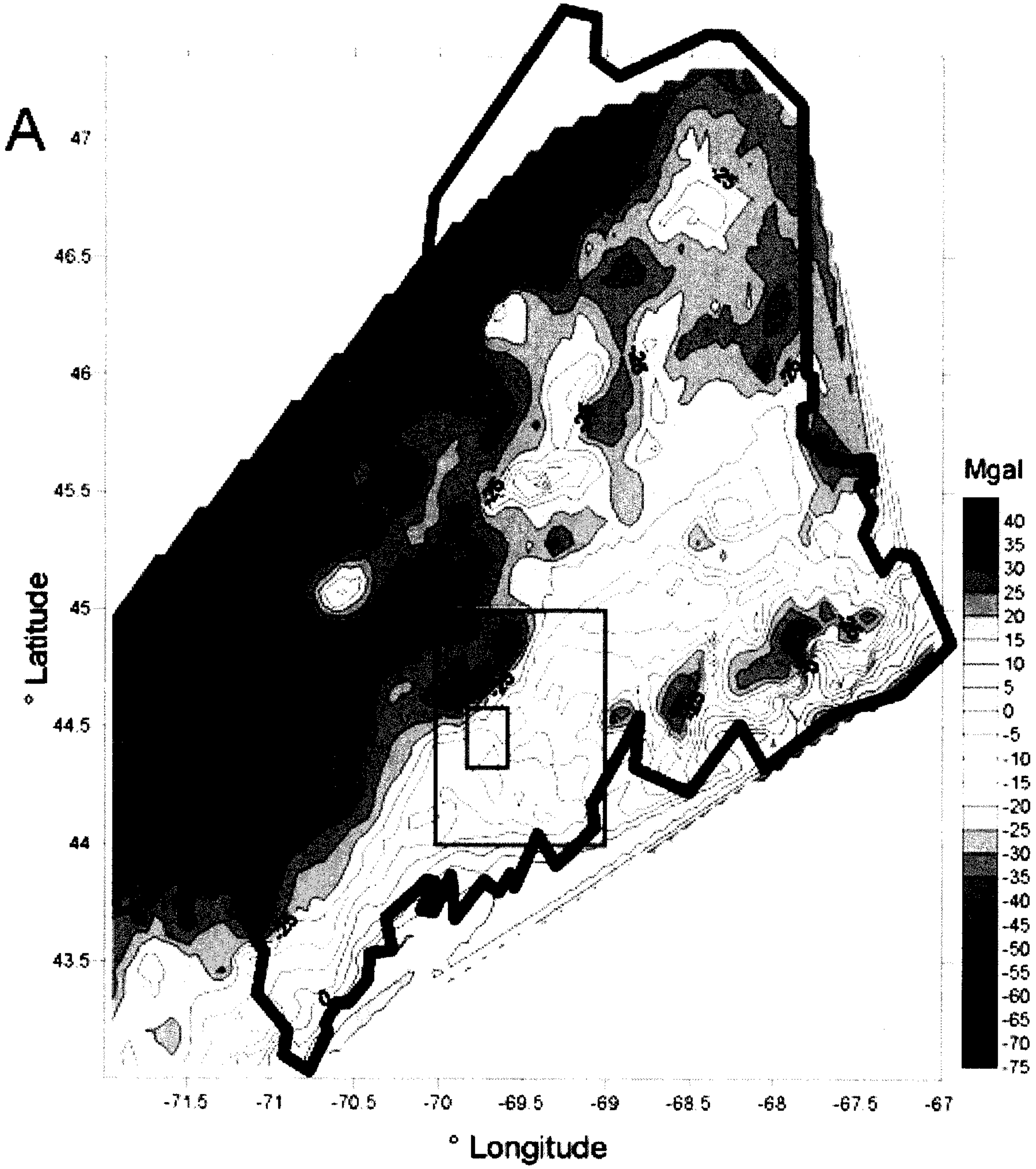
A
47
46.5
46
45.5
45
44.5
44
43.5
° Latitude
-71.5
-71
-70.5
-70
-69.5
-69
-68.5
-68
-67.5
-67
° Longitude
Mgal
40
35
30
25
20
15
10
5
0
-5
-10
-15
-20
-25
-30
-35
-40
-45
-50
-55
-60
-65
-70
-75

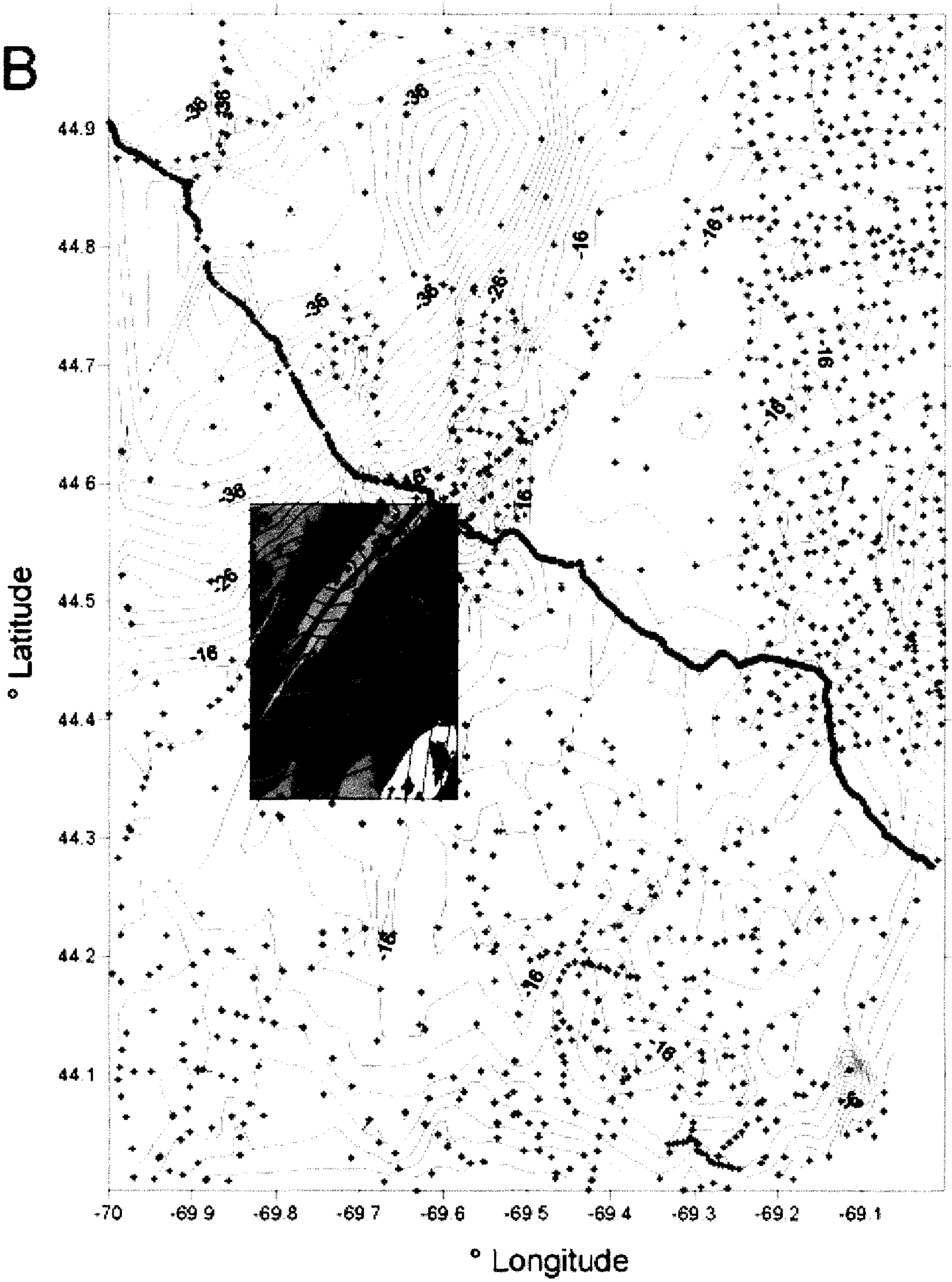

Figure 5.1 Continued.

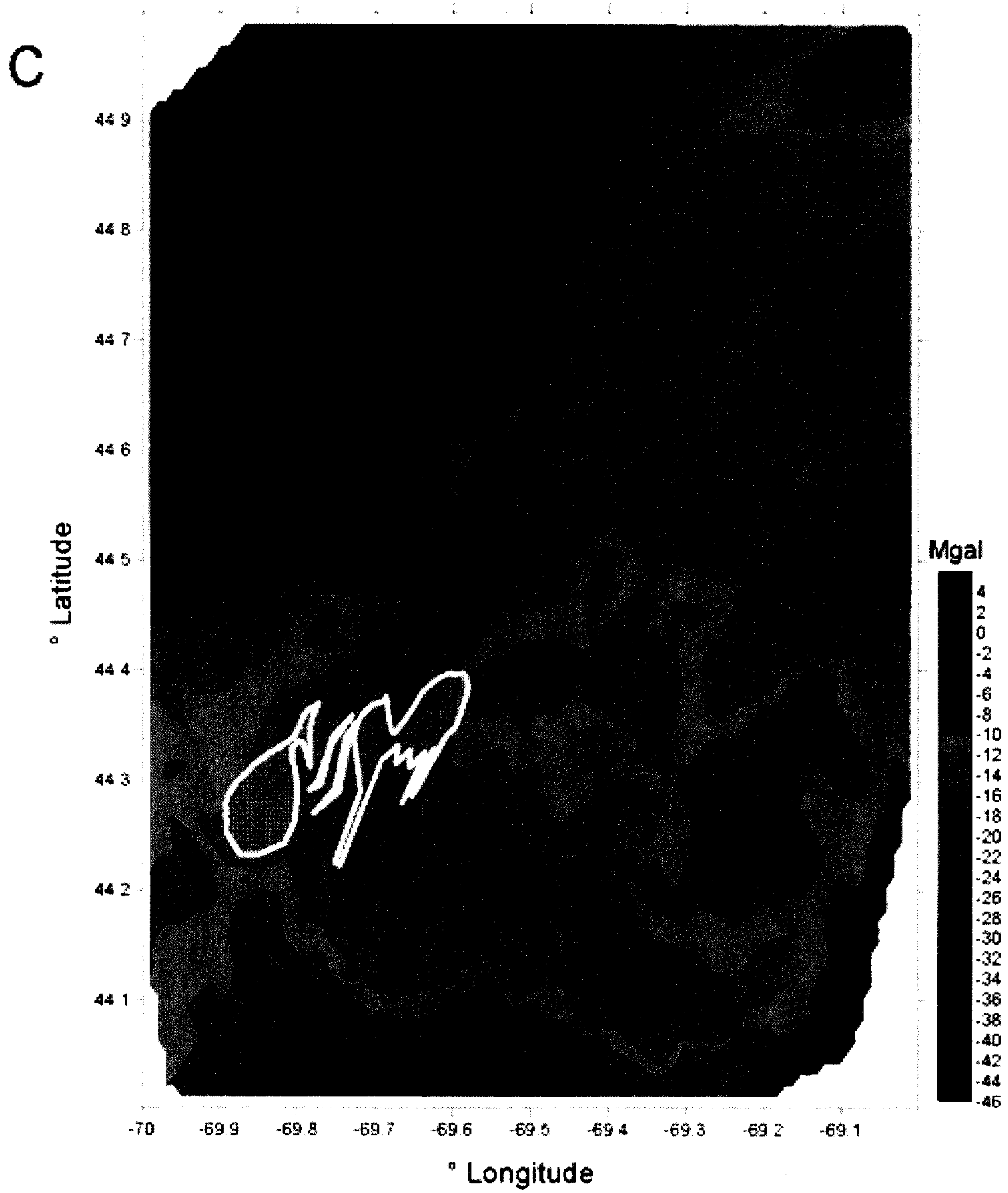

Figure 5.1 Continued.

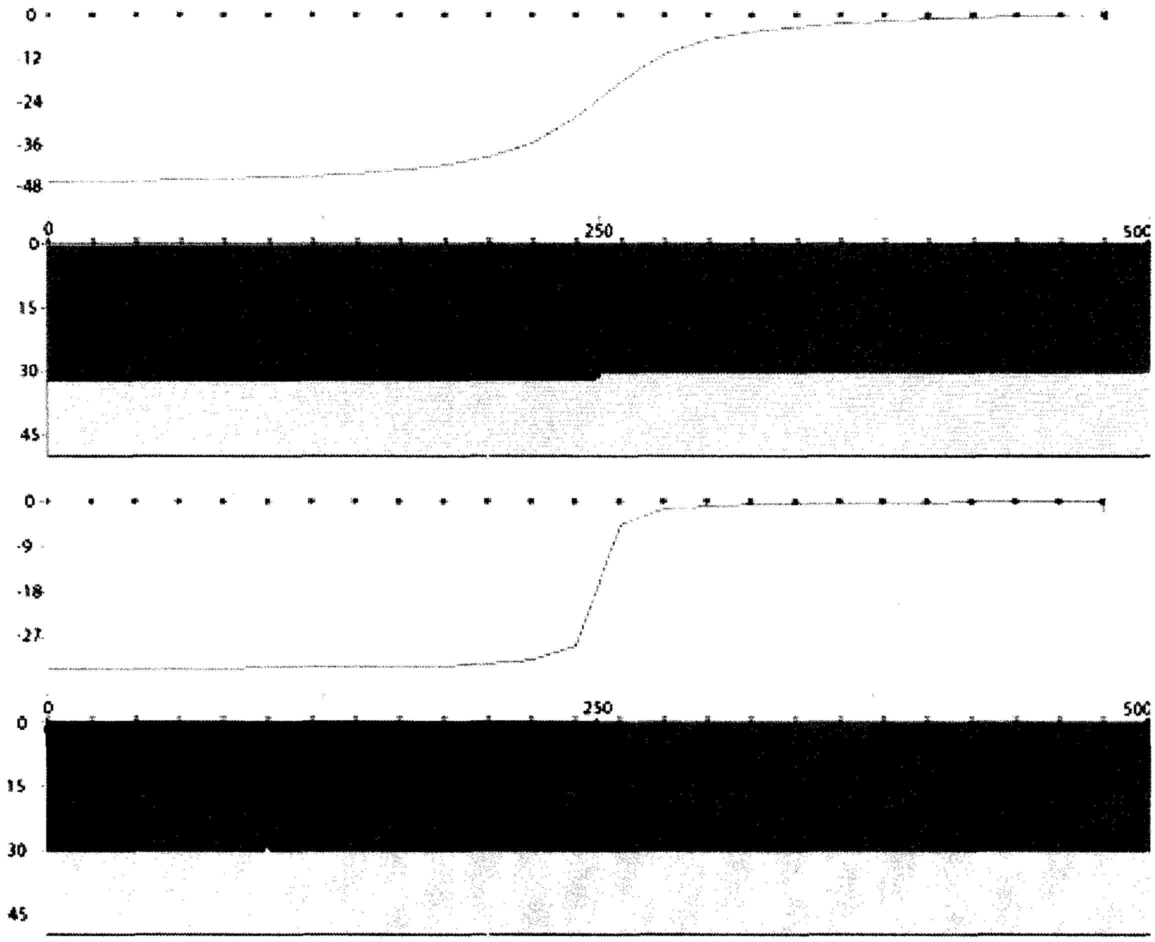

Figure 5.2. Gravity models of a regional mass deficit. Shown are two upper lithospheric cross-sections and their associated gravitational profiles. Dark blue represents low-density plutonic rocks with a density of 267 kg m^{-3}, light blue represents crustal rocks with a density of 275 kg m^{-3}, and orange represents the mantle lithosphere with a density of 335 kg m^{-3}. The upper cross-section looks at the possibility of a thickened crust to explain the gravitational deficit in southern Maine, and the lower cross-section looks at the possibility of low-density plutonic material in the upper crust to explain the same gravitational feature. In the two situations, the gradient in gravity differs.

This geometry is consistent with the sheet-like geometry of other plutons in Maine that was inferred from detailed gravity studies (Joyner, 1963, Nielson et al., 1976, Sweeney, 1976).

Gravity modeling shows that a tabular granitic pluton 2 km thick would produce an anomaly of about -6 mgal (Figure 5.3). This is consistent with what is observed in Augusta. Doubling the thickness of the pluton approximately doubles the magnitude of the anomaly. Thus, a 4 km thick pluton produces an anomaly approximately 12 mgal in magnitude. For this reason, a thin pluton geometry is preferred. If the pluton dipped beneath the surface, the shape of the gravity anomaly would be affected by the dip angle. The gravity data in Augusta is consistent with a dipping pluton because there is an increase in gravity of about 2 mgal 10 km north of the pluton. However, the data is sparse, and there are clearly three-dimensional effects in the regional gravity. These factors make it difficult to make a strong case that the low gradient in gravity is caused by a dipping pluton. Additionally, the gravity models show that 20 km from the edge of the surface exposure of a pluton, the difference between the gravity anomalies produced by plutons dipping at 5° and a 12° is approximately 1 mgal. Given the scarcity of data, it is not possible to distinguish between a dipping and a horizontal pluton let alone 2 plutons of different dip angles. However, for tabular plutons dipping at 5° and 12°, the 12° pluton would need to be thicker than the 5° pluton to produce the same area of surface exposure. Because a 12° pluton would need a thickness of about 4 km, at its maximum, it produces an anomaly of 12 mgal. Despite the quality of the gravity data, it is unlikely that such an anomaly would not be visible in Augusta. For this reason, a horizontal or very shallowly dipping thin pluton is preferred.

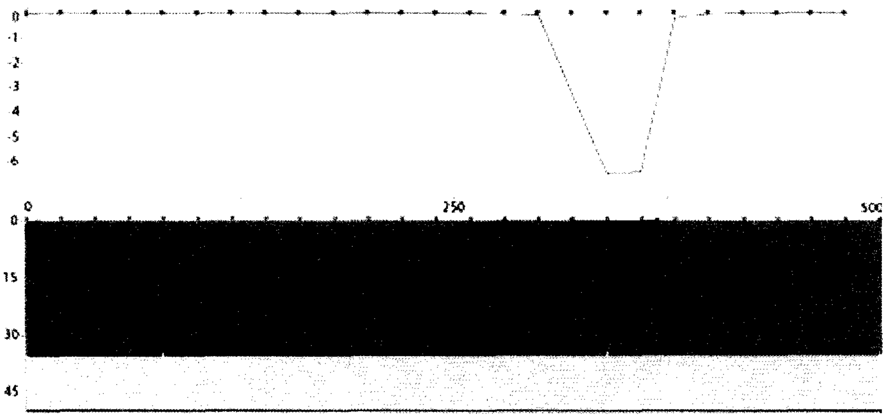
0
-1
-2
-3
-4
-5
-6
0
250
500
0
15
30
45

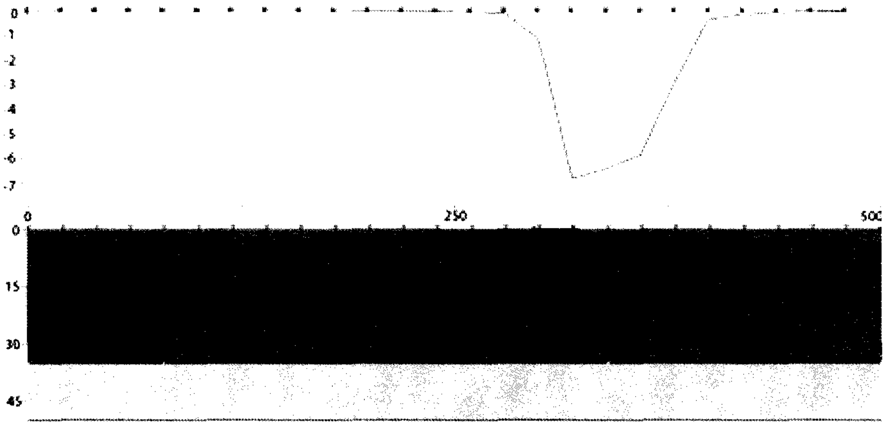
0
-1
-2
-3
-4
-5
-6
-7
0
250
500
0
15
30
45

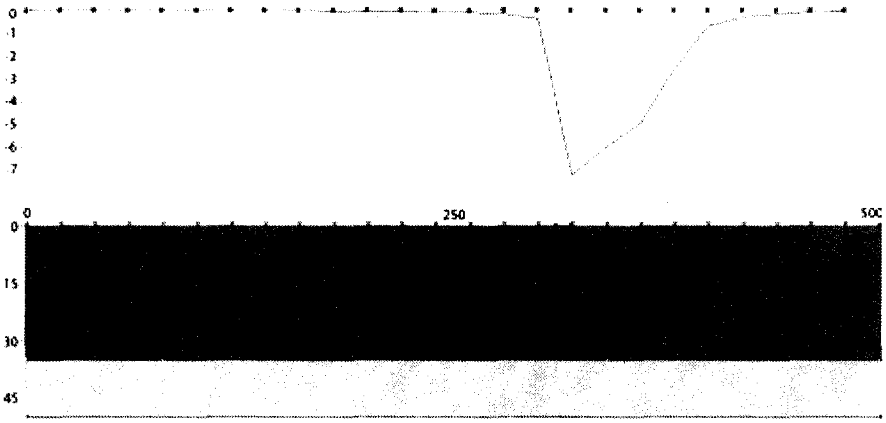
0
-1
-2
-3
-4
-5
-6
-7
0
250
500
0
15
30
45

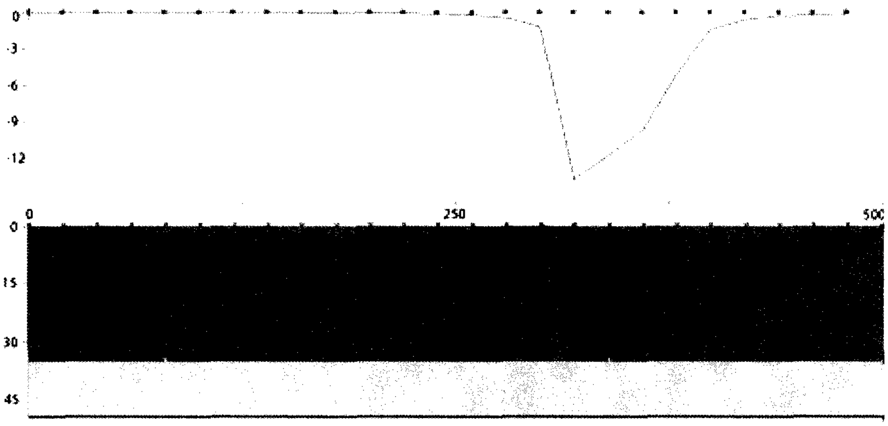
0
-3
-6
-9
-12
0
250
500
0
15
30
45

The possibility that the asthenosphere reached a shallow depth is raised in Chapter 4. The gravitational signature of an elevated asthenosphere evolves with time. If the asthenosphere intrudes into the crust, it displaces crustal material and causes a positive anomaly (Figure 5.4). However, depending on the geometry, there may be a region where the asthenosphere is displacing the more dense lithospheric mantle, and this situation could create a small region of negative gravity. Once the asthenospheric source has cooled, it increases in density. This increase in density will cause the magnitude of the positive anomaly to increase and the region of negative gravity to be incorporated into the positive anomaly. Such a gravitational feature would be difficult to mask. Even a continuous layer of 10 km thick granitic material would not mask a cooled asthenospheric source that had reached a depth of 25 km below the earth's surface. The evolution of such a region would be different if the asthenospheric source extended to, but not into, the crust. In this case, the asthenospheric source initially displaces mantle material creating a region of low gravity (Figure 5.5). When the asthenospheric source has cooled, it is the same density as the adjacent lithosphere, thus the existence of the asthenospheric source is gravitationally invisible.

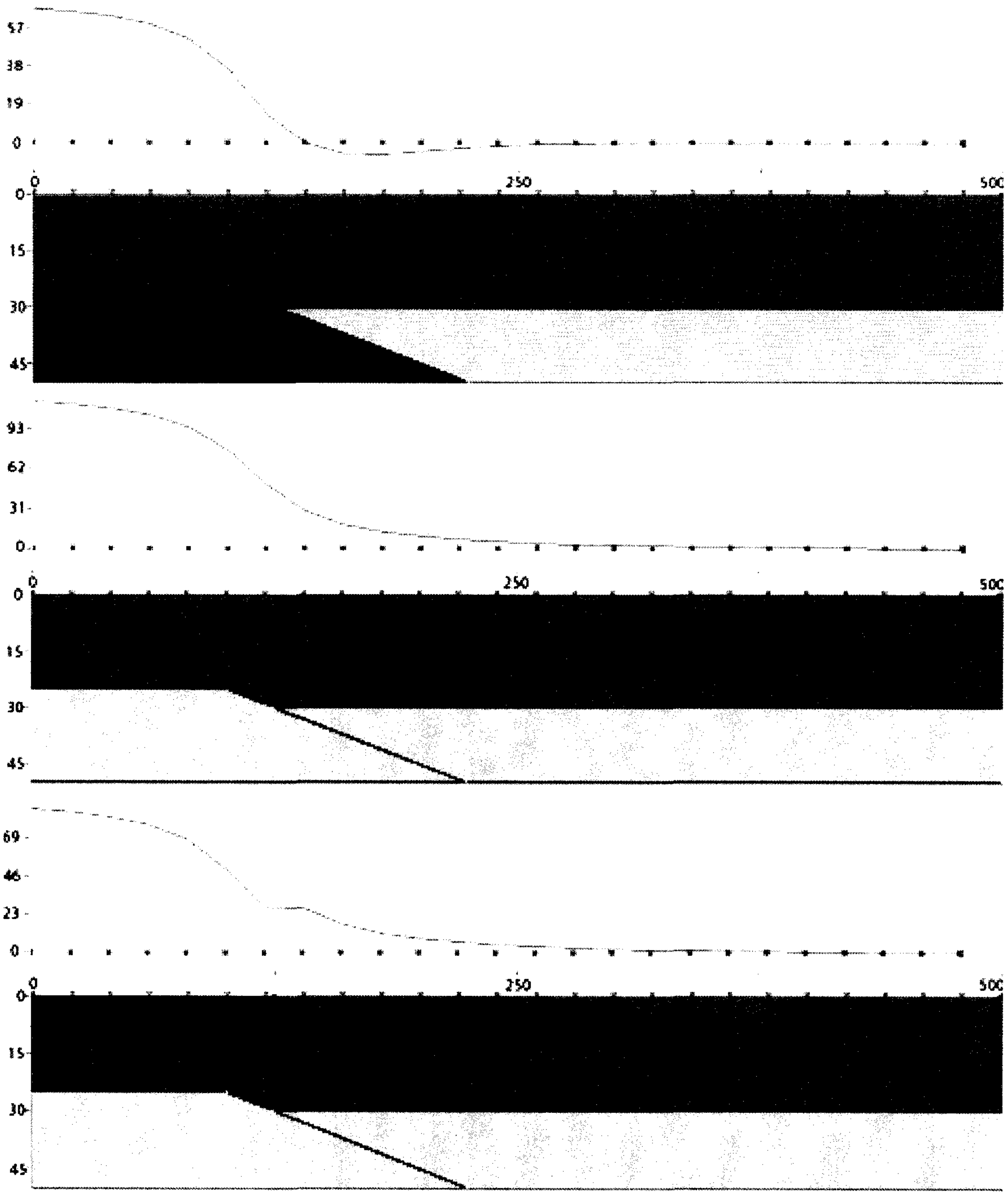
57
38
19
0
0
250
500
0
15
30
45
93
62
31
0
0
250
500
0
15
30
45
69
46
23
0
0
250
500
0
15
30
45

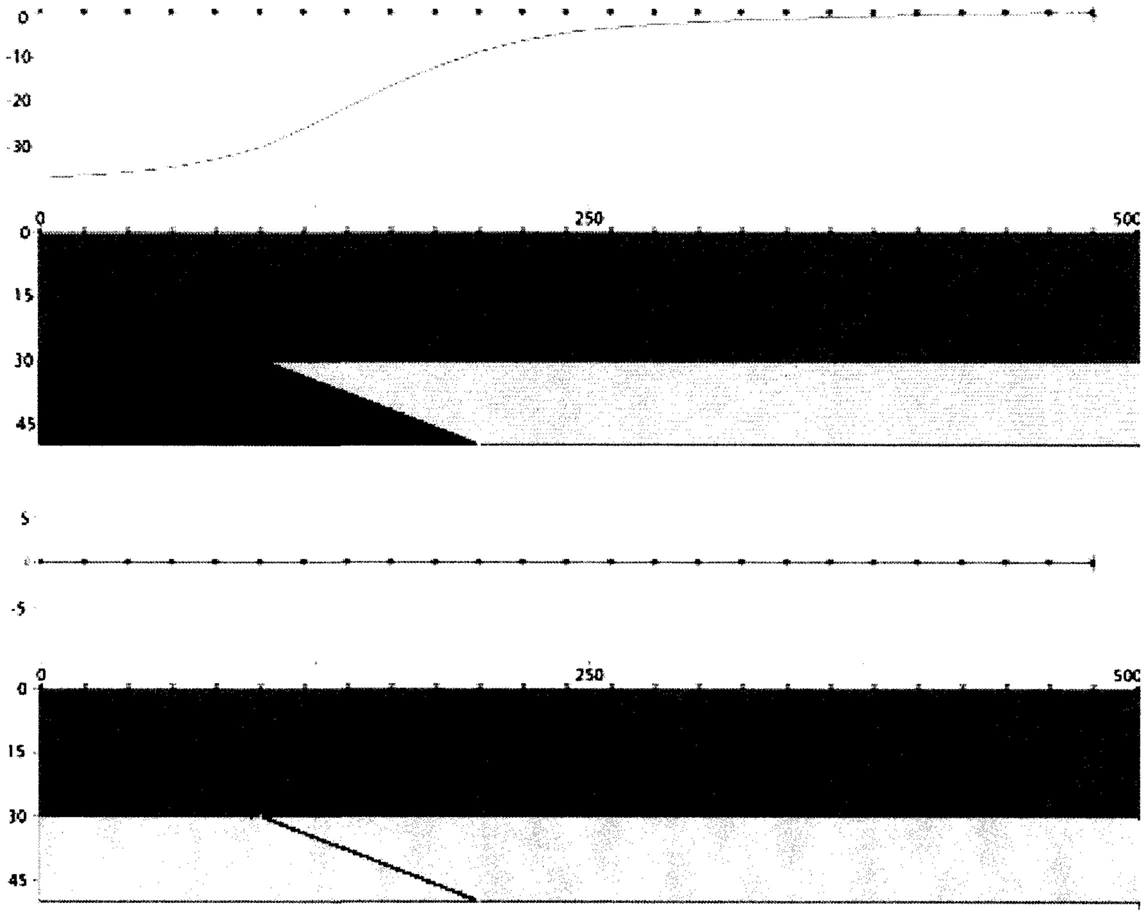

Figure 5.5. Gravitational effects of a shallow asthenosphere with no crustal intrusion. This situation is similar to the one shown in Figure 5.4. However, in this figure the asthenosphere does not intrude into the crust. The color scheme is the same as Figure 5.3. Figure A shows the gravitational signature while the asthenosphere is hot, and figure B shows how the gravitational measurements change when the asthenosphere has cooled.

Chapter 6

MECHANICAL MODELS

6.1. Model Setup

The mechanical models used in this project were modified from numerical models of New Zealand created and used by Upton et al. (2003), Koons et al. (2003), and Upton and Koons (in review).

The mechanical models were created with FLAC^{3D}, a three-dimensional finite difference code (Itasca, 2005). A model created with FLAC^{3D} represents materials as a three-dimensional volume that is broken into a grid of polyhedra. The corners of each polyhedron are assigned velocities and stresses, and the system responds to the imposed conditions according to the equation $\frac{\partial \sigma_{ij}}{\partial x_i} + \rho b_i = \rho \frac{dv_i}{dt}$, where σ_{ij} = the components of the stress tensor, x_i=components of the position vector, ρ=density, b_i=components of the body forces, v_i=the components of the velocity vector, and t=time. This equation is solved explicitly for each time step for which the model is run.

The upper crust is modeled with a Mohr-Coulomb rheology because this rheology is strongly pressure dependant, and the lower crust and mantle lithosphere are modeled with a von Mises rheology (Kohlstedt et al., 1995). In FLAC^{3D}, each of these rheologies is modeled in such a way that the material deforms plastically after it reaches a yield stress. Different equations govern the failure and flow of materials for each type of rheology. The yield condition that governs the Mohr-Coulomb behavior is $\sigma_1 = -\sigma_3 N + 2C\sqrt{N_\phi}$, where σ_1=maximum normal stress, σ_3=minimum normal stress, C=cohesion, $N_\phi = \left(\frac{1+\sin\phi}{1-\sin\phi}\right)$, and ϕ=the internal angle of friction, and the flow law for plastic shear flow $= \sigma_1 - \sigma_3 N_\psi$, where $N_\psi = \left(\frac{1+\sin\psi}{1-\sin\psi}\right)$, and ψ=the dilatation angle. The yield condition that governs the von Mises flow is τ=k, where τ is the shear stress and k is the shear strength, and the flow law for plastic shear flow= τ.

The model setup consists of a rectangular volume with dimensions x=380 km, y=500 km, and z=50 km. Within this volume, the grid spacing is 10 km in the x-direction, 12.5 km in the y-direction, and 2.5 km in the z direction. The transition between the Mohr-Coulomb and von Mises rheologies takes place at 400° C. The transition from a pressure dependent to a thermally activated rheology is based on the ductility of quartz. This transition is typically thought to take place at 350° C, although the value depends on strain rate (Brace and Kohlstedt, 1980). In this model, the rheology was determined every 100° C, as discussed below. For this reason, the brittle-ductile transition was approximated as 400° C. Yield stresses in the von Mises rheology are based on a quartz diorite rheology deforming at a strain rate of 10^{-14} s^{-1} (Ranalli, 1995), and the shear strength is altered incrementally with temperature, following a power law relationship (Brace and Kohlstedt, 1980). The quartz diorite rheology was used throughout the 50 km thickness of the model. Typical upper crustal material will likely have more quartz than a diorite while the upper mantle will have less quartz. The choice of diorite is an approximation from which neither crustal nor upper mantle material will likely diverge widely in behavior. The western edge of the model has an elastic rheology which serves as a backstop to limit x- and y-displacement (Figure 6.1). This backstop simulates the cold non-deforming portion of the Laurentian continent. Such asymmetric

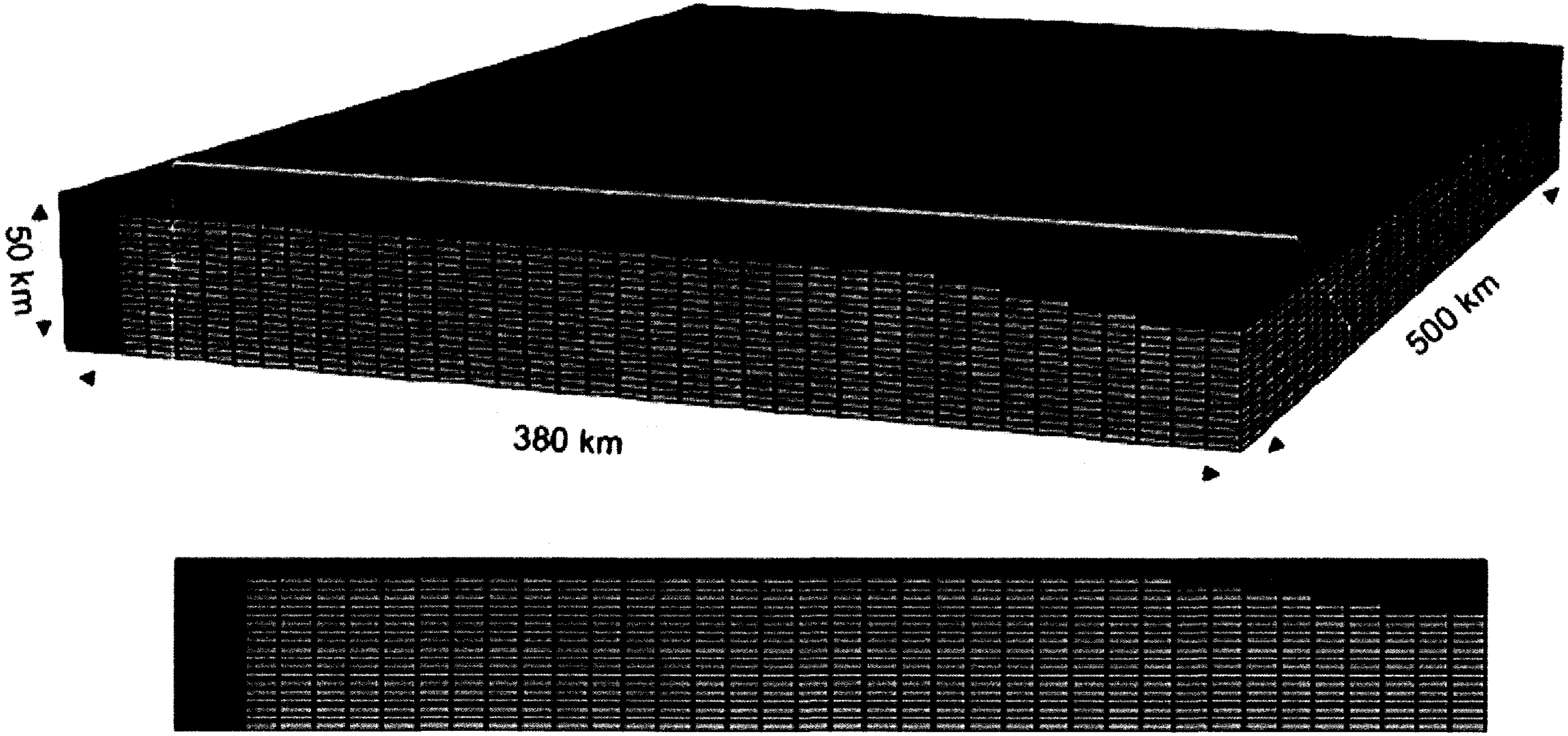

Figure 6.1. Mechanical model setup: rheological distribution. Shown are the locations of the three rheology types used for modeling. Red represents a Mohr-Coulomb rheology, light blue represents a von Mises rheology, and dark blue represents elastic material. The depth of the transition from a Mohr-Coulomb to a von Mises rheology is determined by the temperature.

deformation is observed in a number of modern orogens such as the Southern Alps, the Himalaya, and Taiwan and is well modeled by an indentor that is strong relative to the deforming material (Koons, 1990, Davis et al., 1983).

The rheological structure of the model is based on the thermal structure that resulted from the large-scale modeling described in Chapter 5. In the thermal models, the locations of isotherms, with a 100° C interval, were used as the approximate planes of transition separating material with different shear strengths (Figure 6.2). However, the power law relationship between shear strength and temperature becomes inaccurate at very high temperatures. For this reason, the shear strength was held constant between temperatures of 600° and 1400° C. The rheology is consistent with an asthenospheric source that reached a depth of 30 km below the earth's surface. An additional model was tested in which the asthenosphere only reached a depth of 40 km below the earth's surface. The rheology is heterogeneous across the model; it is assumed that within the overriding slab, the asthenospheric source is not continuous across the length of the model. Thus within the overriding plate, there is a transition from a normal to an elevated thermal rheology along strike. Within the subducting slab, it is assumed that the presence of the high-temperature region is not able to significantly affect the thermal structure of the subducting slab in the upper 50 km of the earth because advection is the dominant mechanism of heat transfer in this portion of the model (Koons et al., 2003, Peacock, 1996). For this reason, the subducting slab was given a normal rheology (Figure 6.3).

Various geometries of the rheologically weakened region were tested. The extent of the weakened region was varied in the y-direction (Figure 6.4). Endmembers with no

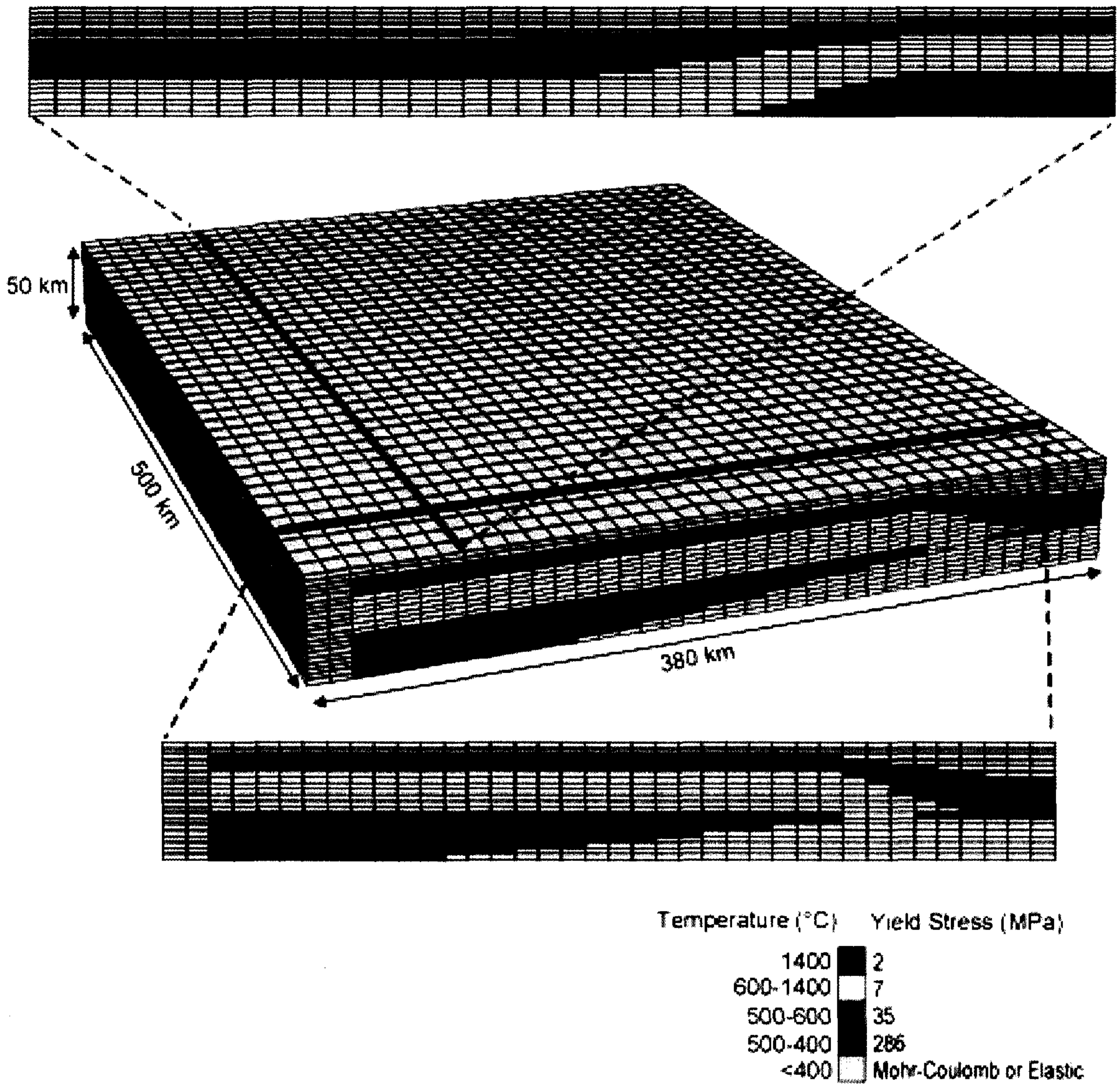

Figure 6.2. Mechanical model setup: rheological weakening. The different shear strengths used in the von Mises rheology are shown. Cross-sections are shown normal to x and normal to y. The cross-section across-strike of the orogen shows that the crust is anomalously weak only in the overriding plate. In the subducting slab, the rheology is normal. The cross-section along the strike of the orogen shows that the weakening is non-continuous along the orogen. In the north, there is a transition back to a normal rheology. Areas with a Mohr-Coulomb or elastic rheology are shown in grey.

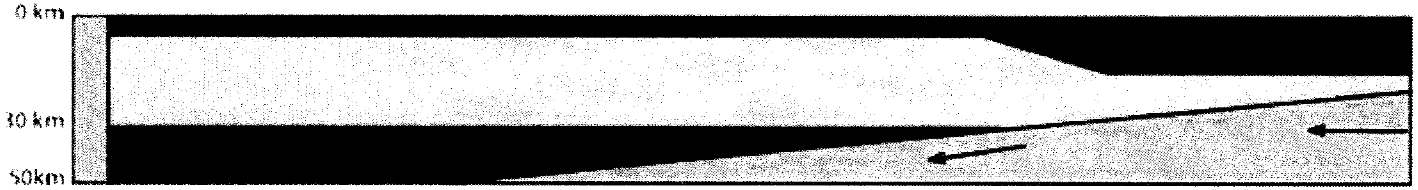

Figure 6.3. A schematic diagram of the model setup. Blue represents the asthenospheric source, yellow represents the region of ductile deformation in the overriding plate, light green represents the subducting slab, which also deforms ductilely, dark green represents the region that deforms brittlely, and pink represents the elastic backstop, which represents the stable, non-deforming continental interior.

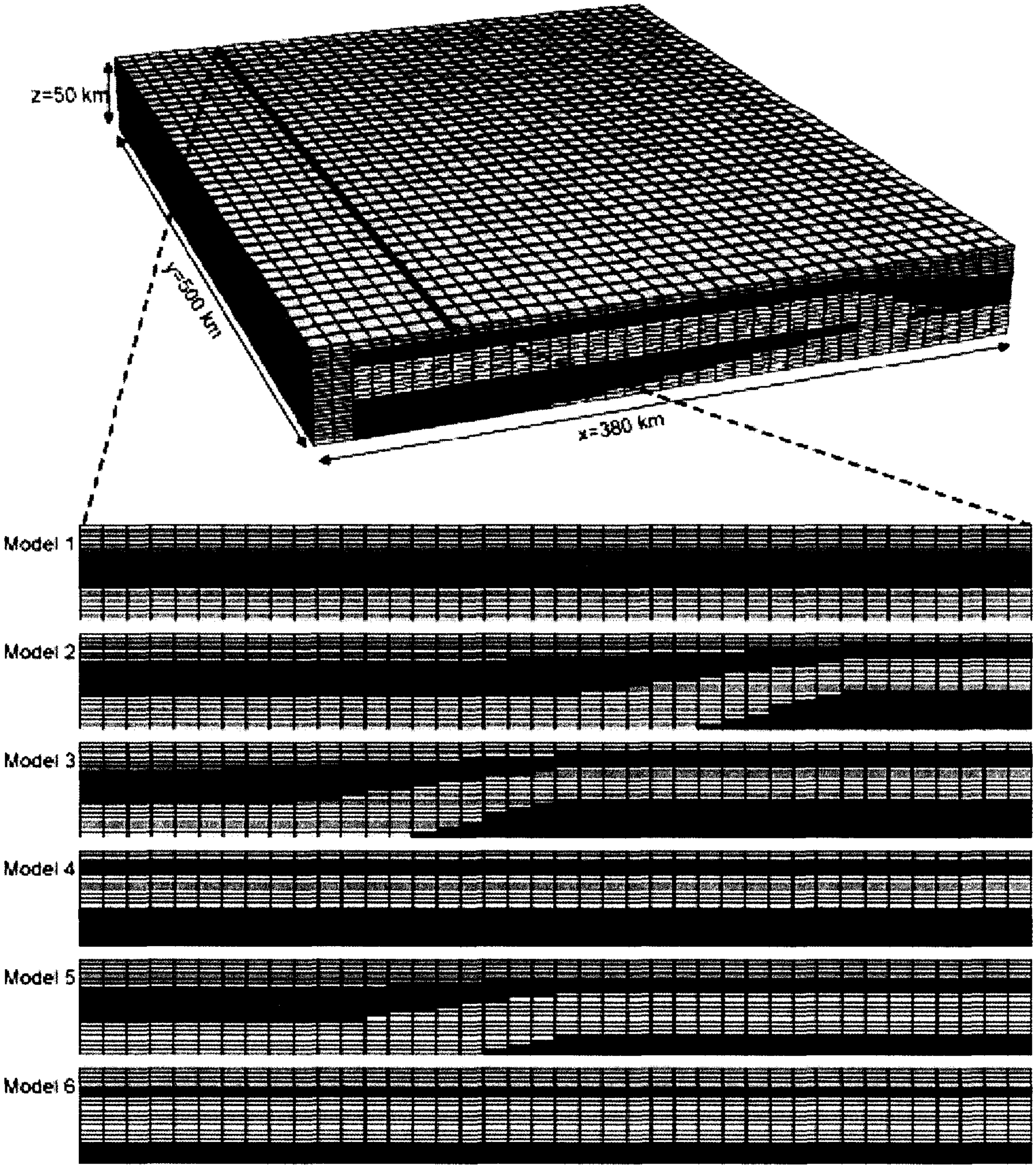

Figure 6.4. Mechanical model setup: variations in geometry. Six different along-strike cross-sections were used in different models. These diagrams show the variations in the horizontal and vertical extent of the weakened region that were tested. Models were tested that had no weakened region, weakening along the entire orogen, two intermediate models, and two models where the asthenosphere only reached a depth of 40 km. Colors are the same as those used in Figure 6.2.

rheological weakening and weakening along the entire y-extent of the model were tested as well.

The eastern side of the model, on which subduction is taking place, has velocity conditions imposed on it (Figure 6.5). The edge and base of the subducting slab are given x- and y-velocities with the y-velocity four times greater than the x-velocity. A study of vorticity within one lithologic unit in central Maine found vorticity to be compatible with an obliquity of 4 to 1 (Short and Johnson, in press). The vorticity of a single lithologic unit cannot necessarily be correlated to orogen-scale obliquity because local effects may be significant. However, because there are not other reliable sources of information about the obliquity and because this obliquity is known to be realistic in other orogens (Upton et al., 2003), it was assumed for the model geometry. The base of the subducting slab is given a z-velocity that increases with proximity to the overriding slab. The z-velocity is, at its maximum, four times smaller than the x-velocity. To avoid imposing unrealistic velocity conditions on the northern and southern sides of the models, the velocities at each y-boundary of the model are taken from velocities calculated within the interior of the model. This assumption is most appropriate when the velocities do not vary significantly in the y-direction between the edge of the model and the x-location from which the boundary conditions are taken.

The model includes erosional conditions in which points between x=-80 km and x=-160 km are eroded if they reach an elevation higher than 50 m. The value of x=-80 km was based on the location of the down-going slab in the model, and the value of x=-160 km is the location of the elastic backstop. This erosion condition was based on patterns of erosion in New Zealand, where the highest levels of erosion are between the

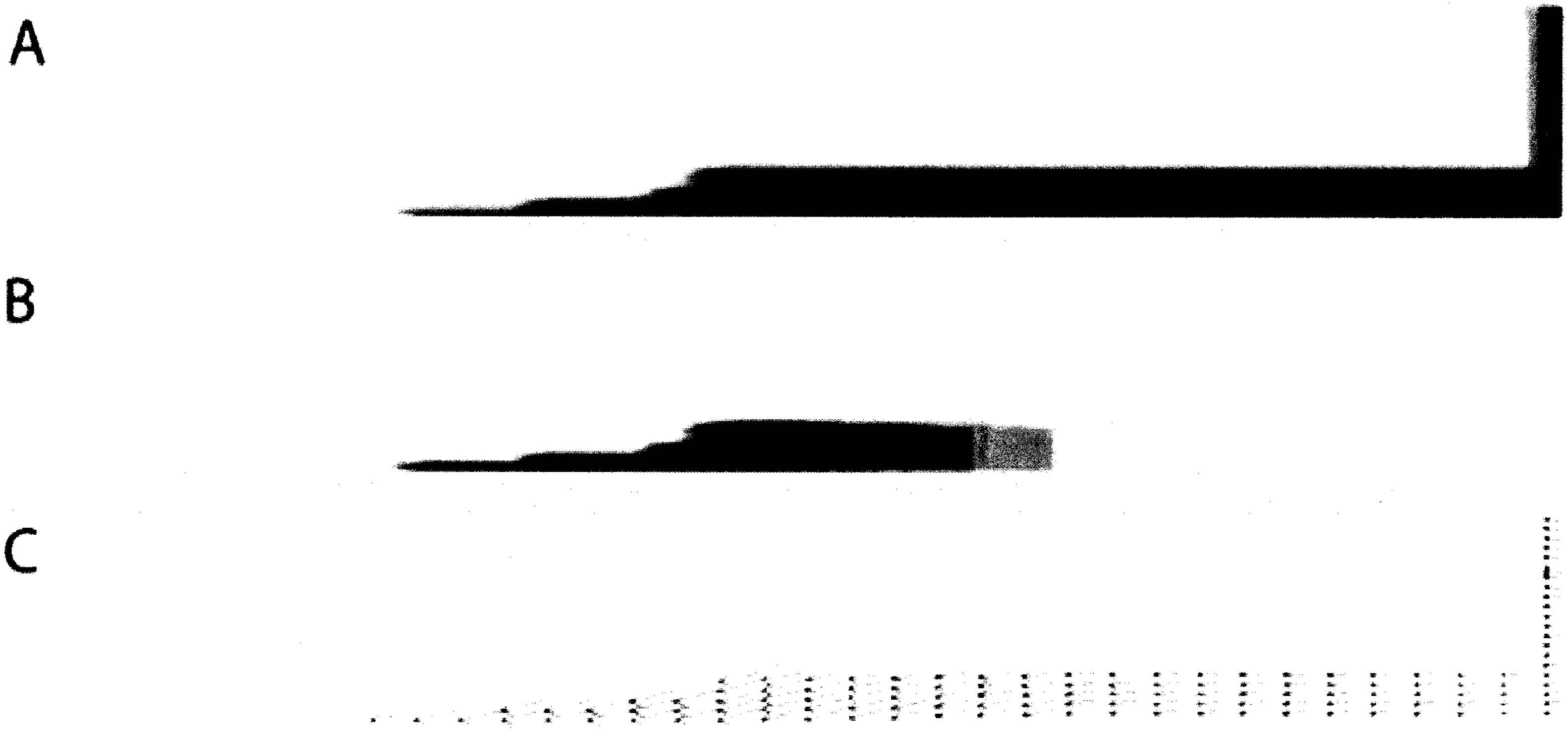

Figure 6.5. Velocity conditions on the model. Image A shows the locations at which x- and y- velocities were applied. Image B shows the locations at which z-velocities were applied. In both of these diagrams, blue represents high velocity while white represents zero velocity. C shows the same velocity conditions represented by vectors.

Main Divide and the west coast (Hicks et al., 1996). As a comparison, a model with no erosion was tested as well.

6.2. Model Results

The results of the mechanical models are represented in map view at a depth of 12 km beneath the earth's surface. Because 12 km is the approximate depth of the erosional surface in central Maine, this representation is intended to make a comparison between the model results and the geology easier. Near the y-boundaries of the models, the results are significantly affected by the oblique boundary conditions. For this reason, the results from the central portion of the model, away from the northeast and southwest boundaries, are the most representative.

Much of this analysis depends on components of strain in the x-y plane. These components are most correctly calculated from velocities. However, if there is no significant evolution in the behavior of the model and if the total displacement is small compared to the size of the model, the displacements can be used as well. The advantage of using displacements under such conditions is that transient features that are seen in the instantaneous velocities are smoothed out. Because these transient features are often unimportant in the overall long-term behavior of the model, they serve as distractions. However, if there are significant changes in the behavior of the orogen with time, using displacements for the calculation of strain will create a time average of these changes leading to a masking of the changes and confusion over the behavior of the orogen. In my case, the deformation is small relative to the size of the orogen and the orogen is deforming in a manner that is close to a steady state. For this reason, the use of displacements in the calculation of strain is appropriate.

6.2.1. Model 1: No Rheological Weakening

When there is no rheological weakening in the model, the x- and y-displacements are nearly constant along the length of the model (Figure 6.6). There is positive z-displacement on the northwest side of the subducting slab with a magnitude of 260 m. There is negative z-displacement farther to the southeast with a magnitude of 260 m. The reason for this negative displacement is that this section of the model is above the downgoing slab, and the downward motion of the slab dominates the kinematics in this part of the viscoelastic model. Farther to the southeast, there is again positive displacement of a magnitude of 80 m. The z-displacements are non-constant along the length of the model with the highest positive displacements in the southwest and the highest negative displacements in the northeast. This is a consequence of the oblique boundary conditions.

Rotation $\left(\frac{1}{2}\left(\frac{\partial D_x}{\partial y}-\frac{\partial D_y}{\partial x}\right)\right)$ and simple shear $\left(\frac{\partial D_x}{\partial y}+\frac{\partial D_y}{\partial x}\right)$ are evaluated in the x-y plane, where x and y are components of the position vector, and D_x and D_y are components of the displacement vector (Figure 6.7) (Koons and Henderson, 1995). The rotation and simple shear are uniform along the length of the model, and the only large along-strike variations are at the boundaries. The rotation and simple shear are both dominated by the term $\partial D_y/\partial x$. Thus the region with high rotation and simple shear is the region in the model where the most along-strike, orogen-parallel motion is accommodated.

Dilatation $\left(\frac{1}{2}\left(\frac{\partial D_x}{dx}+\frac{\partial D_y}{\partial y}\right)\right)$ and pure shear $\left(\frac{\partial D_x}{\partial x}-\frac{\partial D_y}{\partial y}\right)$ were also evaluated in the x-y plane (Figure 6.8). Away from the boundaries, the pure shear and dilatation are dominated by $\partial D_x/\partial x$. Thus the regions with high pure shear and dilatation are the ones where the greatest amount of shortening is being accommodated.

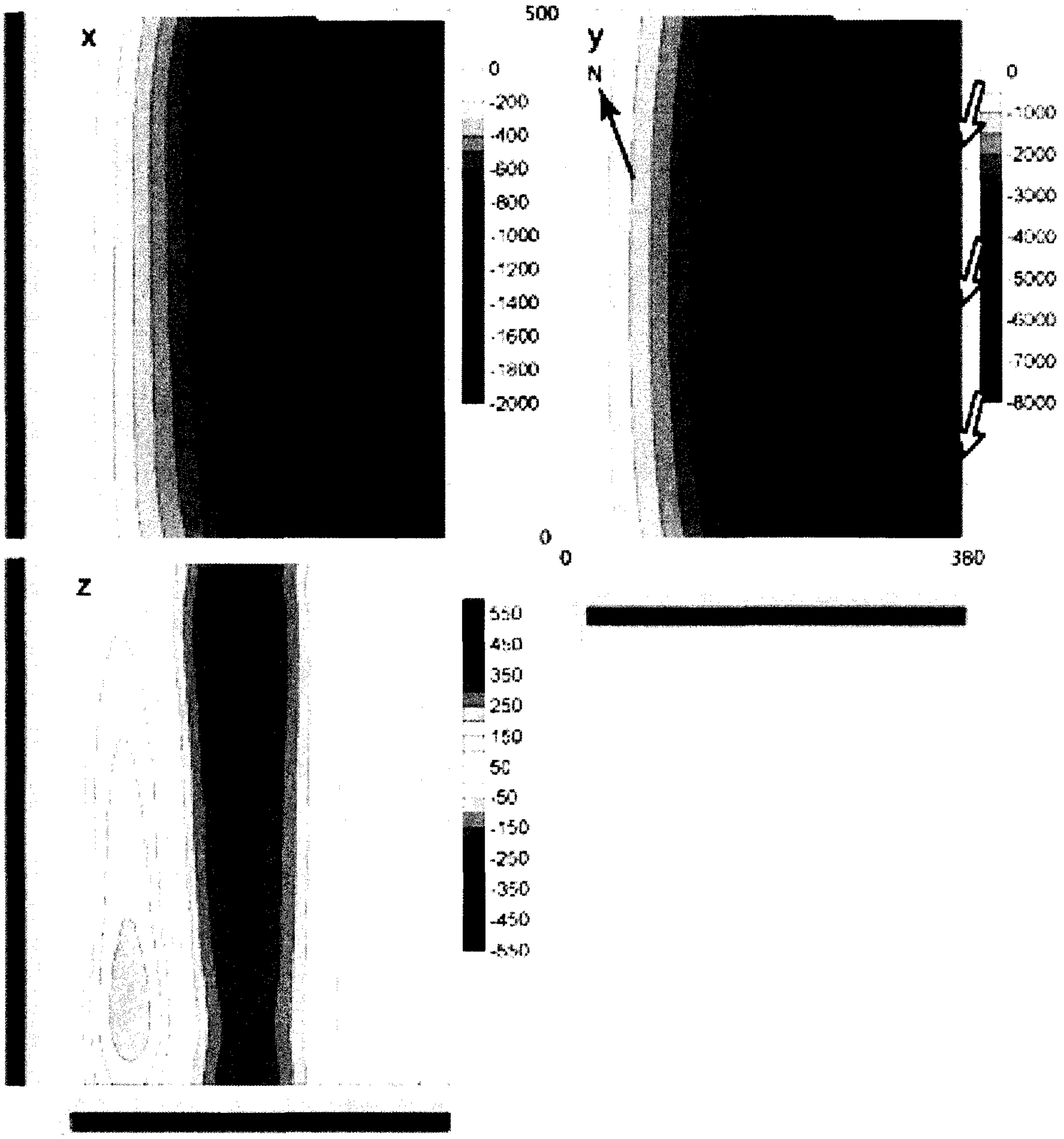

x
500
0
-200
-400
-600
-800
-1000
-1200
-1400
-1600
-1800
-2000
0
y
N
0
-1000
-2000
-3000
-4000
-5000
-6000
-7000
-8000
0
380
z
550
450
350
250
150
50
-50
-150
-250
-350
-450
-550

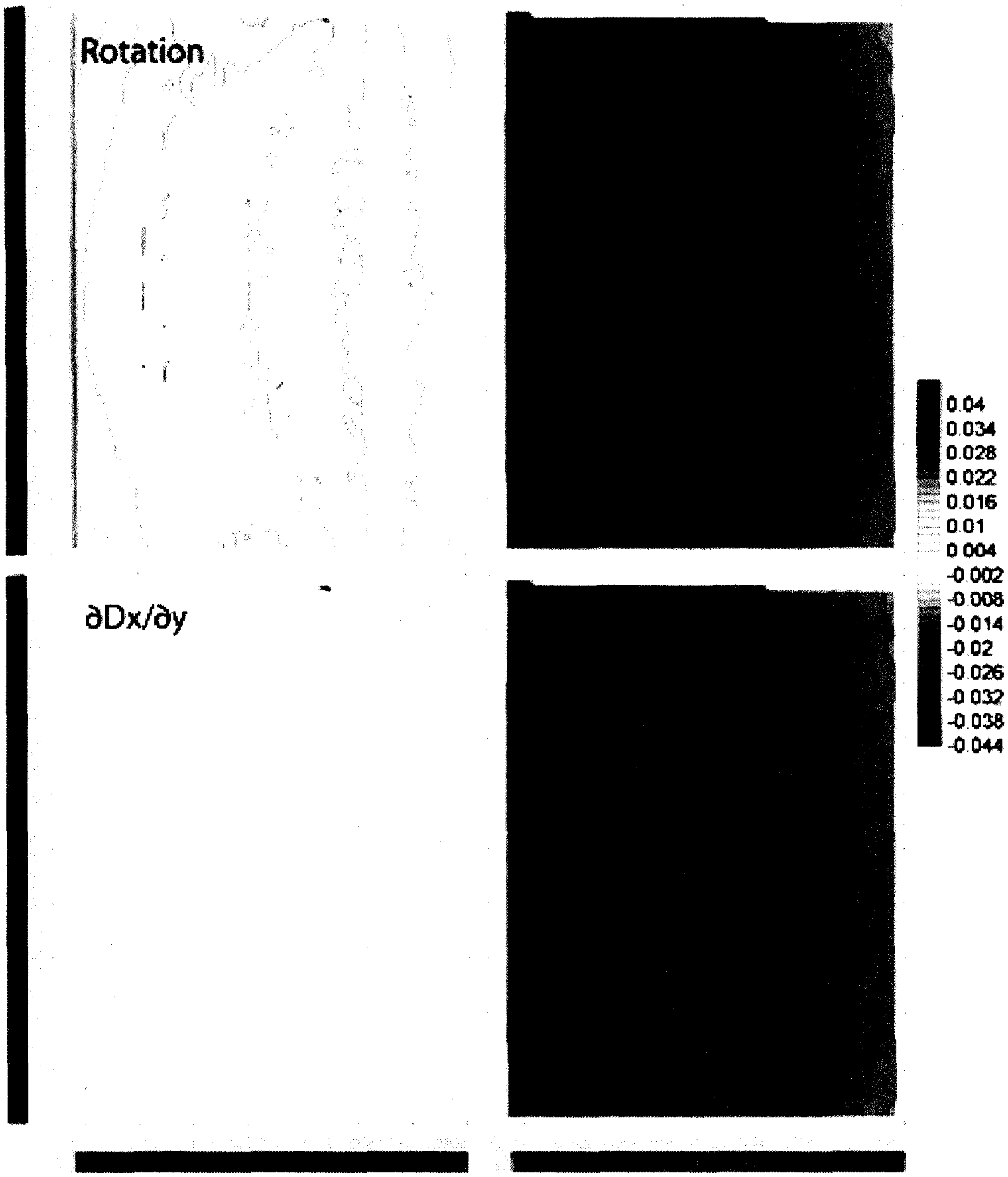

Figure 6.7. Model 1 rotation, simple shear, $\partial D_x/\partial y$, and $\partial D_y/\partial x$. In this x-y plane reference frame, negative values represent sinistral simple shear or counterclockwise rotation while positive values represent dextral shear or clockwise rotation. The contour interval is 0.002. The color scale is the same as the scale used for subsequent plots of rotation and simple shear.

$\partial D_x/\partial y$ is insignificant compared to $\partial D_y/\partial x$. Thus the distribution of $\partial D_y/\partial x$, rotation, and simple shear are all very similar. The high values of each of these factors are distributed over a broad region of the orogen across-strike, but along-strike, there is little variation.

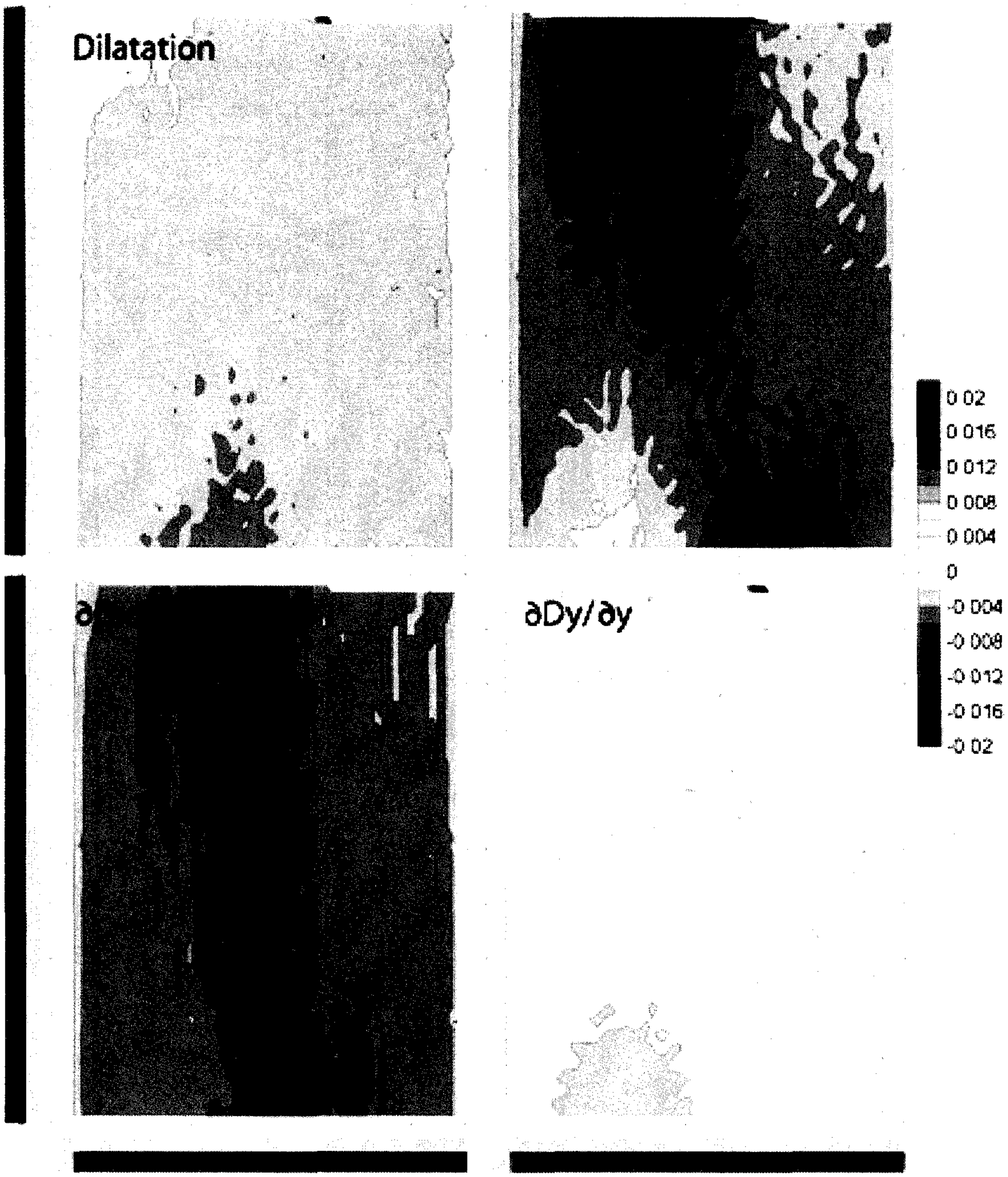

Figure 6.8. Model 1 dilatation, pure shear, $\partial D_x/\partial x$, and $\partial D_y/\partial y$. In the x-y plane negative dilatation indicates shortening in the x and y directions while positive dilatation indicates extension in the x and y directions. Negative pure shear indicates shortening in the x-direction and extension in the y-direction while positive pure shear indicates extension in the x-direction and shortening in the y-direction. The contour interval is 0.002. The color scale used is the same as the scale used for subsequent plots of dilatation and pure shear.

$\partial D_y/\partial y$ is insignificant away from the boundaries. Thus dilatation and pure shear are controlled by $\partial D_x/\partial x$.

6.2.2. Model 2: Weakening in the Southwest

When the southwestern portion of the model is differentially weakened relative to the northeastern portion, the pattern of displacement is significantly different than in model 1 (Figure 6.9). The x-displacement is increased in the region where the transition between the strong and weak rheologies is located. Within the weakened region, the displacement is approximately equal to the displacement in the strong region. It appears that the displacement increases again at the southwestern edge of the model, but this is more likely to be a boundary effect caused by the oblique velocity conditions than a rheological effect. The pattern of the y-displacements seems to be affected very little by the presence of a weak zone, but there are differences from model 1. These changes are difficult to pick out visually, but become more obvious when looking at maps of gradients in y-displacement. The areas of both positive and negative z-displacement have a greater magnitude in this model than in the previous model. The area of uplift has a magnitude of 540 m while the area of negative displacement has a value of -300 m.

In the strong region, the map of $\partial D_y / \partial x$ is very similar to model 1, and has a similar effect on the rotation and simple shear (Figure 6.10). Within the weak region, there is a steep gradient in $\partial D_y / \partial x$ and simple shear. The location of this gradient is parallel to the orogen and occurs at the boundary between the subducting slab and the overriding slab. This region represents an across-strike transition from a strong to a weak rheology, and because it is likely that large rheological contrasts do exist across subduction zones, this kinematic gradient may be realistic in the earth. Unlike model 1, in this model, $\partial D_x / \partial y$ also makes a significant contribution to the rotation and simple shear. As noted above, the transition between the two rheologies represents a region of significant variation in the x-displacement in the y-direction. This causes an increase in clockwise rotation on the strong side of the transition and a decrease on the weak side. Similarly the simple shear decreases on the strong side of the transition and increases on the weak side. In this model, the along-strike variation in $\partial D_x/\partial y$ caused by the weakening does not take place smoothly. This jaggedness is an artifact of the model geometry rather than a result that would be expected in the earth. The reason for these jumps is that the rheology in the model was changed in finite increments. Across the transition zone each rheological layer dips, which causes the thickness of the layers to vary depending on their position relative to the rectilinear grid. The strongest, uppermost ductile layer is very thin and dips shallowly; to approximate the shallow dip, the thickness of this layer varies from 2.5 km to 5 km depending on the position of the layer relative to the grid. Because the thickness of this layer can vary by a factor of two, the strength of the model in the vicinity of this layer is significantly affected by the changes in the thickness of this layer, and at each change in the thickness of this layer, there is a jump in the x-displacement. This problem could be solved by using a finer grid spacing in the z-direction. However, a finer grid spacing also leads to other numerical problems.

The pattern for $\partial D_x/\partial x$ is similar to model 1, but there is a region with high values within the weak zone (Figure 6.11). Values seem to be particularly high at the along-strike rheological transition and are probably related to the perturbation in x-displacement that occurs there. There are high values of $\partial D_y/\partial y$ in the weak zone. These high values are very close to the southwestern boundary of the model, and there was a similar feature in model 1 that I attributed to the boundary. Because of the increase in magnitude relative to model 1, it seems probable that the high values of $\partial D_y/\partial y$ are real, and not entirely a boundary effect. Another interesting feature that is observable in the map of $\partial D_y / \partial y$ is the zone of positive values on the strong side of the along-strike rheological transition. This feature suggests that, like x-displacements, y-displacements are affected by the rheological transition. However, because this effect is of a small magnitude and spatial extent, it is of minor importance in the behavior of the model. The values of $\partial D_x / \partial x$ and $\partial D_y / \partial y$ combine to produce a high negative dilatation value in the weakened region. Pure shear is highest in the rheological transition.

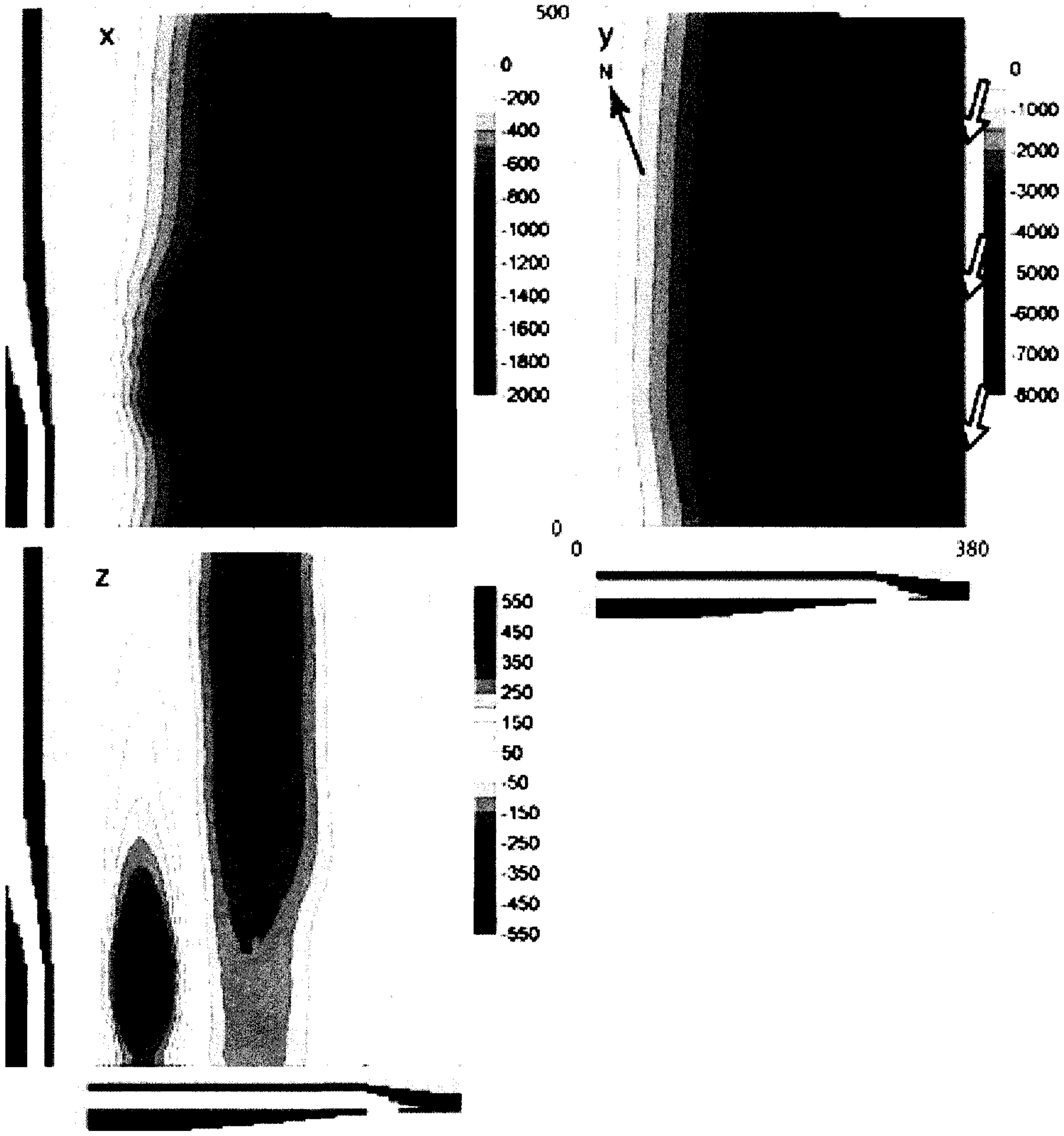

Figure 6.9. Model 2 displacements. x-, y-, and z-displacement is shown for a model with rheological weakening that extends part way along the strike of the model.

The x-displacement is significantly increased at the along-strike rheological transition. The y-displacement is, visibly, not much different from the previous model. The uplift in this model is much larger than the previous model.

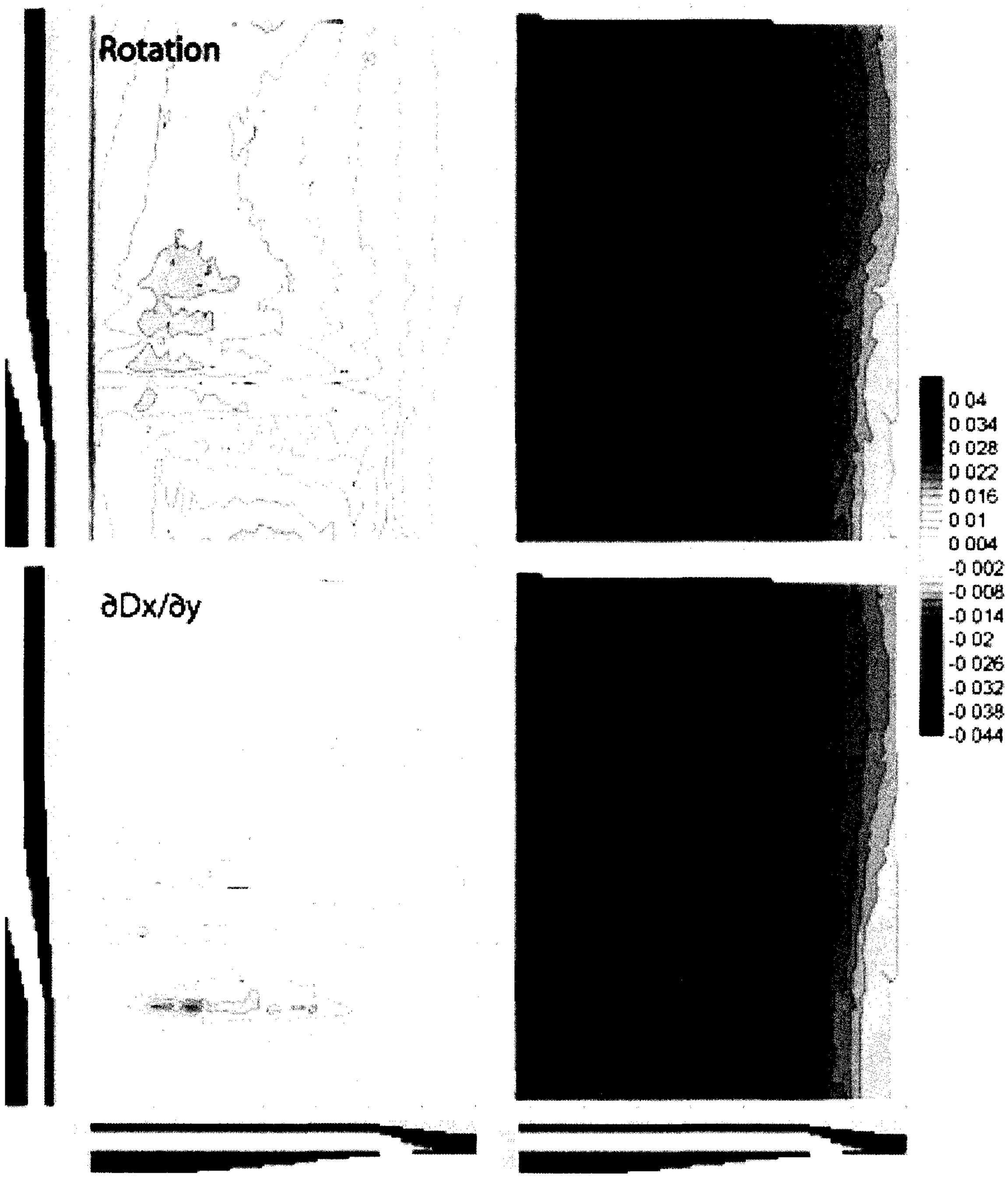

Figure 6.10. Model 2 rotation, simple shear, $\partial D_x/\partial y$, and $\partial D_y/\partial x$.

Plots of $\partial D_y/\partial x$ are similar to model 1 in the strong region but are concentrated into the transition between the two plates in the weakened section, and there is high rotation and simple shear in the areas with high values of $\partial D_y/\partial x$. $\partial D_x/\partial y$ is positive to the north of the along-strike rheological transition and negative to the south. This means that deformation is preferentially taken up through rotation to the north and through simple shear to the south.

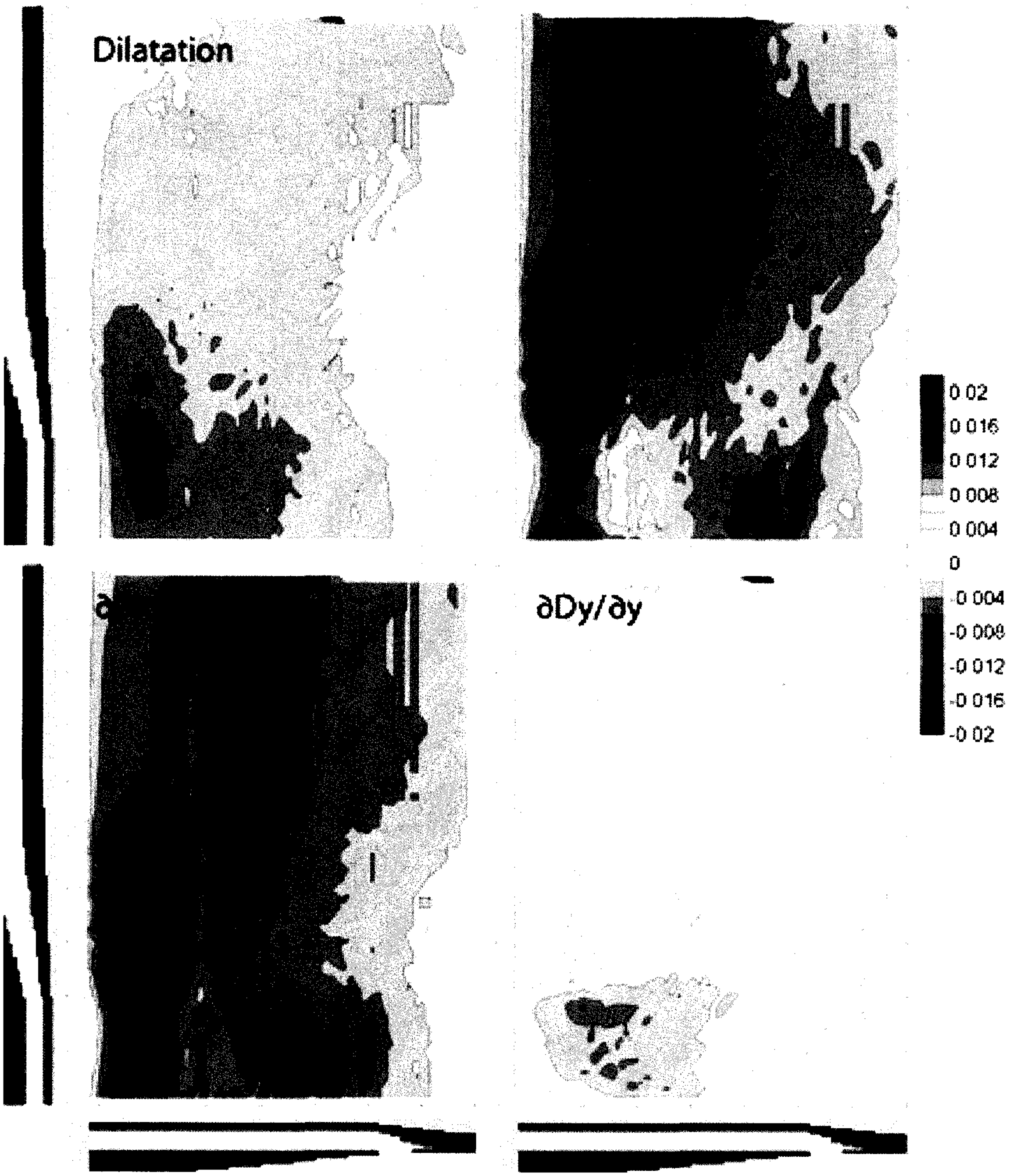

Figure 6.11. Model 2 dilatation, pure shear, $\partial D_x / \partial x$, and $\partial D_y / \partial y$.

There are high values of $\partial D_x / \partial x$ in the weakened zone and especially at the along-strike rheological transition. $\partial D_y / \partial y$ is positive to the north of this rheological boundary and negative to the south of the boundary. This leads to high values of dilatation and pure shear in the weakened zone and transition zone.

6.2.3. Model 3: Weakening in the Southwest — Increased y-Dimension of the Weakened Area

The x-, y-, and z-displacements in this model are similar to model 2 (Figure 6.12). The region of increased x-displacement has been translated to a new y-location that corresponds to the new rheological transition. By comparison to this model, it becomes clear that the increase in displacement along the southwestern boundary observed in model 2 is a boundary effect and not a rheological effect. The magnitude of the z-displacement varies from 450 m to -350 m. The area of high uplift appears to extend along the entire extent of the weakened zone. However, the areas where high uplift can be expected will be further discussed below.

The rotation, simple shear, pure shear, and dilatation show very similar patterns to model 2, but the dominant features have shifted northeast along the length of the orogen (Figure 6.13 and 6.14). The orogen-parallel gradient in simple shear is more easily visible in this model than in model 2 because of the increased length of the weak interface between the slabs. In this model it also becomes clear that along this rheological boundary, there is not only a high gradient in $\partial D_y / \partial x$ but also a localization of the high values into this region. Thus, if there is rheological weakening across the subduction zone, the location of high rotation and simple shear are shifted southeastward such that they coincide with the rheological boundary. In this model, it becomes clear that although there are high $\partial D_x / \partial x$ values throughout the weakened region, the highest values occur only in the along-strike rheological transition. Similarly, the only significant variation in $\partial D_y / \partial y$ away from the boundaries occurs in the transition.

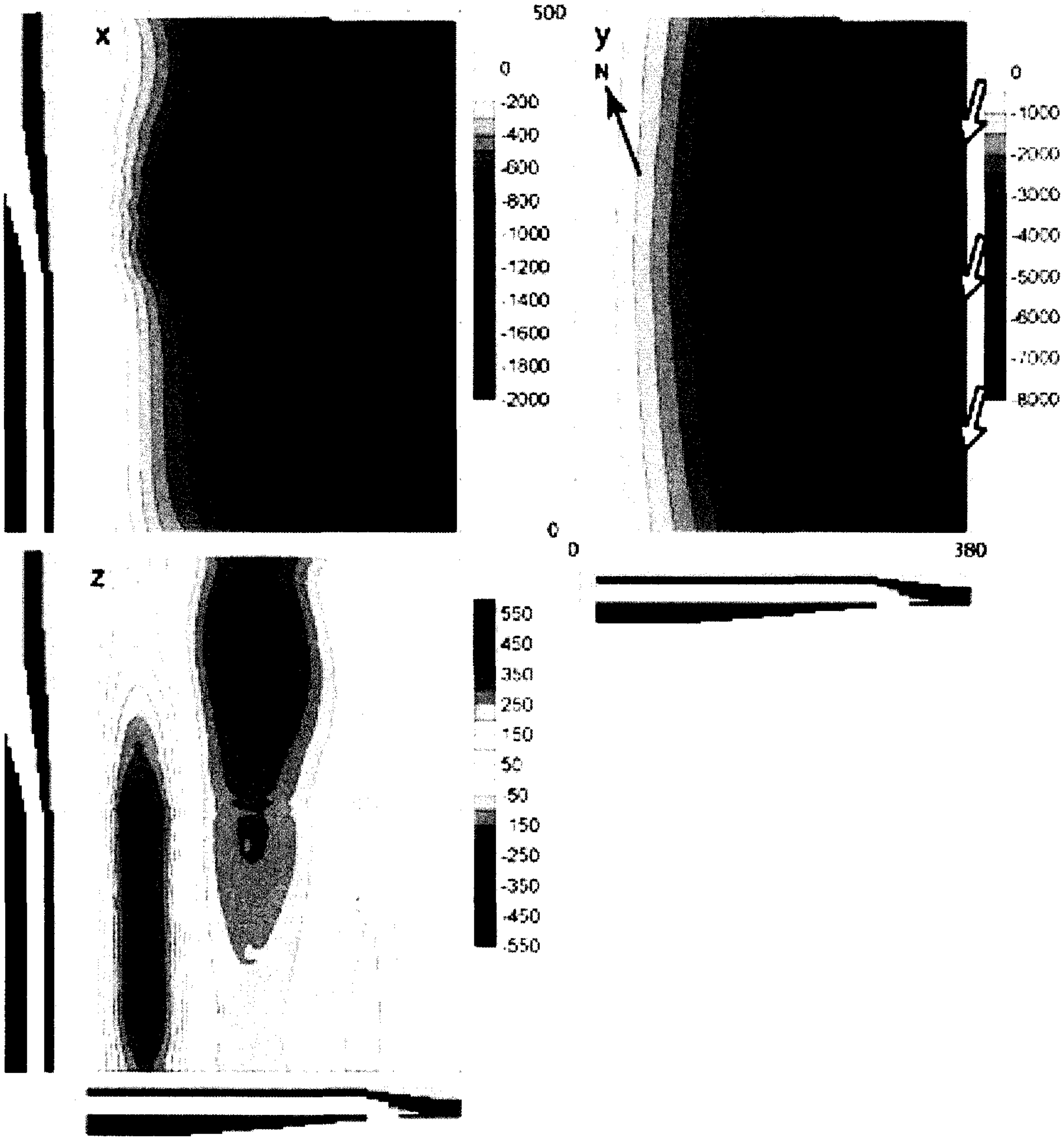

Figure 6.12. Model 3 displacements. In this model there is a larger extent of along-strike rheological weakening than in model 2.

The region of high x-displacement has shifted north relative to model 2 to the new rheological transition. The plot of y-displacement looks very similar to corresponding plots in model 1 and 2. The magnitude of the uplift in the map of z-displacement is smaller than the uplift in model 2, but it is spread over a greater along-strike region of the orogen in model 3.

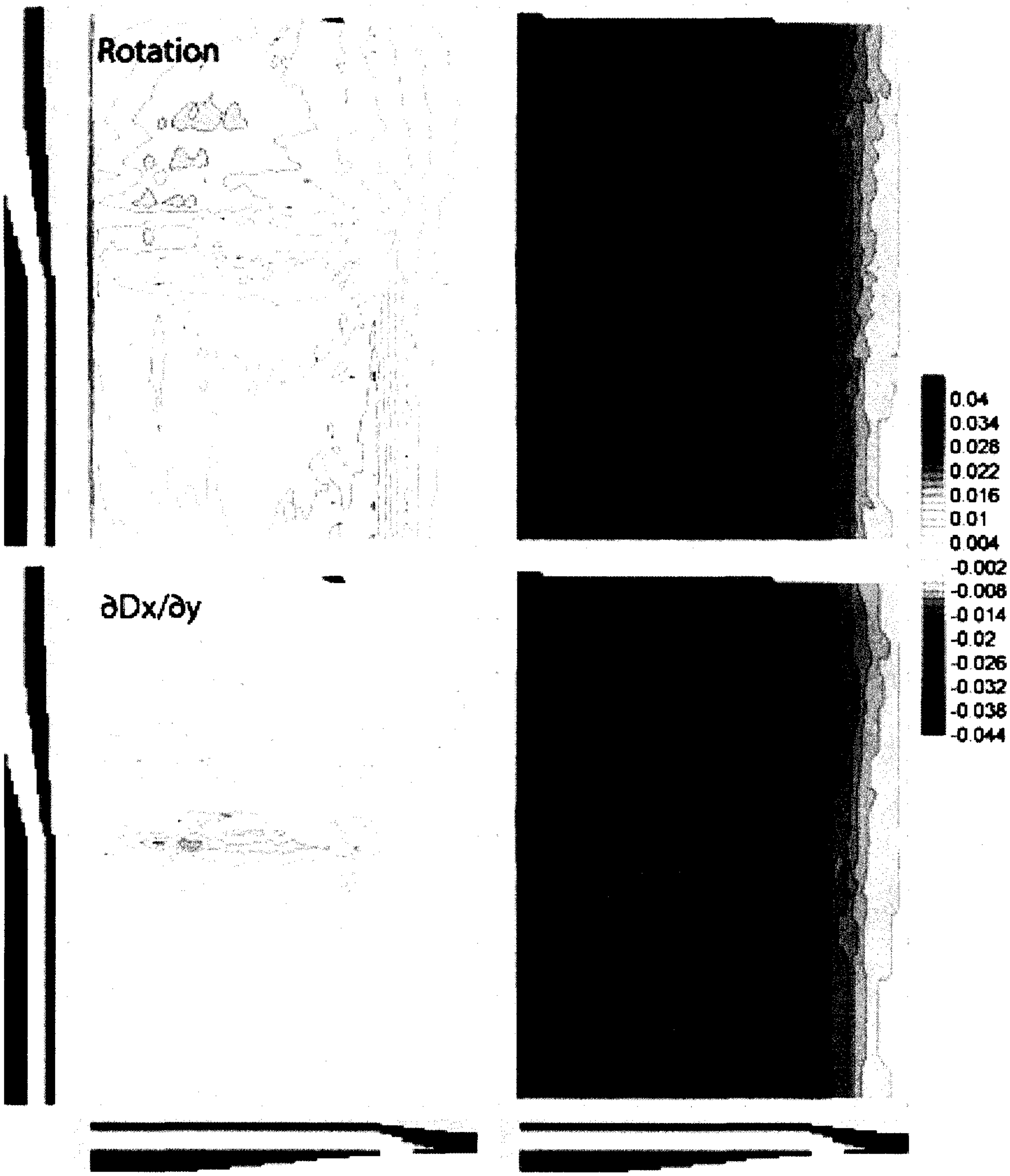

Figure 6.13. Model 3 rotation, simple shear, $\partial D_x / \partial y$, and $\partial D_y / \partial x$.

These maps are very similar to the corresponding maps in model 2. Because there is a greater area of weakening, there is a greater length of the model along which high values of $\partial D_y / \partial x$ are concentrated into the transition between plates. Similarly, the high values of $\partial D_x / \partial y$ have been shifted to the north relative to model 2, where the new along-strike transition is located.

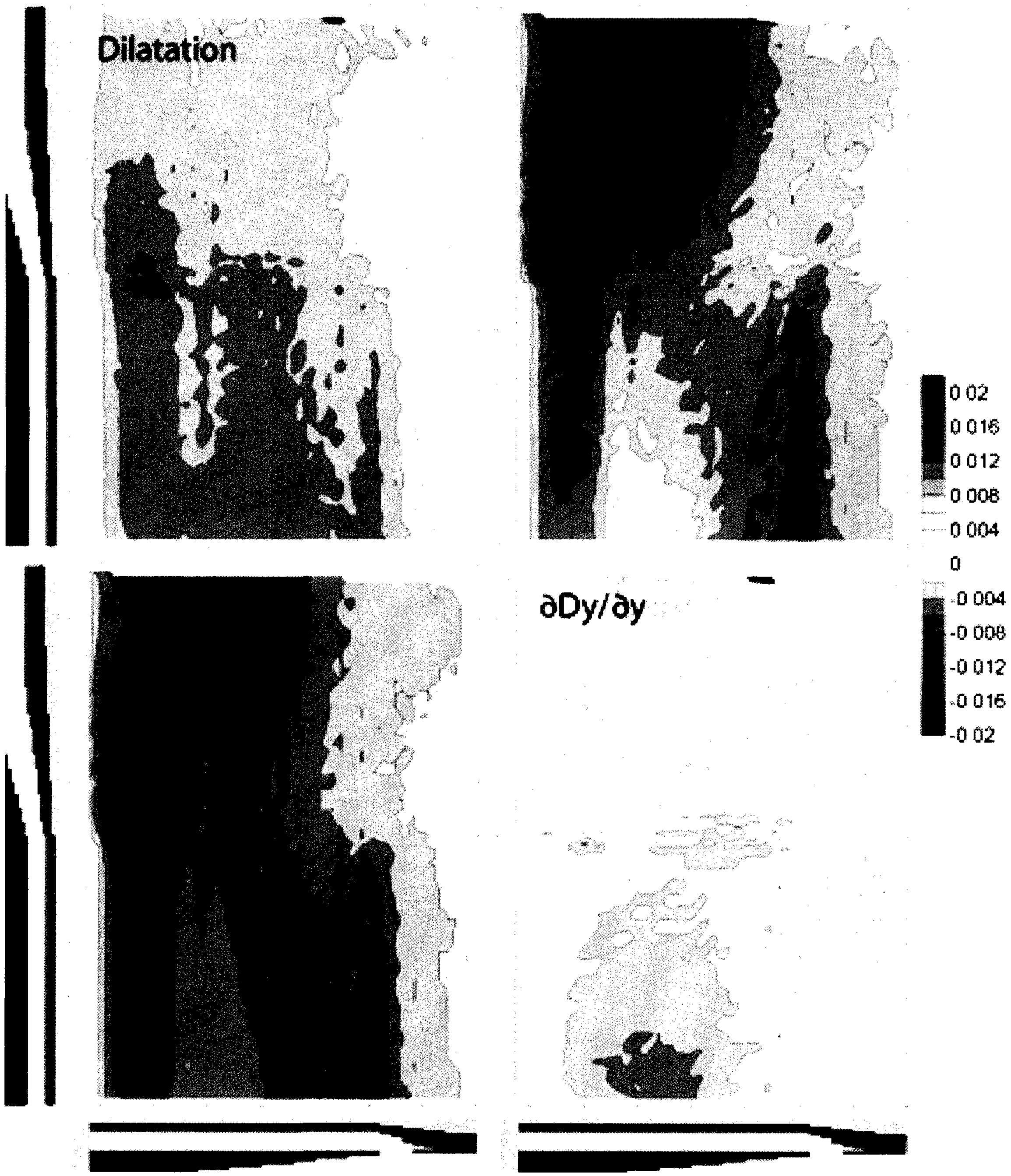

Figure 6.14. Model 3 dilatation, pure shear, $\partial D_x / \partial x$, and $\partial D_y / \partial y$.

These plots are very similar to the corresponding plots from model 2. However, the region where there are high $\partial D_x / \partial x$ values and where $\partial D_y / \partial y$ values switch from positive to negative has shifted north to the new rheological transition zone.

6.2.4. Model 4: Weakening Along the Entire y-Extent

The patterns of displacement look similar to model 1 because x- and y-displacements are nearly uniform across the length of the model (Figure 6.15). However, displacements are higher in the interior of this model; there is a steeper gradient in displacement in this model, and a shorter distance over which deformation is accommodated. The distribution of z-displacement is similar to model 1, but the magnitude of the displacement is different. The magnitude of the z-displacement varies from 360 m to -200 m. Thus, the uplift is greater in this model than in model 1, and the magnitude of downward motion is smaller.

The rotation and simple shear are both nearly uniform across the length of the model (Figure 6.16). As in models 2 and 3, each is strongly affected by the across-strike rheological boundary separating the two slabs. At this location there is a high gradient in strain. Again this feature is caused by a steep gradient in $\partial D_y / \partial x$. As in the model 1, there is very little along-strike variation in dilatation or pure shear away from the boundaries (Figure 6.17).

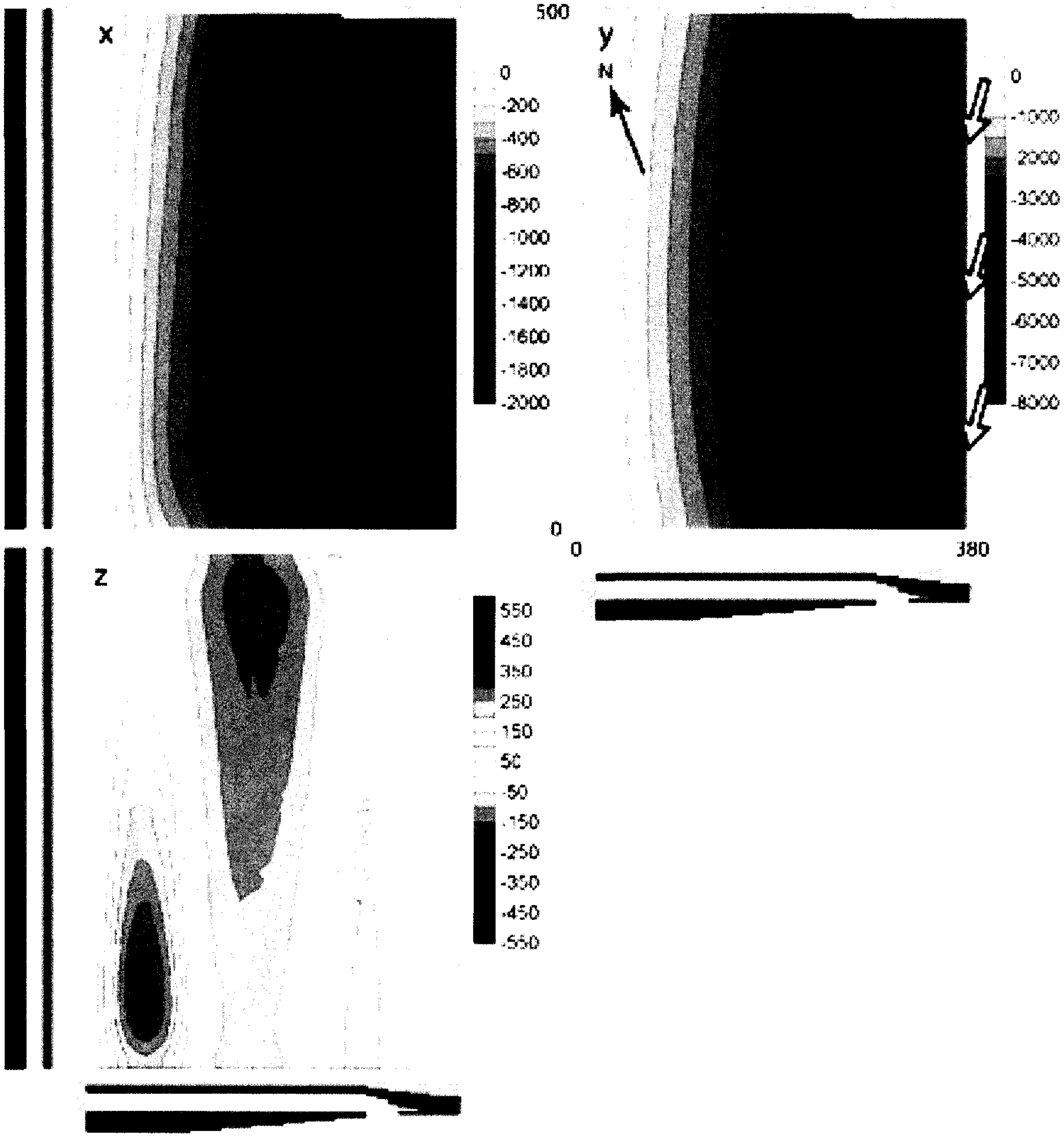

Figure 6.15. Model 4 displacements. In this model there is rheological weakening along the entire y extent of the model.

The plot of x is higher within the interior of the orogen compared to model. In other words, the deformation is taking place over a smaller x-extent. On the eastern side of the model, the y-displacement is higher relative to the y-displacement in model 1, and in the western side of the model, the y-displacements are similar in models 1 and 4. The uplift is greater in model 4 than in model 1, but the distribution of uplift is very similar.

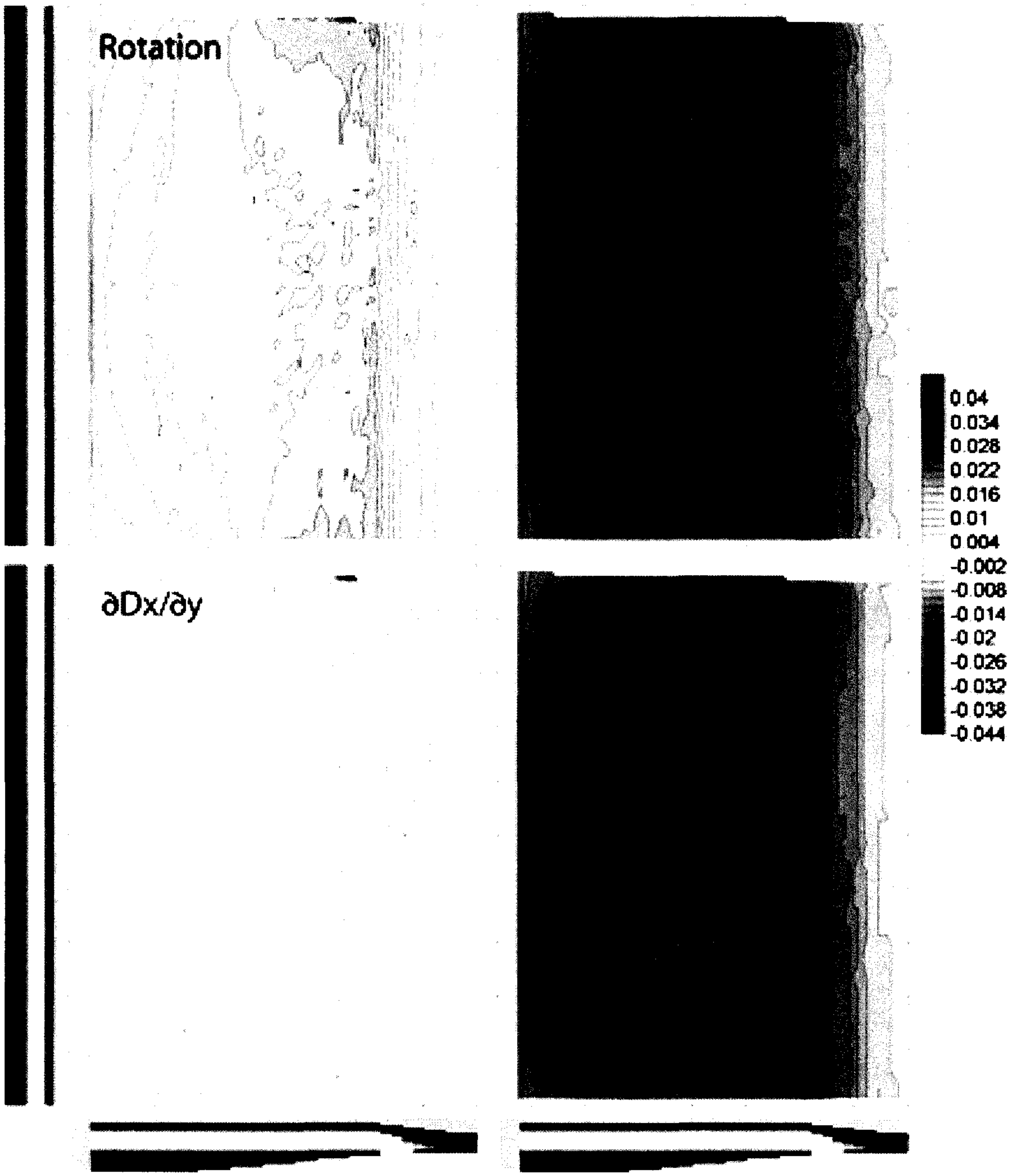

Figure 6.16. Model 4 rotation, simple shear, $\partial D_x / \partial y$, and $\partial D_y / \partial x$.

The plot of $\partial D_y / \partial x$ shows a concentration of this gradient into the plate boundary along the entire y-extent of the model. For this reason, rotation and simple shear are also concentrated into this boundary. As in model 1, $\partial D_x / \partial y$ makes an insignificant contribution to the rotation and simple shear in model 4.

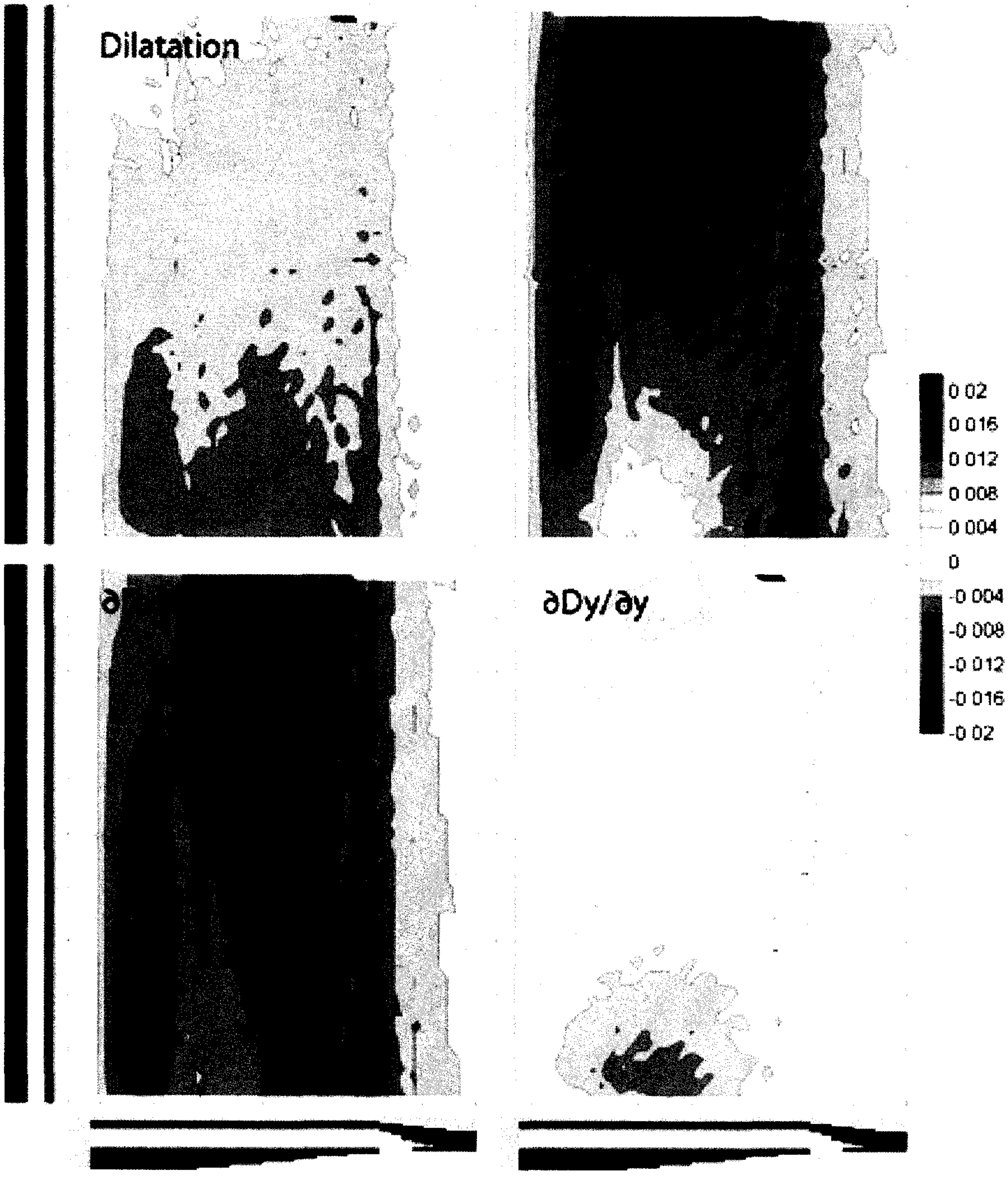

Figure 6.17. Model 4 dilatation, pure shear, $\partial D_x/\partial x$, and $\partial D_y/\partial y$.

As with previous models, there are high values of $\partial D_x/\partial x$ in the weakened zone. Like model 1, the values of $\partial D_y/\partial y$ are insignificant away from the boundaries.

6.2.5. Model 5: Decrease in the Vertical Extent of Weakening & Weakening Only in the Southwest

The patterns of displacement look similar to those in model 3. However, because the weakening does not extend as far into the crust, there is a smaller increase in x-displacement in the along-strike rheological transition zone compared to model 3. Correspondingly, there is a decrease in the uplift in the along-strike transition relative to model 3.

Because the subducting slab dips, a decrease in the vertical extent of the weakened zone results in a net horizontal shift in the across-strike rheological transition, and because the location of the across-strike transition has shifted to the northwest relative to model 3, the region of high $\partial D_y / \partial x$ values has correspondingly shifted to the northwest.

Patterns of dilatation and pure shear are similar to those in model 3. Relative to model 3, there is a decrease in values of $\partial D_x / \partial x$ at the along-strike rheological transition, which is caused by the relative decrease in the perturbation of x-displacement at this boundary. Additionally, there is a shift in the high values of $\partial D_x / \partial x$ to the northwest which corresponds to the shift in the across-strike rheological transition.

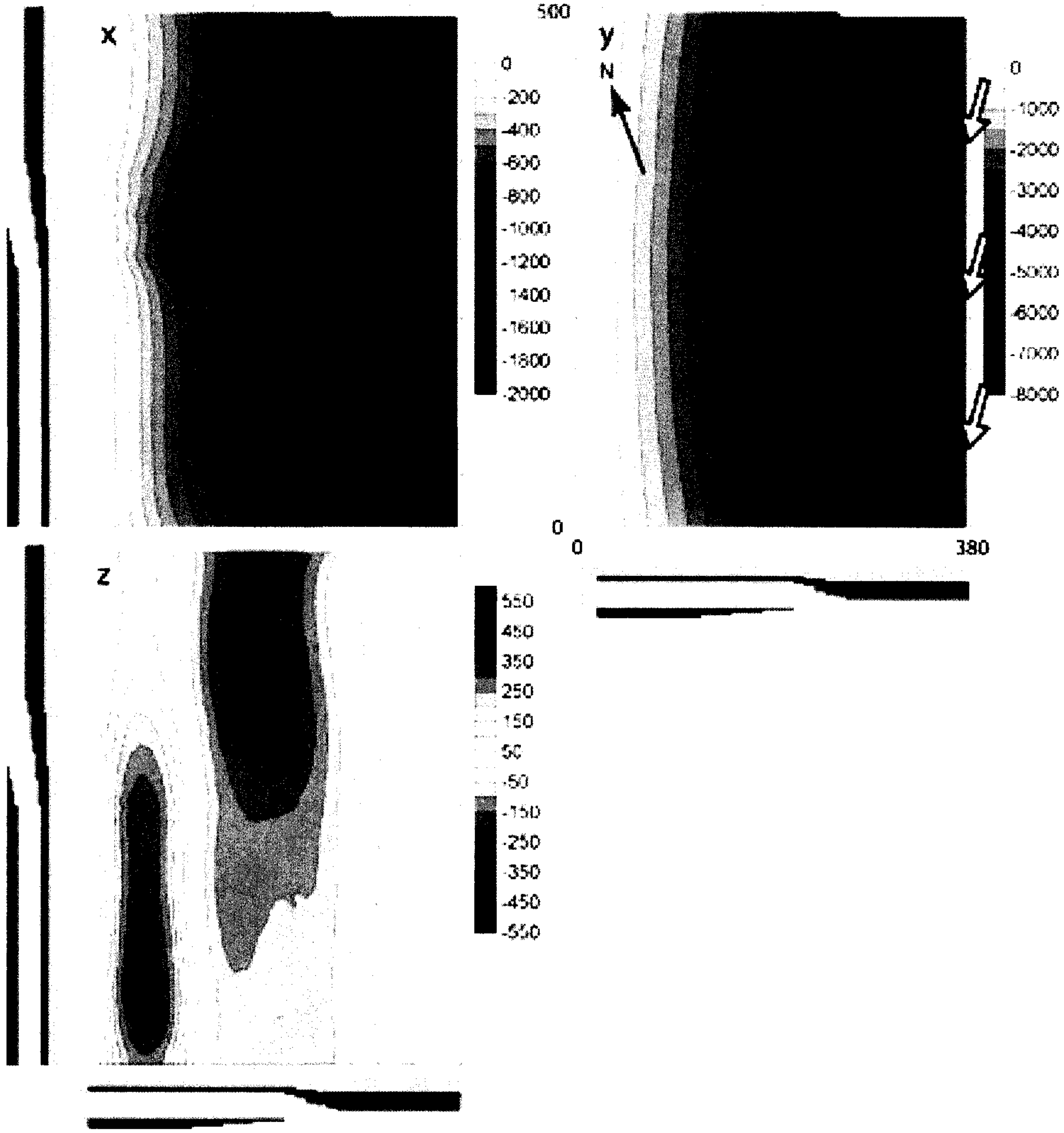

Figure 6.18 Model 5 displacements.

The perturbation in x displacement at the along-strike transition is smaller than in model 3.

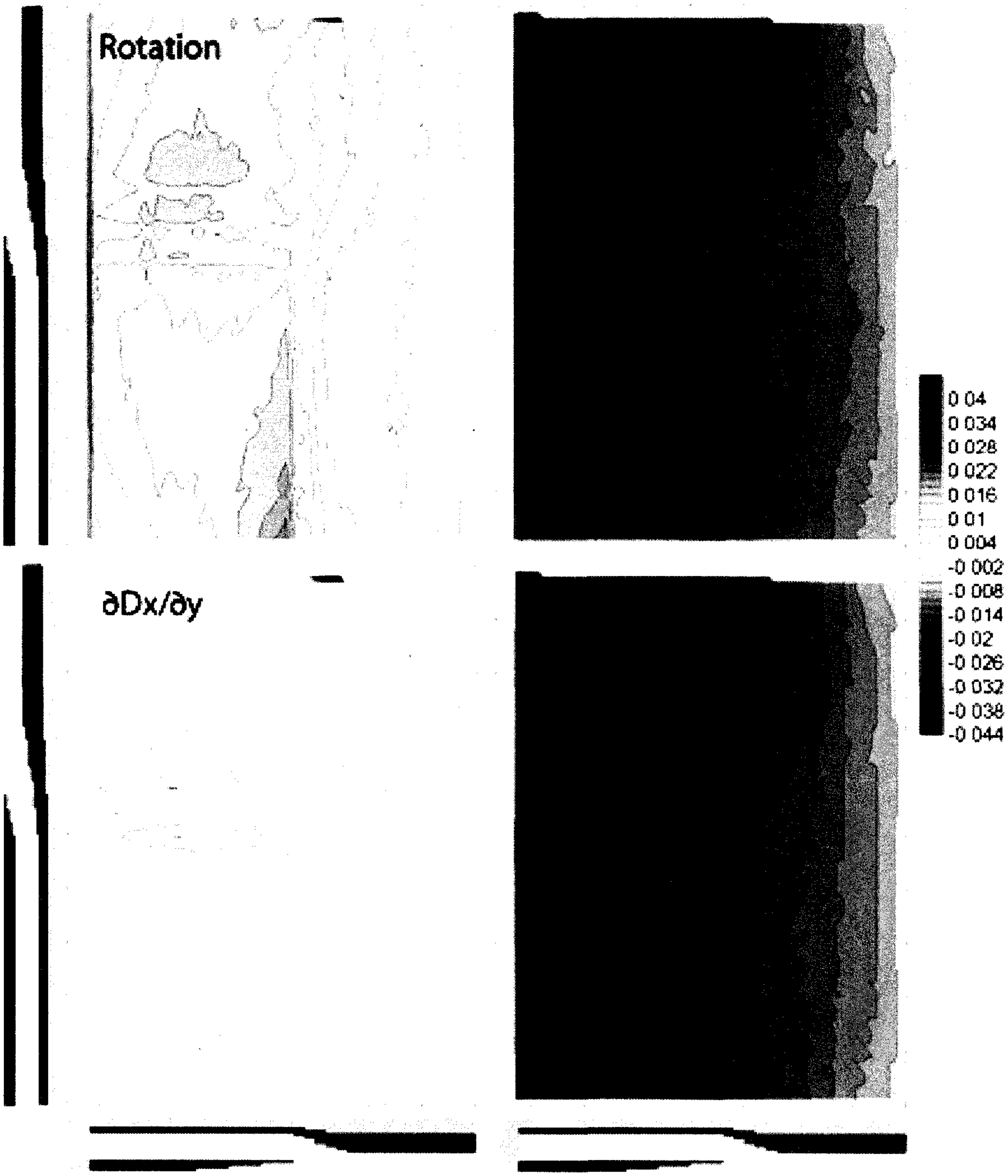

Figure 6.19 Model 5 rotation, simple shear, $\partial D_x/\partial y$, and $\partial D_y/\partial x$.

Regions of high $\partial D_x/\partial y$ values have shifted to the northwest with the new across-strike transition.

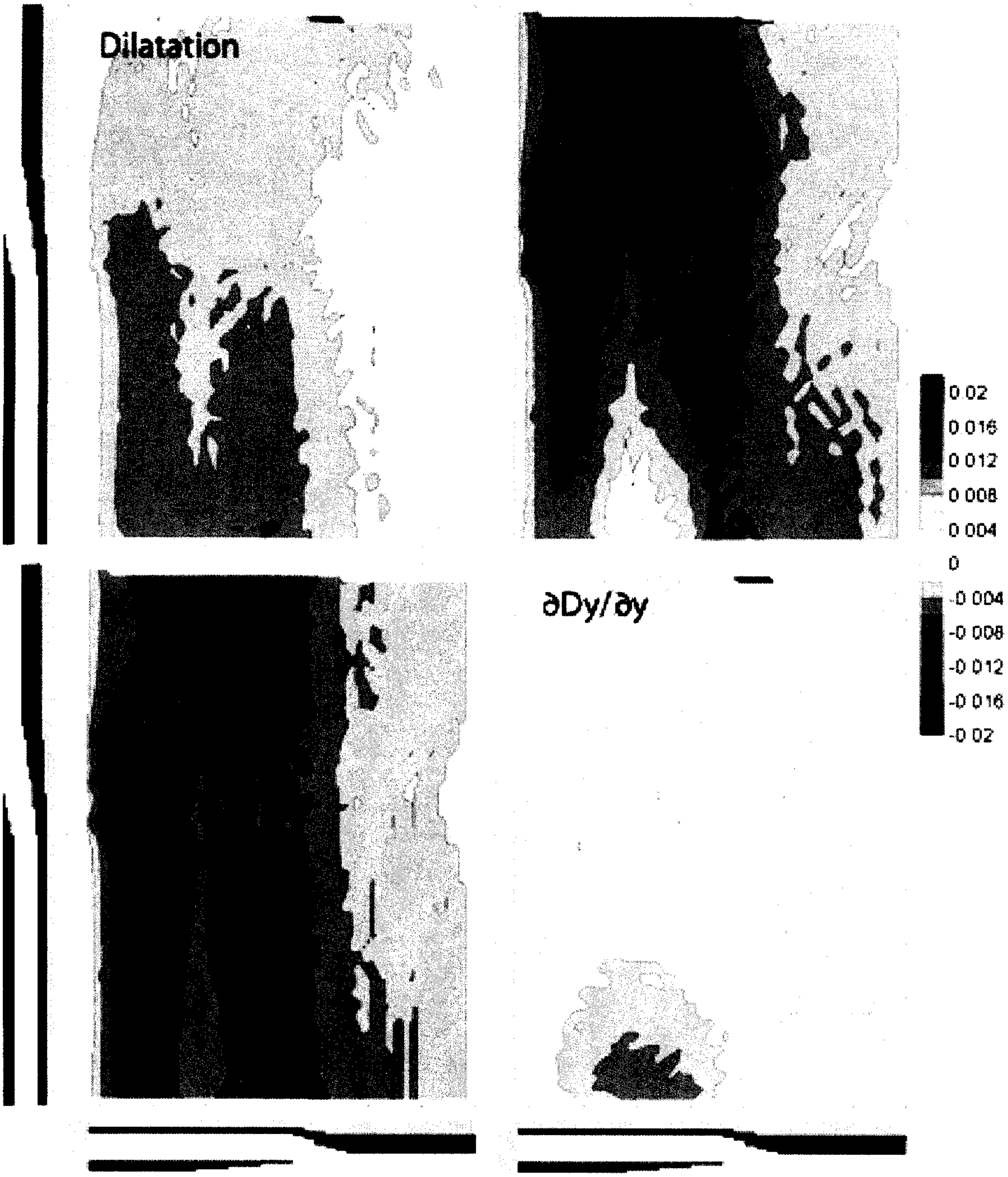

Figure 6.20 Model 5 dilatation, pure shear, $\partial D_x / \partial x$, and $\partial D_y / \partial y$.

Values of $\partial D_x / \partial x$ have decreased relative to model 3 in the transition zone.

6.2.6. Model 6: Decrease in the Vertical Extent of Weakening & Weakening Along the Entire y-Extent

Relative to model 4, it is clear from the x- and y-displacements that the deformation is taking place over a smaller distance in the across-strike direction. The reason for this decrease in length is that the across-strike rheological transition has shifted to the northwest. Because most of the deformation takes place within the weakened region, a decrease in the across-strike width of this region results in a concentration of the deformation into a smaller area. Additionally, in this model the uplift is 440m, an increase relative to model 4.

Compared to model 4, most of the simple shear and rotation are taken up over a smaller area, which matches the pattern of x- and y-displacement noted above. Similarly, because the decrease in y-displacement takes place over a smaller region, values of $\partial D_y / \partial x$ are higher than they were in model 4, where this deformation was slightly less concentrated.

Patterns of pure shear and dilatation are similar to those in model 4, except, as discussed above, they are taken up over a smaller across-strike distance.

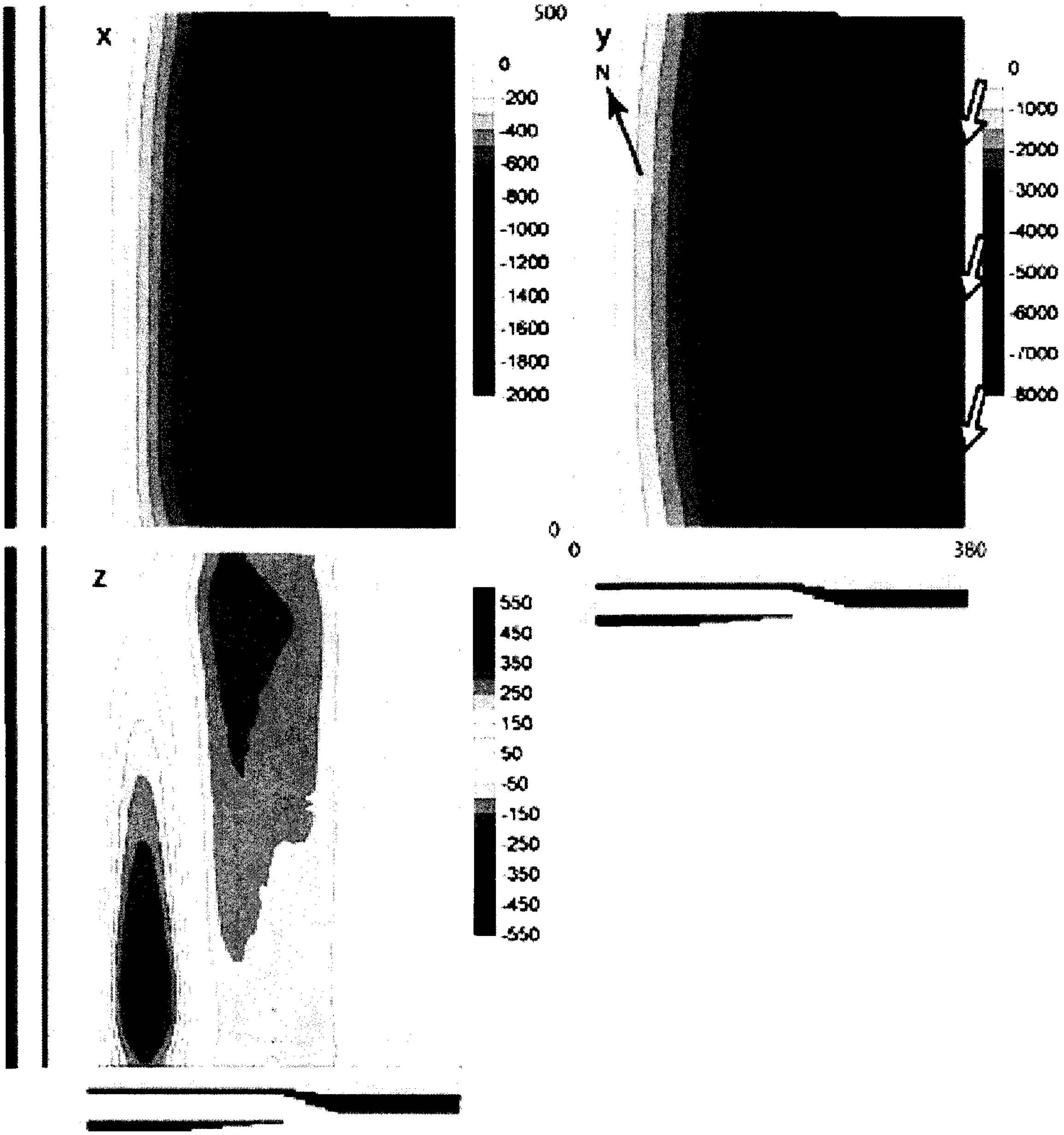

Figure 6.21 Model 6 displacements.

Decreases in x- and y-displacements take place over a smaller region than they did in model 4.

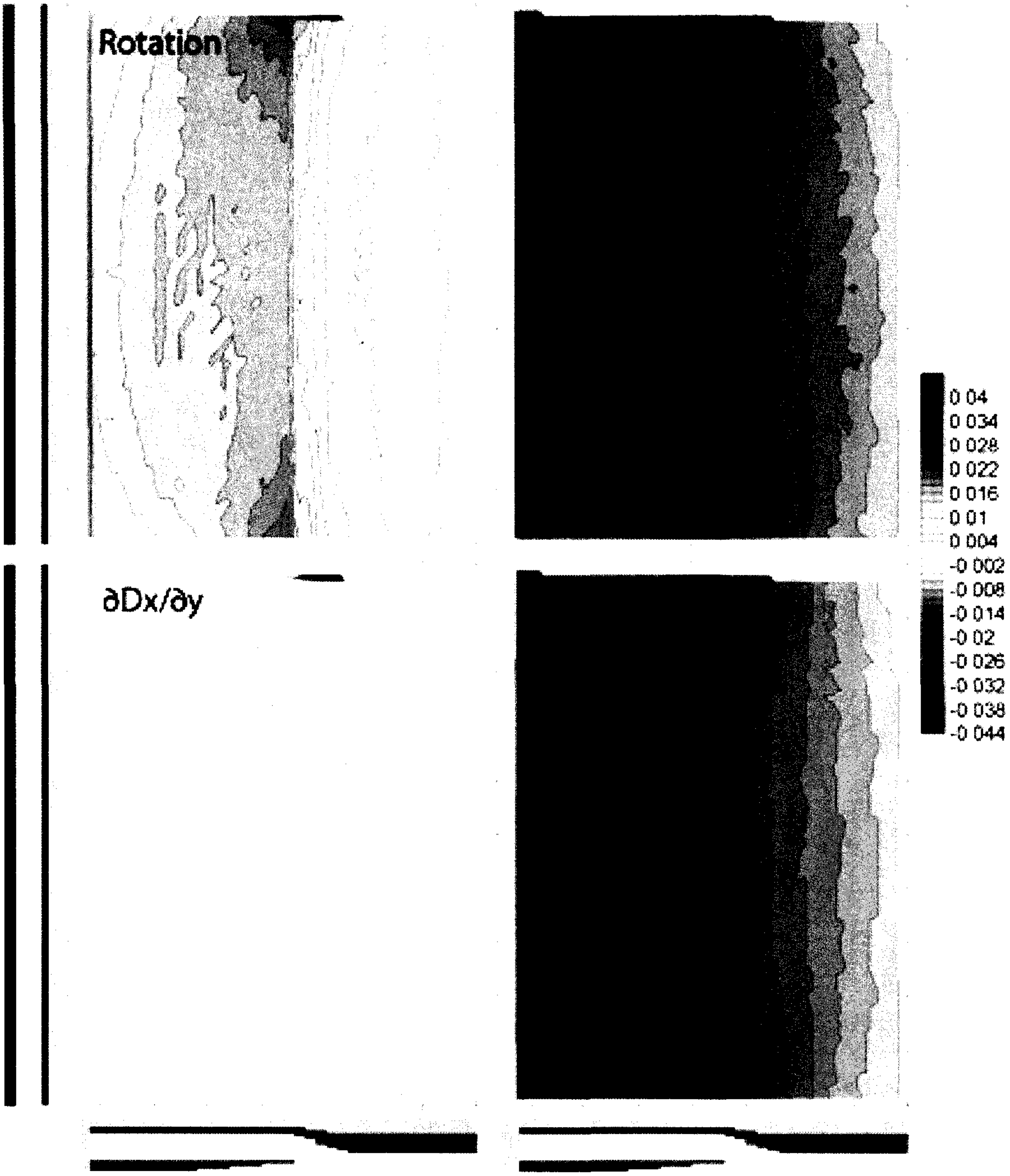

Figure 6.22 Model 6 rotation, simple shear, $\partial D_x/\partial y$, and $\partial D_y/\partial x$.

Values of $\partial D_y/\partial x$ are concentrated into a smaller across-strike width of the model relative to model 4.

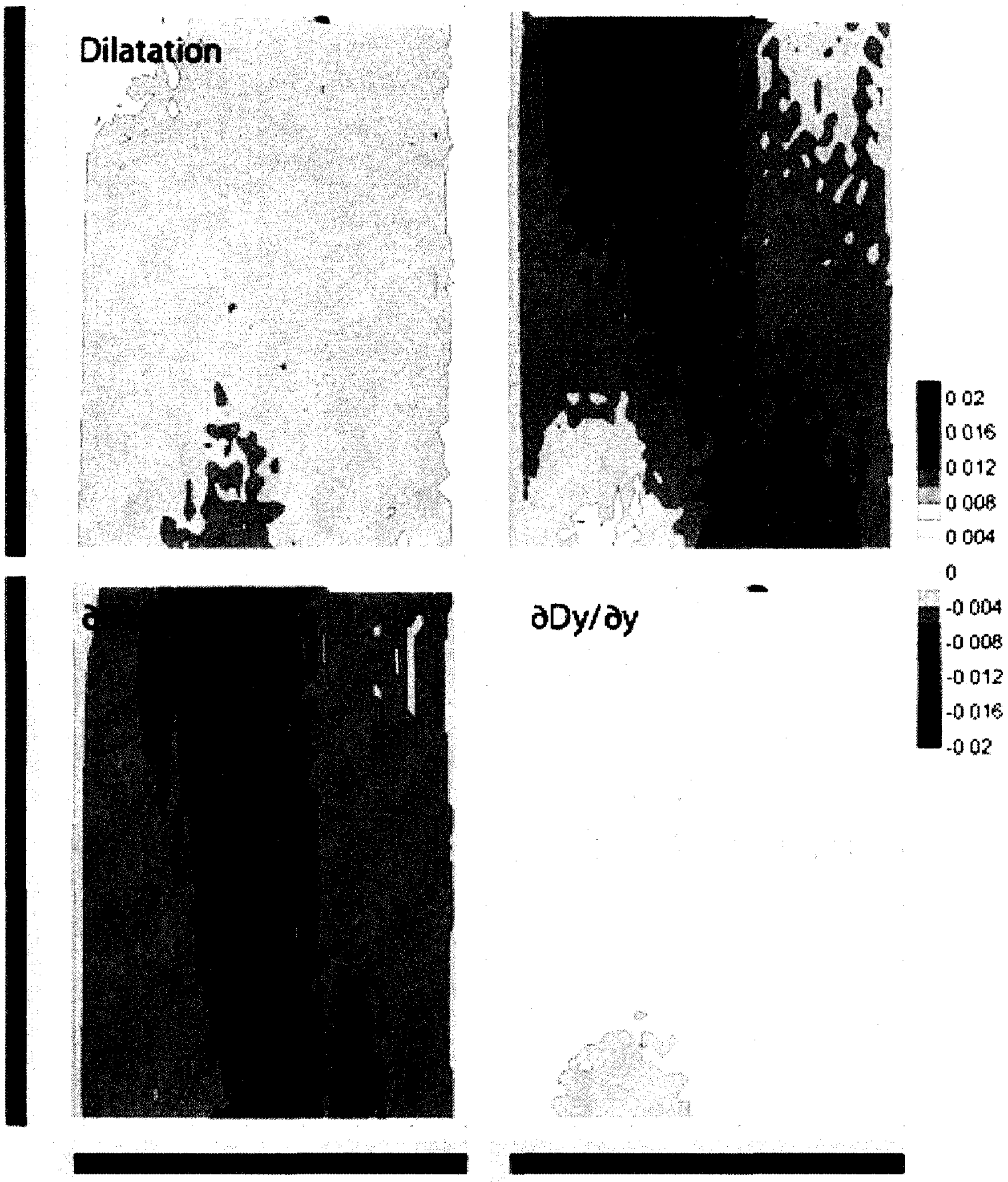

Figure 6.23 Model 6 dilatation, pure shear, $\partial D_x / \partial x$, and $\partial D_y / \partial y$.

Values of $\partial D_x / \partial x$ are concentrated into a shorter across-strike width of the model relative to model 4.

6.2.7. Effect of Erosion

When there is no erosion included in the models, the results are very similar to the previous models, except that the degree of uplift is smaller (Figure 6.18). In the first model the highest uplift was 260 m, and when run with no erosion, the uplift was 200 m. The erosion conditions affect the absolute values of the model but do not seem to affect the qualitative patterns that arise.

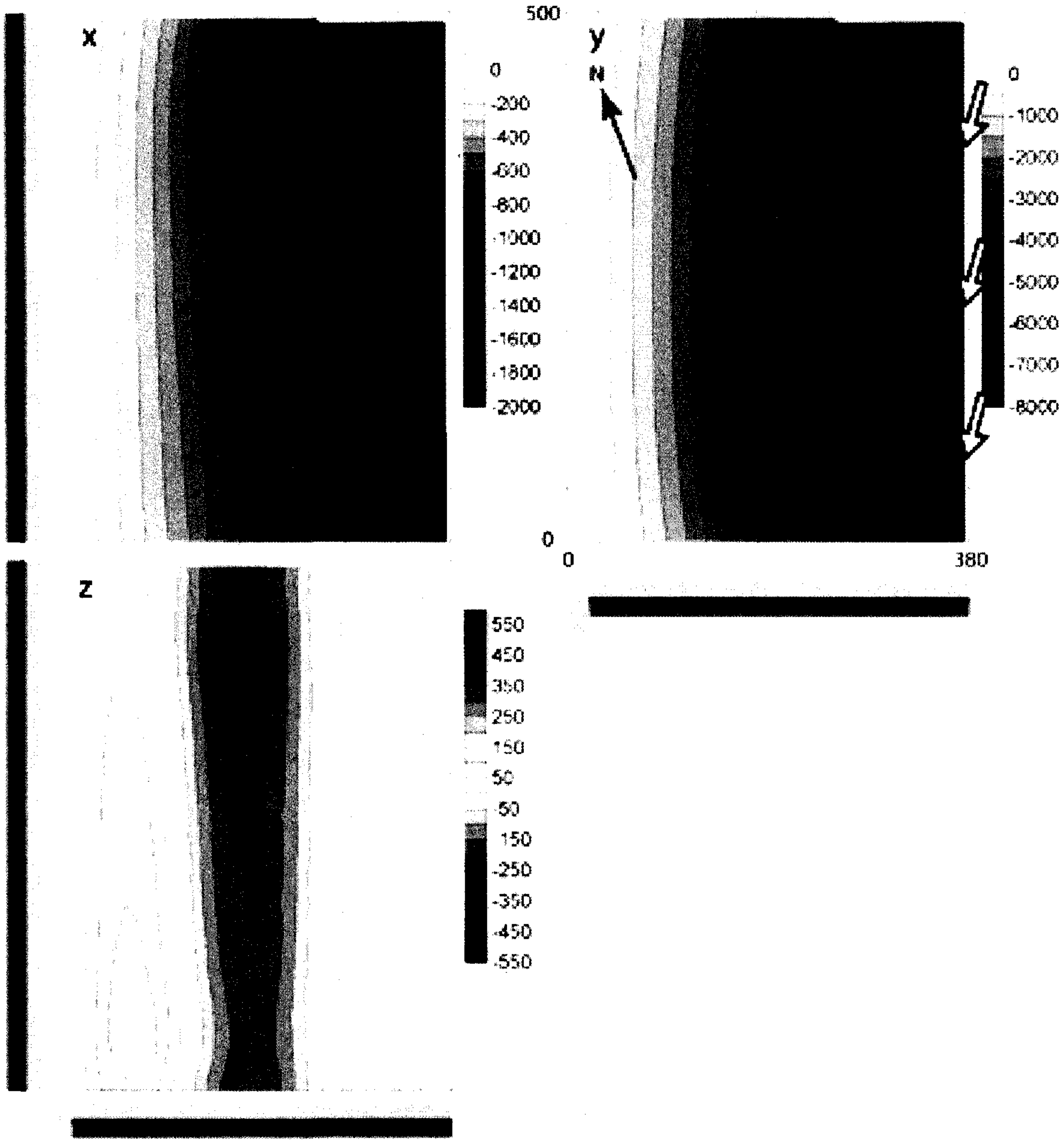

Figure 6.24. Displacements in a model with no erosion. Like model 1, there is no rheological weakening in this model.

These plots are similar to corresponding plots in model 1, but the magnitude of the uplift has decreased.

6.2.8. Summary and Physical Meaning

Differential weakening along-strike in the overriding slab of a subduction zone affects the x-displacement. By comparing models 1 and 4, it appears that a weakened rheology causes a slight increase in displacement. The reason for this increase is that when there is weakening, the strong material on the southeastern side of the model moves as a nearly rigid block and the majority of the deformation takes place within the weakened region. In contrast, when there is no weakening, the deformation is forced to take place in the strong material. Because the rheology is laterally uniform in model 1, deformation takes place fairly uniformly throughout the model when compared to model 4. However, this difference between models 1 and 4 is relatively minor compared to the increase in x-displacement that is found in the along-strike rheological transition of models 2 and 3, but when the depth of the weakened region was increased in model 5, the increase in x-displacement at the transition became less significant. A comparison of y-displacement between models 1 and 4 shows a similar pattern to x-displacement; there is a slight increase in the y-displacement in the weakened model.

The absolute values of z-displacement within a model are of little importance because they depend on the total amount of convergence. However, comparing the degree of uplift between models is useful. When there was no weakening (model 1), the highest uplift was 260 m. When there was weakening in the southwest (model 2), the highest uplift increased to 550 m. When the lateral extent of the weakening was increased along-strike (model 3), the highest value was 450 m, and the area over which the high uplift occurred became more diffuse. When there was weakening along the entire orogen (model 4), the high value was 360 m. When there was weakening along the entire orogen, but the depth of the weakened region was lowered (model 6), the highest value was 440m. Comparing models 1 and 4, it appears that uniform rheological weakening increases the magnitude of the uplift, but it does not increase the spatial extent of this uplift. Comparing models 4 and 6 shows that lowering the depth of the weakened region increases the uplift. This result seems counterintuitive, but decreasing the vertical extent of the weak zone, with this geometry, also decreases the width of the weak zone. It appears that for the limited geometries tested, decreasing the width of the weak zone is more significant than decreasing the vertical extent of the weak zone. When the weak zone is narrow, material is forced upwards during deformation. Although deformation is still focused into the weak zone when the weakened region is wider, this weak area is not able to support the high shear stresses that are associated with uplift. Thus, with this geometry, there is a balance between an increase in depth and a decrease in width. This result is likely to be highly dependent on geometry; for some geometries increasing the depth of the weakened region may be the dominant factor. In contrast to models 1, 4, and 6, model 3 does show an increase in the y-extent of the high uplift. It is possible that two separate effects are visible in this model. One is a region of high uplift on the southwestern boundary, which is similar to the pattern of uplift visible in model 1. The other effect is a separate region of uplift in the along-strike transition between the strong and weak rheologies. This idea is supported by model 2, which has the highest uplift of all the models. The high uplift in this model may be the result of having the rheological transition close to the southwestern boundary of the model, and the two regions of high uplift may overlap such that they appear as one region of extremely high uplift.

Rotation and simple shear are significant in all of the models because of the obliquity. In models 1 and 4, these two strain components are uniform along the length of the model because the rheology is uniform along strike, and because there is very little along-strike variation in displacement, the $\partial D_y/\partial x$ term controls rotation and simple shear. Thus, simple shear and rotation in these two models represent areas where high attenuation of the y-velocity is occurring. In a discontinuous medium, this region might represent one where an orogen-parallel fault zone may develop. In model 4, the region of high orogen-parallel shear was in a different location within the model than in model 1, and the shear was concentrated into a narrower region in the x-direction. Specifically, weakening the overlying slab transfers the majority of the shear to the southeast and localizes the high shear into a narrow zone at the boundary between the two slabs. This steep gradient indicates that the orogen-parallel velocity is not well transmitted from the strong to the weak region; the high simple shear is the result of a rapid decrease in the y-velocity. Thus, if there is a rheological change between the two slabs, it is likely that this region will represent a mechanical and kinematic boundary as well as a rheological boundary. This localization of the y-displacement gradient also matches the displacement structure noted above in which the y-displacements were greater in the weakened model. In the east the y-displacement is greater in the weakened model, but much of this displacement is taken up at the plate boundary, and the gradients are lower in model 4 on the northwestern side of the model. When the weakening was discontinuous across the length of the model, there was an additional region of rotation and simple shear caused by the curvature in the x-displacement. This curvature led to positive values of $\partial D_x/\partial y$ on the northeastern side of the transition and negative values on the southwestern side. Thus there is a decrease in rotation on the southwestern side, an increase in rotation on the northeastern side, an increase in simple shear on the southwestern side, and a decrease in simple shear on the northeastern side.

When there is a uniform rheology along the length of the orogen (models 1 and 4), dilatation and pure shear are dominated by $\partial D_x / \partial x$. As with simple shear, in model 4, there is some concentration of high $\partial D_x / \partial x$ values into the transition between the two plates. In model 4 there is also some concentration of $\partial D_x / \partial x$ on the northwestern side of the model as the displacement decreases at the backstop. This suggests that the velocities within the orogen are higher when there is weakening, and that the velocities must decrease rapidly as the material approaches the backstop. This is supported by the increased displacements in model 4 that were noted above. The elastic backstop represents the cold non-deforming continent. It is unlikely that the transition between an asthenospheric heat source and the cold continent would take place over as short a distance as it does in these models. A more gradual change in rheology may force the decrease in velocity to take place over a broader area than it did in model 4.

When there is differential weakening in the rheology (models 2 and 3), there is an additional region with high $\partial D_x / \partial x$ values at the along-strike rheological transition. The reason for the high $\partial D_x / \partial x$ values near the along-strike rheological transition is the same as the reason for the high $\partial D_x / \partial x$ values near the backstop; there are high x-velocities in the transition zone, and these velocities decrease rapidly with proximity to the backstop. The gradient in $\partial D_x / \partial x$ in front of the backstop explains the high z-displacement that occurs on the northwestern side of the orogen, and the high displacements at the transition zone explain why there are two zones of high uplift that occur along strike as discussed above. Increased uplift in the weakened models is explained through increased x-velocities in the interior of the model and increased x-velocity gradients and shortening near the backstop. Similarly, the high uplift near the transition is explained through high displacements in the transition zone, which attenuate rapidly at the backstop.

Values of $\partial D_y / \partial y$ are insignificant when there is no along-strike rheological variation. When there is differential weakening, there are positive $\partial D_y / \partial y$ values on the northeast side of the along-strike rheological border while there are negative values on the southwestern side. This gradient is the result of a slight curvature in the map of y-displacements. The velocity gradients $\partial D_x / \partial x$ and $\partial D_y / \partial y$ result in a pattern of pure shear that, in the weak zone, is concentrated in two locations. There is high pure shear in the southeast at the boundary between the two slabs and in the northwest near the backstop. In the strong region, pure shear is more evenly distributed across the orogen, but it is strongly concentrated at the along-strike rheological boundary. Similarly, dilatation is highest near the backstop and the along-strike rheological transition.

Chapter 7

DISCUSSION

The metamorphism in Maine implies that there was a large region of the crust that was anomalously hot during the Acadian orogeny. The steepest parts of the gradient in temperature on the edges of this anomaly are well modeled by plutonic activity. However, it is the steepness of the thermal gradients produced by this type of heat source that make it improbable that plutons could sustain a thermal anomaly over long wavelengths. Thus, I have modeled the heat source for the large-scale anomaly as a shallow asthenosphere, and this explanation is capable of producing the observed thermal effects within error. Although, this anomaly can account for the metamorphism in Maine, it is still possible that other or multiple heat sources could be used to explain the metamorphic record (Gerbi et al., 2006, Hochstein 1995). Future modeling could evaluate other heat sources for suitability to the Acadian orogen.

Mechanical modeling has shown an increase in uplift above the thermally weakened region. This phenomenon provides a mechanism for increasing the erosional depth in southern Maine. Additionally, the presence of a shallow asthenosphere requires the lithosphere to have thinned, and if the lithospheric thinning were accomplished through preferential removal of the mantle lithosphere, as opposed to uniform thinning, this event could provide an isostatic component to the uplift. However, the uplift caused by weakening may be partially the result of the abrupt change in rheology between the asthenosphere and the backstop in the models. Future modeling could explore the sensitivity of the models to this rheological transition, and determine if uplift can be expected when there is more gradual transition. An additional problem is that this mechanical model predicts a prominent curvature in the orogen at the edge of the thermal anomaly, which is not observed in Maine. There are several ways of explaining this discrepancy. One possibility is that the kinematics of the mechanical model do not adequately reflect the complexity of the orogen. Modern orogens with regions of lithospheric thinning and a shallow asthenosphere frequently display some degree of slab rollback. By ignoring this possible dynamic of the subducting slab, I have simplified the kinematics such that regions of extension are not produced in my models. It is possible that by combining a rheology consistent with slab rollback with boundary conditions consistent with a stable subduction point, I have produced some features that would be unrealistic in a natural orogen. Future modeling could attempt to address this issue. It may be possible to dynamically change the velocity conditions on the base of the model as it is running in an attempt to simulate slab rollback.

Another possibility is that the asthenospheric source was at a depth greater than I tested in my models. The variation in depths tested in the mechanical models suggests that the curvature in the orogen decreases when the heat source is deeper. Because the heat source is required to produce metamorphism, there are thermal limitations on the depth of the heat source. For a horizontal erosional surface, the heat source cannot be significantly deeper than 40 km, the deepest asthenospheric level tested with the mechanical models. However, for a dipping erosional surface, the heat source can be much deeper than 40 km. Further numerical testing could explore the effect of asthenospheric depth on orogen curvature.

Another parameter that should be explored further numerically is the obliquity of the model. Because the along-strike transitional effects appear to be associated almost entirely with the x-velocity, changes in the obliquity of the model could have a significant effect on the overall curvature observed in the model.

A fourth possibility is that the heat source extended farther to the north. This possibility would explain the lack of curvature in the orogen, but another mechanism would be needed to increase the uplift in the south. One possibility is that an episode of flat subduction in southern Maine thickened the crust, leading to net isostatic uplift in the southern part of the state relative to the north. Thus the high-temperature metamorphism would be exposed only in the south, and the lateral extent of the high-temperature region at depth would be poorly constrained.

In this scenario, central Maine would represent an erosional transition rather than a thermal transition. It is known that the rocks of southern Maine were metamorphosed at a greater depth than those of northern Maine, and it is possible that central Maine represents a rapid increase in the erosional depth instead of a rapid increase in temperature at a nearly constant depth. The geobarometry for the region is not accurate enough to reliably distinguish between a gradual change in depth and an abrupt nonlinear change (Ferry, 1980).

The regional gravitational data is consistent with underplating, but it is unable to provide definitive evidence of flat subduction. As discussed previously, there is a mass deficit over southern Maine that is suggestive of thickened crust, and the thickened crust could be the result of underplating. Additionally, the sequence of events in which underplating follows a period of lithospheric thinning provides a mechanism by which the high-density signature of a thinned crust could be removed. Another important consideration about the gravitational data is that, if the region of shallow asthenosphere extended farther north and underplating exposed the metamorphism in the south, the gravitational limit on the depth of the asthenosphere to no shallower than 30 km may still apply. If differential thermal weakening is adopted in place of underplating as the cause of uplift, a new mechanism must be found to explain the gravity data. However, in general in an orogen with a protracted history and a high degree of deformation, it is unclear that gravitational evidence for a shallow asthenosphere would be well preserved. Because of the curvature that is expected with differential along-strike weakening and because gravitational data provides marginally more support for underplating than for differential weakening, underplating is the model which is tentatively favored.

Underplating could have been accomplished through the overriding of a plume that kinematically prevented subduction, the partial subduction of continental material, or the subduction of oceanic sediments. Murphy et al. (1999) used the possibility that the subduction zone had overridden a mantle plume to explain many of the features of the volcanism in the Acadian orogeny. The effect of a mantle plume below a subduction zone is complex. The increase in temperature associated with a plume would decrease the viscosity and decrease the density contrast between the subducting slab and the asthenosphere. Both of these factors would increase the forces on the slab favoring subduction. Thus, to cause flat subduction, the upward velocity of the plume and the thermally induced thinning and density changes of the overlying slab would need to overcome all the forces promoting subduction. Another consequence of plume-related flat subduction is that the underplating would last only as long as the plume was active, and it is unclear that crustal thickening would persist beyond the life of the plume and the subduction zone. Additionally, there are numerous examples of flat-slab geometry that have been documented, which do no invoke the presence of a plume (Gutcher and Peacock, 2003). For these reasons, it is unclear that the presence of a plume is a realistic model. The partial subduction of continental material and the subduction of ocean sediments are similar mechanism to each other and similar to what is taking place in Taupo, New Zealand. In Taupo, it is known that there is high temperature metamorphism taking place and rapid uplift. Thus Taupo suggests that this method of underplating is compatible with the features seen in Maine. For these reasons, the subduction of sediments or continental material is the preferred method of underplating.

REFERENCES

Aleinikoff, J. N. and Moench R. H., 1987; U-Pb geochronology and Pb isotopic systematics of plutonic rocks in northern New Hampshire; ensimatic vs. ensialic sources; Abstracts with Programs - Geological Society of America, vol.19, no.1, pp.1-2.

Barr, S. M., White, C. E., Miller, B. V., 2002b; The Kingston Terrane, southern New Brunswick, Canada; evidence for an Early Silurian volcanic arc; Geological Society of America Bulletin, vol.114, no.8, pp.964-982.

Barr, S. M., White, C. E., Miller, B. V., van Staal, C. R., 2002a; The myth of "Avalonia"; did it constitute a single terrane or several different terranes in the early Paleozoic?; Abstracts with Programs - Geological Society of America, vol.34, no.1, pp.28.

Bibby, H. M., Caldwell, T. G., Davey, F. J., Webb, T. H., 1995; Geophysical evidence on the structure of the Taupo volcanic zone and its hydrothermal circulation; Journal of Volcanology and Geothermal Research, vol.68, no.1-3, pp.29-58.

Bourne, M. and Stuart, G., 2000; ScSp observed on North Island, New Zealand; implications for subducting plate structure; Geophysical Journal International, vol.142, no.3, pp.925-932.

Brace, W.F., Kohlstedt, D., 1980; Limits on lithospheric stress imposed by laboratory experiments; Journal of Geophysical Research, 89, 6248-6252.

Bradley, D. C., 1983; Tectonics of the Acadian Orogeny in New England and adjacent Canada; Journal of Geology, vol.91, no.4, pp.381-400.

Bradley, D. C. and Kidd, W. S. F., 1991; Flexural extension of the upper continental crust in collisional foredeeps; with Suppl. Data 91-27; Geological Society of America Bulletin, vol.103, no.11, pp.1416-1438.

Bradley, D. C. and Tucker, R., 2002, Emsian synorogenic paleogeography of the Maine Appalachians; Journal of Geology, vol.110, no.4, pp.483-492.

Bradley, D. C., Tucker, R. D., Lux, D. R., Harris, A. G., McGregor, D. C., 1998; Migration of the Acadian Orogen and foreland basin across the Northern Appalachians. Open-File Report - U. S. Geological Survey, Report: OF 98-0770, 79 pp.

Cloos, M., 1993; Lithospheric buoyancy and collisional orogenesis; subduction of oceanic plateaus, continental margins, island arcs, spreading ridges, and seamounts; Geological Society of America Bulletin, vol.105, no.6, pp.715-737.

Cloos, M., Sapiie, B., 1998; Continental margin subduction, collision, and lithospheric delamination in New Guinea; Abstracts with Programs - Geological Society of America, vol.30, no.7, pp.208.

Dallmeyer, R. D. and van Breeman, O., 1981; Rb-Sr whole-rock and ^{40}Ar/ ^{39}Ar mineral ages of the Togus and Hallowell quartz monzonite and Three Mile Pond granodiorite plutons, South-central Maine; their bearing on post-Acadian cooling history; Contributions to Mineralogy and Petrology, vol.78, no.1, pp.61-73.

Davis, D., Suppe, J., and Dahlen, F. A., 1983; Mechanics of fold-and-thrust belts and accretionary wedges; Journal of Geophysical Research. B, vol.88, no.2, pp.1153-1172.

DeYoreo, J.J., Lux, D. R., Decker, E. R., Osberg, P. H., 1989; The Acadian thermal history of western Maine; Journal of Metamorphic Geology, vol.7, no.2, pp.169-190.

DeYoreo, J. J., Lux, D. R., Guidotti, C. V., 1991; Thermal modelling in low-pressure/high-temperature metamorphic belts; Tectonophysics, vol.188, no.3-4, pp.209-238.

Dutrow, B. L. and Foster, C. T., 2002; Spatial and temporal characteristics of temperature and fluid flow during metamorphism around tabular plutons; Abstracts with Programs - Geological Society of America, vol.34, no.6, pp.501.

Eberhart-Phillips, D. and Reyners, M., 1999; Plate interface properties in the Northeast Hikurangi subduction zone, New Zealand, from converted seismic waves; Geophysical Research Letters, vol.26, no.16, pp.2565-2568.

Eusden Jr., J. D. and Barreiro, B., 1988; The timing of peak high-grade metamorphism in central-eastern New England; Maritime Sediments and Atlantic Geology, vol.24, no.3, pp.241-255.

Eusden Jr., J. D., Garesche, J. M., Johnson, A. H., Maconochie, J., Peters, S. P., O'Brien, J. B, Widmann, B. L., 1996; Stratigraphy and ductile structure of the Presidential Range, New Hampshire; tectonic implications for the Acadian Orogeny; Geological Society of America Bulletin, vol.108, no.4, pp.417-436.

Ferry, J. M. 1976; Metamorphism of calcareous sediments in the Waterville-Vassalboro area, South-central Maine; mineral reactions and graphical analysis; American Journal of Science, vol.276, no.7, pp.841-882.

Ferry, J. M. 1976; P, T, f_{CO2} , and f_{H2O} during metamorphism of calcareous sediments in the Waterville-Vassalboro area, South-central Maine; Contributions to Mineralogy and Petrology, vol.57, no.2, pp.119-143.

Ferry, J. M., 1980; A comparative study of geothermometers and geobarometers in pelitic schists from South-central Maine; American Mineralogist, vol.65, no.7-8, pp.720-732.

Ferry J. M., 1982; A comparative geochemical study of pelitic schists and metamorphosed carbonate rocks from south-central Maine, USA; Contributions to Mineralogy and Petrology, vol.80, no.1, pp.59-72.

Gerbi, C. C., Johnson, S. E., Koons, P. O., 2006; Control on low-pressure anatexis; Journal of Metamorphic Geology, vol.24, no.2, pp.107-118.

Gerbi, C., Johnson, S. E., Paterson, S. R., 2004; Implications of rapid, dike-fed pluton growth for host-rock strain rates and emplacement mechanisms; Journal of Structural Geology, vol.26, no.3, pp.583-594.

Guidotti, C. V., 1970; Metamorphic petrology, mineralogy and polymetamorphism in a portion of N.W. Maine, in Guidebook for field trips in the Rangeley lakes-Dead River basin region, western Maine; N. Engl. Intercoll. Geol. Conf., Syracuse, New York.

Guidotti, C. V., 1985; Metamorphic map of Maine, in Osberg, P. H., Hussey, A. M., II, and Boone, G. M. (eds.), Bedrock geologic map of Maine; Maine Geological Survey., scale 1:500,000.

Guidotti, C. V., 1989; Metamorphism in Maine: an overview, in Studies in Maine geology; papers to commemorate the 150th anniversary of C. T. Jackson's reports on the geology of Maine ed. Tucker, R. D., Marvinney, R. G.; Studies in Maine geology; papers to commemorate the 150th anniversary of C. T. Jackson's reports on the geology of Maine, pp. 1-17.

Gutscher, M.-A., Peacock, S. M., 2003; Thermal models of flat subduction and the rupture zone of great subduction earthquakes; Journal of Geophysical Research, B, Solid Earth and Planets, vol.108, no.1, 16 pp.

Hess, P. C., 1969; The metamorphic paragenesis of cordierite in pelitic rocks; Contributions to Mineralogy and Petrology, vol.24, no.3, pp.19107.

Hibbard, J. P., van Staal, C. R., Rankin, D. W., and Williams, H., 2006; Lithotectonic map of the Appalachian Orogen, Canada-United States of America; Geological Survey of Canada, Map 2096A, scale1:1,500,000.

Hicks, D. M., Hill, J., Shankar, U., 1996; Variation of suspended sediment yields around New Zealand; the relative importance of rainfall and geology; IAHS-AISH Publication, vol.236, pp.149-156.

Hochstein, M. P., 1995; Crustal heat transfer in the Taupo volcanic zone (New Zealand): comparison with other volcanic arcs and explanatory heat source models; Journal of Volcanology and Geothermal Research, vol.68, no.1-3, pp.117-151.

Holdaway, M. J., Guidotti, C. V., Novak, J. M., Henry, W. E., 1982; Polymetamorphism in medium- to high-grade pelitic metamorphic rocks, West-central Maine; Geological Society of America Bulletin, vol.93, no.7, pp.572-584.

Itasca, 2005; FLAC3D (Fast Lagrangian Analysis of Continua in 3 Dimensions), Minneapolis.

Johnson, J. E., Koons, P. O., Guidotti, C. V., manuscript in preparation; Emplacement-related strain rates from conductive cooling times in static and dynamic pluton aureoles: example from the Maine Appalachians, U.S.A.

Joyner, W. B., 1963; Gravity in north-central New England; Geological Society of America Bulletin, vol.74, no.7, pp.831-857.

Keppie, J. D. and Dostal, J., 1994; Late Silurian-Early Devonian transpressional rift origin of the Quebec Reentrant, Northern Appalachians; constraints from geochemistry of volcanic rocks; Tectonics, vol.13, no.5, pp.1183-1189.

Kohlstedt, D. L., Evans, B., Mackwell, S. J., 1995; Strength of the lithosphere; constraints imposed by laboratory experiments; Journal of Geophysical Research,B, Solid Earth and Planets, vol.100, no.9, pp.17,587-17,602.

Koons, P. O., 1990; Two-sided orogen; collision and erosion from the sandbox to the Southern Alps, New Zealand; Geology, vol.18, no.8, pp.679-682.

Koons, P. O., Henderson, C. M., 1995; Geodetic analysis of model oblique collision and comparison to the Southern Alps of New Zealand; New Zealand Journal of Geology and Geophysics, vol.38, no.4, pp.545-552.

Koons, P.O., Norris, R.J., Craw, D., Cooper, A.F., 2003; Influence of exhumation on the structural evolution of transpressional plate boundaries: An example from the Southern Alps, New Zealand; Geology. 31, 3-6.

Koons, P. O., Upton, P., Terry, M. P., 2003a; Three-dimensional mechanics of UHPM terrains and resultant P-T-t paths; EMU Notes in Mineralogy, vol. 5, ch. 13, pp. 415-441.

Ludman, A., Hopeck, J. T., and Brock, P. C., 1993; Nature of the Acadian Orogeny in eastern Maine; Special Paper - Geological Society of America, vol.275, pp.67-84.

Lux, D. R. and Guidotti, C. V., 1985; Evidence for extensive Hercynian metamorphism in western Maine; Geology, vol.13, no.10, pp.696-700.

McKerrow, W. S. and Ziegler, A. M., 1971; The lower Silurian paleogeography of New Brunswick and adjacent areas; Journal of Geology, vol.79, no.6, pp.635-646.

McMahon, T. P., 2000a; Magmatism in an arc-continent collision zone: an example from Irian Jaya (western New Guinea), Indonesia; Buletin Geologi, vol. 32, no. 1, pp. 1-22.

McMahon, T. P., 2000b; Origin of syn- to post-collisional magmatism in New Guinea; Buletin Geologi, vol. 32, no. 2, pp. 89-104.

Murphy, J. B., van Staal, C. R., Keppie, J. D., 1999; Middle to late Paleozoic Acadian Orogeny in the Northern Appalachians; a Laramide-style plume-modified orogeny?; Geology, vol.27, no.7, pp.653-656.

National Image and Mapping Agency (NIMA); 2001[modified 2005, accessed 2005]; GeoNet - United States Gravity Data Repository System; U.S. Geological Survey, University of Texas at El Paso, Arizona State University, Pan American Center for Earth and Environmental Studies (PACES), National Oceanographic and Atmospheric Agency(NOAA), National Science Foundation (NSF), National Aeronautic and Science Administration (NASA), and National Geospatial-Intelligence Agency (NGA); http://paces.geo.utep.edu/gdrp/.

Nelson, K. D., 1992; Are crustal thickness variations in old mountain belts like the Appalachians a consequence of lithospheric delamination?; Geology, vol.20, no.6, pp.498-502.

Nielson, D. L., Clark, R. G., Lyons, J. B., Englund E. J., Borns, D. J., 1976; Gravity models and mode of emplacement of the New Hampshire Plutonic Series; Memoir - Geological Society of America, no.146, Studies in New England geology; northern New England, pp.301-318.

Northwest Geophysical Associates, Inc, 2004; GM-SYS Version 4.9, Corvallis, Oregon.

Osberg, P. H., 1968; Stratigraphy, structural geology, and metamorphism of the Waterville-Vassalboro area, Maine; Bulletin - Maine Geological Survey, 64 pp.

Pattison, D. R. M., Spear, F. S., Cheney, J. T., 1999; Polymetamorphic origin of muscovite + cordierite + staurolite + biotite assemblages; implications for the metapelitic petrogenetic grid and for P-T paths; Journal of Metamorphic Geology, vol.17, no.6, pp.685-703.

Peacock S. M., 1996; Thermal and petrologic structure of subduction zones; Geophysical Monograph, vol.96, pp.119-133.

Ranalli, G., 1995; Rheology of the Earth. 2nd ed. London: Chapman & Hall.

Reyners, M., Eberhart-Phillips, D., Stuart, G., 1999; A three-dimensional image of shallow subduction; crust structure of the Raukumara Peninsula, New Zealand; Geophysical Journal International, vol.137, no.3, pp.873-890.

Robinson, P., Tucker, R. D., Bradley, D., Berry IV, H. N., Osberg, P. H., 1998; Paleozoic orogens in New England, USA; GFF, vol.120, no.2, pp.119-148.

Short H. A. and Johnson S. E., in press; Estimation of vorticity from fibrous calcite veins, central Maine, USA; Journal of Structural Geology.

Solar, G. S. and Brown, M., 2001; Deformation partitioning during transpression in response to Early Devonian oblique convergence, Northern Appalachian Orogen, USA; Journal of Structural Geology, vol.23, no.6-7, pp.1043-1065.

Spear, F. S, 1993; Metamorphic phase equilibria and pressure-temperature-time paths; Mineralogical Society of America, Washington, DC, United States.

Spear, F. S. and Cheney, J. T., 1989; A petrogenetic grid for pelitic schists in the system SiO_2 -Al_2O_3 -FeO-MgO-K_2 O-H_2O; Contributions to Mineralogy and Petrology, vol.101, no.2, pp.149-164.

Stern, T. A. and Davey, F. J., 1987; A seismic investigation of the crustal and upper mantle structure within the central volcanic region of New Zealand; New Zealand Journal of Geology and Geophysics, vol.30, no.3, pp.217-231.

Stewart, D. B., Wright, B. E., Unger, J. D., Phillips, J. D., and Hutchinson, D. R., 1993; Global Geoscience Transect 8; Quebec-Maine-Gulf of Maine Transect, southeastern Canada, northeastern United States of America; Miscellaneous Investigations Series - U. S. Geological Survey, Report: I-2329, 17 pp.

Swanson, M. T., 1999; Kinematic indicators for regional dextral shear along the Norumbega fault system in the Casco Bay area, coastal Maine; Special Paper - Geological Society of America, ed. Ludman, A, West, D. P., Jr., vol.331, pp.1-23.

Swanson, M. T., 1992; Late Acadian-Alleghenian transpressional deformation; evidence from asymmetric boudinage in the Casco Bay area, coastal Maine; Journal of Structural Geology, vol.14, no.3, pp.323-341.

Sweeney, J. F., 1976; Subsurface distribution of granitic rocks, south-central Maine; Geological Society of America Bulletin, vol.87, no.2, pp.241-249.

Tucker, R. D., Osberg, P. H., Berry IV, H. N., 2001; The geology of a part of Acadia and the nature of the Acadian Orogeny across central and eastern Maine; American Journal of Science, vol.301, no.3, pp.205-260.

Turcotte, D. L. and Schubert, G., 2002; Geodynamics; Cambridge University Press, Cambridge, United Kingdom, 456 pp.

Tuttle, O. F., Bowen, N. L., 1958; Origin of granite in the light of experimental studies in the system $NaAlSi_3O_8$-$KAlSi_3O_8$-SiO_2-H_2O; Geological Society of America Memoir, 74, 54-63.

Upton, P., Craw, D., Caldwell, T.G., Koons, P.O., James, Z., Wannamaker, P.E., Jiracek, G.J., Chamberlain, C.P., 2003a; Upper Crustal Fluid Flow in the Outboard Region of the Southern Alps, New Zealand; Geofluids 3, 1-12.

Upton, P., and Koons, P. O., in review; Three-dimensional geodynamic framework for the Central Southern Alps, New Zealand: Intergrating geology, geophysics and mechanical observations; Geophysical Monograph.

Upton, P., Koons, P.O. Eberhart-Phillips, D., 2003b; Extension and strain-partitioning in an oblique subduction zone, New Zealand: Constraints from three-dimensional numerical modeling; Tectonics, vol.22, no.6, 14 pp.

Van Staal, C. R., Barr, S. M., Fyffe, L. R., McNicoll, V., Pollock, J. C., Reusch, D. n., Thomas, M. A., Valverde-Vacquero, P., Whalen,J., 2002; Ganderia; an important peri-Gondwanan terrane in the Northern Appalachians; Abstracts with Programs - Geological Society of America, vol.34, no.1, pp.28.

West, D, P., Jr., Lux, D. R., Hussey II, A. M., 1988; $^{40}Ar/^{39}Ar$ hornblende ages from southwestern Maine; evidence for late Paleozoic metamorphism; Maritime Sediments and Atlantic Geology, vol.24, no.3, pp.225-239.

White, S. M., Crisp, J. A., Spera, F. J., 2006 (in press); Long-term volumetric eruption rates and magma budgets; Geochemistry Geophysics Geosystems, vol. 7.

Xu, G, Will, T. M., Powell, R., 1994; A calculated petrogenetic grid for the system K_2O-FeO-MgO-Al_2O_3 -SiO_2 -H_2O, with particular reference to contact-metamorphosed pelites; Journal of Metamorphic Geology, vol.12, no.1, pp.99-119.

Zartman, R. E. Hurley, P. M. Krueger, H. W., Giletti, B. J., 1970; A Permian disturbance of K-Ar radiometric ages in New England; its occurrence and cause; Geological Society of America Bulletin, vol.81, no.11, pp.3359-3374.

BIOGRAPHY OF THE AUTHOR

Lucy E. Brown was born in Boston, Massachusetts in 1981. She was raised in Belmont, Massachusetts, and she graduated from Belmont High School in 1999. From 1999 to 2003 she attended Wellesley College, where she received a Bachelor of Arts degree in geology. In 2003 she entered the Graduate School at the University of Maine.

Lucy is a candidate for the Master of Science degree in Earth Sciences in December, 2006.